Metal Borohydrides beyond Groups I and II: A Review

Karina Suárez-Alcántara * and Juan Rogelio Tena García

Morelia Unit of Materials Institute Research, National Autonomous University of Mexico, Morelia, Michoacán 58190, Mexico; kse_91@hotmail.com

* Correspondence: karina_suarez@iim.unam.mx; Tel.: +52-55-5623-7300 (ext. 37889)

Abstract: This review consists of a compilation of synthesis methods and several properties of borohydrides beyond Groups I and II, i.e., transition metals, main group, lanthanides, and actinides. The reported properties include crystal structure, decomposition temperature, ionic conductivity, photoluminescence, etc., when available. The compiled properties reflect the rich chemistry and possible borohydrides' application in areas such as hydrogen storage, electronic devices that require an ionic conductor, catalysis, or photoluminescence. At the end of the review, two short but essential sections are included: a compilation of the decomposition temperature of all reported borohydrides versus the Pauling electronegativity of the cations, and a brief discussion of the possible reactions occurring during diborane emission, including some strategies to reduce this inconvenience, particularly for hydrogen storage purposes.

Keywords: borohydrides; transition metals; lanthanides

1. Introduction

To date, several reviews on the alkali or alkali earth metal borohydrides for hydrogen storage have been published [1,2]. This great interest is due to the high hydrogen content of some of them, e.g., $LiBH_4$. However, other metal borohydrides can be important for several applications, including, but not limited to, hydrogen storage. For example, the transition metal borohydrides present dehydrogenation temperatures which are usually lower than those of Group I and Group II borohydrides. In some cases, the hydrogen content is interesting (6–8 wt.%) due to the oxidation states (+2, +3) that translate into a high number of $[BH_4]^{-1}$ ions (ligands) [3] (See Figure 1). Recently, bimetallic and trimetallic materials with high hydrogen content have emerged (See Figure 2). Non- alkali or alkali earth metal borohydrides have many exciting characteristics that can help design new materials and applications beyond hydrogen storage. For example, lately, borohydrides have gained attention as high-temperature conductors in the solid-state or even when melted [4–6]. Borohydrides can also act as precursors to the corresponding metal boride [7–10] for the CVD-growing of thin films [11,12]. Rare earth metal borohydrides are emerging as new materials [13] for ion conductivity [5,14], catalysis [15,16], luminescence [17,18], or magnetic [19,20] applications.

Legend:
* 2THF
** probably solvated, no experimental crystal data
ʁ 2THF and 3THF solvated
§ not isolated form other reaction products

Main table:

$LiBH_4$ 18.51 wt% 663 K	$Be(BH_4)_2$ 20.8 wt% 396 K															
$NaBH_4$ 10.66 wt% 773 K	$Mg(BH_4)_2$ 14.9 wt% 572 K											$Al(BH_4)_3$ 16.91 wt% 400 K				
KBH_4 7.47 wt% 823 K	$Ca(BH_4)_2$ 11.56 wt% 628 K		$Ti(BH_4)_3$ 13.1 wt% 298-333 K	$V(BH_4)_3$ 12.67 wt% 343-463 K	$Cr(BH_4)_2$ * 9.87 wt% 253-298 K	$Mn(BH_4)_2$ 9.53 wt% 413-433 K	$Fe(BH_4)_2$ 9.43 wt% 263-273 K			$CuBH_4$ 5.14 wt% 261-273 K	$Zn(BH_4)_2$ **	$GaH(BH_4)_2$ 9 wt% 228 K				
$RbBH_4$ 4.02 wt% 773 K	$Sr(BH_4)_2$ 6.87 wt% 653 K	$Y(BH_4)_3$ 9.06 wt% 460 K	$Zr(BH_4)_4$ 10.71 wt% 355 K							$AgBH_4$ 3.28 wt% 243 K	$Cd(BH_4)_2$ 5.67 wt% 348 K	$In(BH_4)_3$ ʁ 7.6 wt% 263 K				
$CsBH_4$ 2.73 wt% 695 K	$Ba(BH_4)_2$ 4.83 wt% > 773 K		$Hf(BH_4)_4$ 6.78 wt% 473 K									$TlBH_4$ § 1.84 wt%				

Lanthanides/Actinides:

$La(BH_4)_3$ 6.6 wt% 523-573 K	$Ce(BH_4)_3$ 6.55 wt% 498-563 K	$Pr(BH_4)_3$ 6.52 wt% 520-533 K	$Nd(BH_4)_3$ 6.41 wt% 523 K		$Sm(BH_4)_2$ 4.48 wt% 608 K / $Sm(BH_4)_3$ 6.21 wt% 473 K	$Eu(BH_4)_2$ 4.44 wt% 668 K / $Eu(BH_4)_3$ 6.16 wt% 298 K	$Gd(BH_4)_3$ 5.99 wt% 508-543 K	$Tb(BH_4)_3$ 5.95 wt% > 523 K	$Dy(BH_4)_3$ 5.84 wt% > 523 K	$Ho(BH_4)_3$ 5.77 wt% 523 K	$Er(BH_4)_3$ 5.71 wt% 559 K	$Tm(BH_4)_3$ 5.71 wt% > 523 K	$Yb(BH_4)_3$ 5.56 wt% 618 K / $Yb(BH_4)_2$ 3.98 wt%	$Lu(BH_4)_3$ 3.94 wt%
	$Th(BH_4)_4$ 5.53 wt%	$Pa(BH_4)_4$ 5.55 wt%	$U(BH_4)_4$ 5.42 wt% 373-423 K	$Np(BH_4)_3$ 4.3 wt% 298K	$Pu(BH_4)_3$ 4.19 wt% 293 K									

Figure 1. "Periodic table" of experimentally reported single homoleptic borohydrides showing hydrogen content in wt.% and decomposition temperature (or range). An editable version is in the supplementary file.

Figure 2. "Periodic table" of experimentally reported mixed-cation homoleptic borohydrides of transition metals, main group, lanthanides, and actinides. An editable version is in the supplementary file.

In the late 1970s, a timely and comprehensive review of transition metals, lanthanide, and actinide borohydride complexes was reported [21]. In 2015, an update which specialized in crystal chemistry was published [22]. Since 2017, an important review of borohydrides and derivates (including heteroleptic materials of the type $M_x(BH_4)_y(NH_2)_z$ and $M_x(BH_4)_y \cdot nNH_3$) has been available for consultation [23]. In 2020, a highly informative paper on several hydrogen storage materials, including some borohydrides, was published [24]. In the last decade, research on the synthesis and characterization of bimetallic, trimetallic, anion-substituted (halide-substituted being more specific), and reactive composite mixtures of borohydrides has emerged, and it deserves a compilation. This work is a comprehensive review of the homoleptic borohydrides of transition metals, lanthanides, actinides, and main group block elements (Figures 1 and 2, editable versions of these figures are in the supplementary file), focusing on the hydrogen storage area, yet covering (when available) data for other applications. When considered necessary, halide-substituted borohydrides are also mentioned.

In the last sections, an overview of the thermodynamics (stability) of borohydrides is included. A section called "the boron problem" is included to discuss the contradictory problem of desirable low-temperature dehydrogenation and the release of B_xH_y compounds.
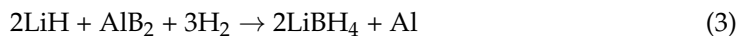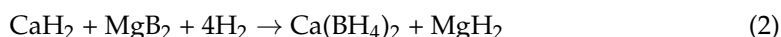
2. Synthesis

Details of the synthesis are presented for each borohydride; however, in this short section, a recount of the generals of borohydrides' syntheses is presented. Synthesis methods can be divided roughly into two types: (i) "wet" synthesis methods in different organic solvents, and (ii) ball-milling synthesis. Wet synthesis has the advantages of better controlling the reaction conditions and products with higher purity, particularly with the new tendency of using mixtures of solvents or co-solvents during reactions and for product extraction. Some borohydrides have actually been produced only by this type of synthesis. Its drawbacks are the use of non-ecofriendly solvents and that some solvated materials are difficult to dry without them decomposing. For its part, ball-milling techniques produce impure borohydrides due to side reactions, by-products, and co-products (e.g., in the metathesis reactions). All these impurities may not always be inert during further reactions (i.e., during dehydrogenation reactions). The advantages of ball-milling are fast production, the possibility of scaling-up, and the chance to control temperature, pressure, and atmospheres during gas–solid reactions.

As additional types of synthesis method, we can include the "combined methods." Combined methods generally start with the pre-milling of raw materials, followed by their reaction in solvents and solvent extraction or, recently, the use of $S(CH_3)_2 \cdot BH_3$ as both a solvent and a reactant [13,25]. In all cases, precautions must be taken due to the materials' sensitivity to oxygen and moisture; handling, synthesis, storage, and characterization must be performed under protective atmospheres (argon, nitrogen, etc.) of high purity.

The general synthesis routes of homoleptic borohydrides can be classified as follows [23,26,27]:

1. Direct synthesis from elements. Usually, this kind of synthesis requires high pressure and temperature. Reducing particle size can (but not always) accelerate reaction kinetics. An example is the synthesis of $LiBH_4$ from Li, B, and H_2 at 150 bar and a temperature of 975 K [26].
2. Syntheses using B_2H_6: For example, during wet synthesis, reagents such as $Mg(CH_2CH_3)_2$ and B_2H_6 can react to produce the corresponding Mg-borohydride [28]. In solid–gas-type reactions, a metal hydride and B_2H_6 can react during ball milling. Notice that B_2H_6 is a toxic and unstable gas.
3. Reactive composites of metals or metal hydrides and metal borides. This type of synthesis has been widely demonstrated for Li, Na, and Ca-borohydrides. The metal borides serve as a B-source, enhancing the kinetics and reducing thermodynamic constraints. Importantly, this kind of synthesis has demonstrated some degree of reversibility, particularly if MgH_2 and MgB_2 are involved.

$$2MH + MgB_2 + 4H_2 \rightarrow 2MBH_4 + MgH_2, \text{ for } M = Li, Na \tag{1}$$

$$CaH_2 + MgB_2 + 4H_2 \rightarrow Ca(BH_4)_2 + MgH_2 \tag{2}$$

$$2LiH + AlB_2 + 3H_2 \rightarrow 2LiBH_4 + Al \tag{3}$$

4. Metathesis. This type of reaction is the most widely used synthesis method for borohydrides beyond Groups I and II, both by wet chemistry and ball-mill assisted synthesis. Usually, LiBH$_4$ or (to a minor extent) NaBH$_4$ are the preferred reagents due to their commercial availability. However, considering hydrogen storage applications, this kind of synthesis is useful only if the new material has better dehydrogenation kinetics, low dehydrogenation temperature, or better reversibility than the original LiBH$_4$ or NaBH$_4$. This statement is made because, normally, the hydrogen content of the new borohydride decreases compared to LiBH$_4$; thus, other advantages over LiBH$_4$ must be necessarily obtained. Additionally, unless proper separation of other metathesis products is accomplished, a significant decrease of the full mixture's hydrogen content is unavoidable. The general reaction is:

$$nMBH_4 + M'X_n \rightarrow M'(BH_4)_n + nMX \tag{4}$$
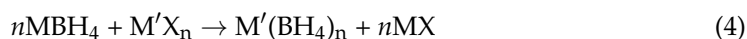
A recent variation of this method involves the use of bulky anions and cations in solvents such as toluene, CH$_2$Cl$_2$, or CHCl$_3$. For example [29]:

$$ZnCl_2 + 2NaBH_4 + [cat]BH_4 \rightarrow [cat][Zn(BH_4)_3] + 2NaCl \tag{5}$$

$$M[an] + [cat][Zn(BH_4)_3] \rightarrow M[Zn(BH_4)_3]\downarrow + [cat][an] \tag{6}$$
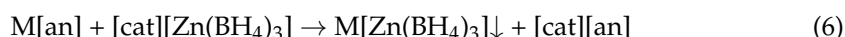
where [cat] = [Ph$_4$P]$^+$ or [nBu$_4$N]$^+$; [an] = [Al{OC-(CF$_3$)$_3$}$_4$]$^-$ or [B{3,5-(CF$_3$)$_2$C$_6$H$_3$}$_4$]$^-$, M = Li, Na, K.

5. Metathesis-addition [23]. As described in the next sections, there is a relationship between metal electronegativity and dehydrogenation temperature [30]. Thus, in principle, the production of bimetallic and trimetallic borohydrides opens the way to tune the thermodynamics of dehydrogenation. For this purpose, the metathesis-addition reaction can be a useful tool.

$$(x + ny)MBH_4 + yM'X_n \rightarrow M_xM'_y(BH_4)_{x+ny} + nyMX \tag{7}$$
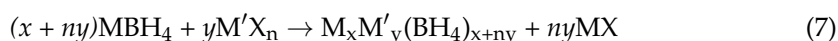
6. Synthesis using metal hydrides and S(CH$_3$)$_2$·BH$_3$. This type of synthesis has evolved mainly for rare-earth (RE) metal borohydrides (RE(BH$_4$)$_x$). The synthesis reaction is preceded by the formation or conditioning of the corresponding metal hydride by mechanical milling. The reaction itself is carried out for a long time (even days of stirring with moderate heating) in toluene. Co-solvents such as dimethyl sulfide (DMS) can be used [13,17,31]. This reaction can be described as a nucleophilic addition mechanism [17]. Finally, extraction of the solvating S(CH$_3$)$_2$ molecules is performed by careful drying [13,31].

$$REH_3 + 3S(CH_3)_2 \cdot BH_3 \rightarrow RE(BH_4)_3\,S(CH_3)_2 + 2S(CH_3)_2 \tag{8}$$
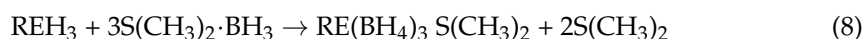
Special care must be taken during the drying process of borohydrides prepared in THF or ether. Some materials are simply delicate. In others, such as transition metals and RE-borohydrides, the solvent molecules cannot be removed without decomposing the borohydride. The use of low-coordination ability solvents [32] might be an option [24].

3. Bonding and Structure of Metal Borohydrides

The bonding and structure details of each borohydride are given, when available, in each element subsection. In this section, general trends are commented on only in

terms of tetrahydroborates complexes (only $[BH_4]^{-1}$ as ligands), monometallic (i.e., no bimetallic or trimetallic) compounds, and without bridging between two different metal centers. All these exceptions reflect the richness of the chemistry of metal borohydrides. A significant difference in comparison to the alkaline and alkaline earth borohydrides must be mentioned: for metals in Groups I and II, the bonding between $[BH_4]^{-1}$ and the metal ions is considered of an ionic nature [33]. This bonding type translates, as in any ionic compound, to highly stable materials, i.e., compounds with high dehydrogenation temperatures (Figure 1). In the transition metal borohydrides, the bonding spans from ionic to covalent coordination, which gives interesting properties of hapticity, H-mobility, H-exchange within the $[BH_4]^{-1}$ ligand or with other H-containing ligands, and reduced thermal stabilities in general (Figures 1 and 2) [34–36]. The interaction of the $[BH_4]^{-1}$ ion with the transition metals occurs through bridging H atoms; thus, the hapticity can be η^1, η^2, or η^3 (Figure 3). Due to the closeness of B atoms with the central metal in some η^3 compounds, even an η^4 interaction has been proposed [34]. The structures of the borohydride complexes around the metal center can have trigonal-planar, tetrahedral, square planar, trigonal-bipyramidal, or square-pyramidal octahedral geometry, especially if other ligands are present or if some H atoms of the $[BH_4]^{-1}$ are considered as a ligand. η^1-, η^2-, or η^3-$[BH_4]^{-1}$ ligands are considered as two-, four-, or six-electron donor ligands in the borohydride metal–ligand interactions; therefore, some compounds such as $M(\eta^3$-$BH_4)_4$ (M = Zr, Y or Hf) do not "follow" the 18-electron rule [37]. However, the 18-electron count is still obtained when symmetry restrictions account for orbital interactions [34]. The formation of compounds that exceed 18-electrons preferentially produces ionic complexes [37]. Another point to consider is the mean distance between the metal center and the B atoms: in general, for the three η^1, η^2, or η^3 interaction modes, metals on the right side of the periodic table show larger distances than those on the left [34]. Moreover, first-row transition metals form shorter distances than those of the third row [34]. The integration of ligands different from $[BH_4]^{-1}$ can reduce hapticity, and change the symmetry and the ionic or covalent bond nature. Manipulation of all these factors may prove useful in the hydrogen storage area.
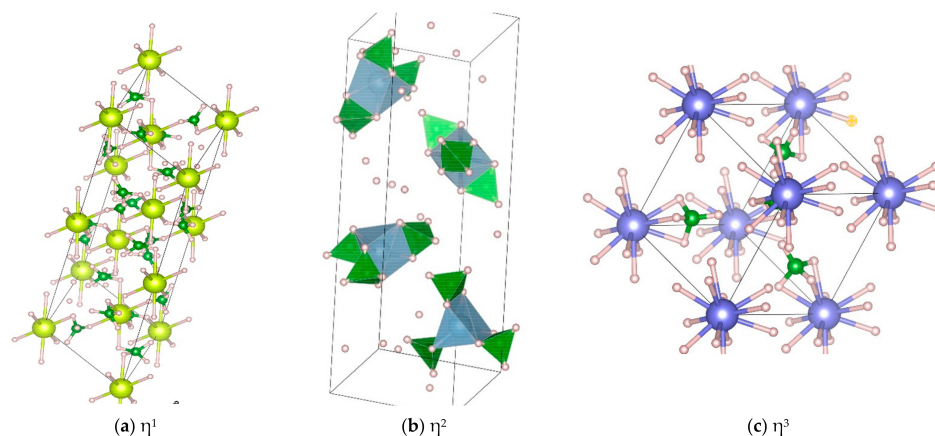
Figure 3. Examples of η^1, η^2, and η^3 bonding between metals and $[BH_4]^{-1}$ ions: (**a**) crystal structure of r-Ce(BH$_4$)$_3$; (**b**) crystal structure of α-Al(BH$_4$)$_3$; (**c**) crystal structure of Zr(BH$_4$)$_3$. Yellow balls—Ce, grey balls—Al, purple balls—Zr, green balls—B, and light pink balls—H.

Vibrational spectroscopy (infrared and Raman) is very useful for characterizing the structure of all borohydrides [38], i.e., for characterization of the coordination modes of borohydrides. Marks et al. resumed the observed bands in mononuclear borohydrides, as shown in Table 1 [21]:

Table 1. Infrared and Raman bands typically observed in covalent metal–borohydrides [21].

Coordination Modes of $[BH_4]^{-1}$	Frequency $[cm^{-1}]$ and Type of Vibration
η^1	2300–2450: B-H(terminal) stretching ~2000: B-H(bridge) stretching ~2000–1700: M-H(bridge) stretching 1000–1150: BH_3 deformation
η^2	2400–2600: B-H(terminal) stretching 1650–2150: B-H(bridge) stretching 1300–1500: Bridge stretching 1100–1200: BH_2 deformation
η^3	2450–2600: B-H(terminal) stretching 2100–2200: B-H(bridge) stretching 1200–1250: Bridge deformation data

An excellent source (downloadable library) of IR-spectra of many borohydrides is the work of D´Anna et al. [39].
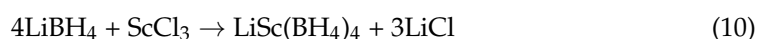
## 4. Transition Metal Borohydrides

4.1. Group 3: Scandium and Yttrium

In 2006, Nakamori et al. reported the formation of **Sc(BH₄)₃** in the solid-state by a metathesis reaction between $LiAlH_4$ and $ScCl_3$, activated by mechanical milling (5 h) [30]:

$$3LiBH_4 + ScCl_3 \rightarrow Sc(BH_4)_3 + 3LiCl \tag{9}$$
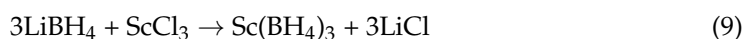
The calculated structural parameters of $Sc(BH_4)_3$ are collected in Table 2 [30]. In the report by Nakamori, the onset and peak dehydrogenation temperatures of the mixture $3LiBH_4 + ScCl_3$ were 450 K and 550 K (as read approximately from a thermal desorption profile plot) [30]. The equivalent of Equation (9) in THF produced the mono-solvated material [40]. Further experiments indicated that the scandium borohydride reported in [30] was most probably **LiSc(BH₄)₄**, because no confirmation of the $Sc(BH_4)_3$ was reported. Data published in 2008 demonstrated that a change in the molar ratio of reaction Equation (9) produced $LiSc(BH_4)_4$ (Table 2) instead of $Sc(BH_4)_3$ [41,42]:

$$4LiBH_4 + ScCl_3 \rightarrow LiSc(BH_4)_4 + 3LiCl \tag{10}$$

In $LiSc(BH_4)_4$, the scandium borohydride is, in fact, a complex ion: $[Sc(BH_4)_4]^{-1}$ (See Figure 4). The formation of complex borohydride ions is a characteristic shared with transition metal borohydrides, frequently facilitated by changes in the precursors' molar ratio.
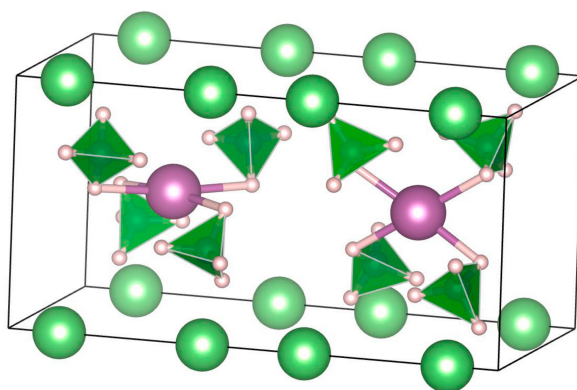
Figure 4. Crystal structure of $LiSc(BH_4)_4$, highlighting the $[Sc(BH_4)_4]^{-1}$ complex ion: $[BH_4]^{-1}$—green tetrahedra, Sc—pink ball, and Li—green ball. Detailed crystallographic information is available in Table 2.

Černý et al. found a significant mass loss (decomposition) of LiSc(BH$_4$)$_4$ in a range between 415 K and 535 K [43]. Employing DFT modeling, Kim et al. confirmed the stability of LiSc(BH$_4$)$_4$ at room temperature [44]. They proposed a complex multistep dehydrogenation reaction in which LiBH$_4$, LiB$_{12}$H$_{12}$, and ScH$_2$ would act as intermediaries, while LiH, ScB$_2$, and ScB$_{12}$ (in addition to H$_2$) would be the final products [44]. Kim et al. confirmed the formation of ScB$_2$ upon heating to 673 K and between 0.1 and 0.3 MPa hydrogen pressure [44]. Re-hydrogenation at 673 K and 7 MPa H$_2$ pressure increased the Li$_2$B$_{12}$H$_{12}$ content while forming a small amount of LiBH$_4$ [44]. No more recent reports were found describing the dehydrogenation/rehydrogenation reactions of LiSc(BH$_4$)$_4$.

NaSc(BH$_4$)$_4$ and **KSc(BH$_4$)$_4$** also have been produced, and their crystallographic properties characterized (Table 2). For the production of NaSc(BH$_4$)$_4$, Černý et al. tried different stoichiometric ratios between NaBH$_4$ and ScCl$_3$. Independently of the ratio, the synthetic reaction promoted by ball-milling was described as [43]:

$$4NaBH_4 + 2ScCl_3 \rightarrow NaSc(BH_4)_4 + Na_3ScCl_6 \tag{11}$$
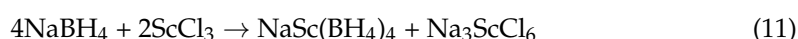
NaBH$_4$ might be regenerated during the first dehydrogenation step of NaSc(BH$_4$)$_4$ (440–490 K) [43]. Na$_3$ScCl$_6$ participates in further dehydrogenation reactions. In the second step (495–540 K), NaBH$_4$ (remanent from the synthesis and also formed during the first decomposition step) reacts with Na$_3$ScCl$_6$; a solid solution of Na(BH$_4$)$_{1-x}$Cl$_x$ is proposed to be formed. NaCl and ScB$_x$ are among the final dehydrogenation products [43].

Several theoretical studies [45–48] followed the experimental report of Černý et al. [43]. Kim proposed, based on first-principle calculations, that the decomposition reaction would be [47,48]:
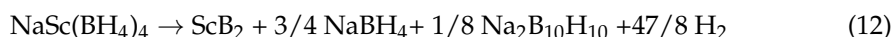
$$NaSc(BH_4)_4 \rightarrow ScB_2 + 3/4\ NaBH_4 + 1/8\ Na_2B_{10}H_{10} + 47/8\ H_2 \tag{12}$$

Table 2. Crystal structures of Sc-borohydrides.

| Material and Hydrogen Content [wt.%]	Structural Parameters [Å, °]	Atomic Positions	Reference and Comments
Sc(BH$_4$)$_3$, 13.51	Space group: trigonal *R-3* (148) a = b = 7.262; c = 18.194 α = β = 90; γ = 120	**Sc:** 0, 0, 0.3210. **B:** 0.3503, 0.3123, 0.4079. **H1:** 0.4002, 0.3671, 0.3423. **H2:** 0.3691, 0.4611, 0.4432. **H3:** 0.1636, 0.1647, 0.4130. **H4:** 0.4588, 0.2370, 0.4329	Theoretical calculation [30]
	Space group: orthorhombic *C222$_1$* (20) a = 8.34, b = 11.94; c = 7.90 α = β = γ = 90	**Sc:** 0.1882, 0, 0. **B1:** 0.3254, 0.1593, 0.9642. **B2:** 0.5, 0.4978, 0.25. **H1:** 0.4045, 0.2411, 0.9457. **H2:** 0.3191, 0.0983, 0.8355. **H3:** 0.3770, 0.0950, 0.0770. **H4:** 0.1854, 0.1775, 0.0036. **H5:** 0.1167, 0.0597, 0.2407. **H6:** 0.5192, 0.4369, 0.3732	Theoretical calculation [44]
LiSc(BH$_4$)$_4$ 14.49	Space group: tetragonal *P-42c* (112) a = b = 6.0759(1); c = 12.0338(1) α = β = γ = 90	**Li:** 0, 0, 0.104(2). **Sc:** 0.5, 0.5, 0.25. **B:** 0.75, 0.6722(6), 0.6386(3). **H1:** 0.7939, 0.6688, 0.7251. **H2:** 0.8960, 0.6926, 0.5891. **H3:** 0.6394, 0.8072, 0.6234. **H4:** 0.6705, 0.5201, 0.6166	Refinement of high-resolution synchrotron powder diffraction and comparison to DFT calculations [42]
	Space group: tetragonal *I-4* (82) a = b = 6.479; c = 12.043 α = β = γ = 90	**Li:** 0, 0.5, 0.25. **Sc:** 0, 0, 0.5. **B:** 0.3534, 0.2469, 0.8889. **H1:** 0.7621, 0.6206, 0.3339. **H2:** 0.5416, 0.2551, 0.8711. **H3:** 0.2852, 0.4221, 0.8705. **H4:** 0.3325, 0.2111, 0.9890	Theoretical calculation [44]
NaSc(BH$_4$)$_4$ 12.67	Space group: orthorhombic *Cmcm* (63) a = 8.170(2), b = 11.875(3), c = 9.018(2). α = β = γ = 90	**Na:** 0, 0, 0.5. **Sc:** 0.5, 0.1462(7), 0.75. **B1:** 0.5, 0.255(1), 0.957(2). **H11:** 0.5, 0.163(1), 0.989(2). **H12:** 0.5, 0.163(1), 0.989(2). **H13:** 0.613(2), 0.274(1), 0.889(2). **B2:** 0.724(2), 0.036(1), 0.75 **H21:** 0.837(2), −0.020(1), 0.75. **H22:** 0.762(2), 0.127(1), 0.75. **H23:** 0.649(2), 0.017(1), 0.852(2)	Experimental synchrotron powder diffraction [43]
	Space group: orthorhombic *C222$_1$* (20) a = 8.318, b = 11.827, c = 9.117 α = β = γ = 90	**Na:** 0.07322, 0, 0. **Sc:** 0, 0.34577, 0.25. **B1:** −0.49941, 0.26614, −0.4569. **B2:** 0.27125, 0.04152, −0.25031. **H1:** −0:49327, 0.32151, 0.43233. **H2:** 0.39351, 0.29602, −0.37049. **H3:** 0:12897, 0.23042, 0.38793. **H4:** −0.35012, 0.48568, −0.25753. **H5:** 0.24323, 0.14288, −0.27103. **H6:** 0.3702, 0.01058, −0.34298. **H7:** 0.16075, 0.46621, 0.3703. **H8:** 0.47365, 0.16592, −0.4863	Theoretical calculation [45]

Table 2. *Cont.*

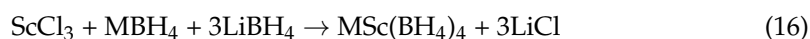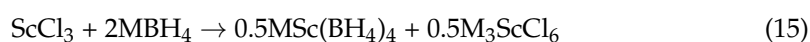| Material and Hydrogen Content [wt.%]	Structural Parameters [Å, °]	Atomic Positions	Reference and Comments
KSc(BH$_4$)$_4$ 11.24	Space group: orthorhombic *Pnma* (62) a = 11.8558(47), b = 7.7998(34); c = 10.1258(63) $\alpha = \beta = \gamma = 90$	**K:** 0.1947(16), 0.25, 0.6527(17). **Sc:** 0.0640(16), 0.25, 0.2152(15). **B1:** 0.1647(32), 0.25, 0.0150(23). **H11:** 0.2342(48), 0.25, 0.0939(74). **H12:** 0.2050(75), 0.25, −0.0881(39). **H13:** 0.1097(33), 0.37018(21), 0.0271(41). **B2:** 0.3819(21), 0.25, 0.3840(45). **H21:** 0.3790(37), 0.25, 0.2706(45). **H22:** 0.2917(28), 0.25, 0.4251(69). **H23:** 0.4286(26), 0.37018(21), 0.4201(43). **B3:** 0.0901(15), 0.0137(21), 0.3431(18). **H31:** 0.080(13), −0.1071(38), 0.4069(53). **H32:** 0.058(12), −0.0137(51), 0.2383(28). **H33:** 0.183(10), 0.052(18), 0.339(10). **H34:** 0.0386(90), 0.124(22), 0.3886(94)	Experimental data [49]
RbSc(BH$_4$)$_4$ 8.50	Space group: orthorhombic *Pbcm* (57) a = 7.6514, b = 11.1821, c = 11.2443 $\alpha = \beta = \gamma = 90$	**B1:** 0.23519, 0.02670, −0.58184. **H11:** 0.36413, 0.04382, −0.64732. **H12:** 0.27076, −0.02575, −0.49111. **H13:** 0.17172, 0.12656, −0.55910. **H14:** 0.12514, −0.02621, −0.64381. **H21:** 0.94449, 0.21868, −0.83832. **H32:** 0.22785, 0.29877, −0.66164. **Rb1:** 0.55522, 0.25, −0.5. **Sc1:** 0.16021, 0.13182, −0.75. **B2:** 0.86828, 0.17635, −0.75. **H22:** 0.71314, 0.19760, −0.75. **H23:** 0.89853, 0.06708, −0.75. **B3:** 0.32462, 0.30552, −0.75. **H31:** 0.41624, 0.21334, −0.75. **H33:** 0.41306, 0.39492, −0.75	Computationally optimized [50]
CsSc(BH$_4$)$_4$ 6.80	Space group: monoclinic *P2$_1$/c* 14 a = 9.5870, b = 10.7270, c = 12.2280 $\alpha = 90$, $\beta = 126.3510$, $\gamma = 90$	**Cs22:** 0.82694, 0.3427, 0.75062. **B1:** 0.21177, 0.01695, 0.27563. **H2:** 0.23203, 0.12082, 0.32887. **H3:** 0.15239, −0.05817, 0.31159. **H4:** 0.11686, 0.03374, 0.15052. **H5:** 0.3566, −0.01335, 0.30707. **B6:** 0.59468, 0.22457, 0.38529. **H7:** 0.53578, 0.28562, 0.27965. **H8:** 0.74057, 0.25675, 0.47509. **H9:** 0.48976, 0.23768, 0.41267. **H10:** 0.58853, 0.11248, 0.35595. **B11:** 0.13689, 0.33158, 0.1196. **H12:** 0.20824, 0.31906, 0.24318. **H13:** 0.03689, 0.41819, 0.07083. **H14:** 0.25418, 0.34173, 0.10504. **H15:** 0.06144, 0.23137, 0.06534. **B16:** 0.33930, 0.08443, 0.04155. **H17:** 0.39476, 0.19319, 0.07405. **H18:** 0.35291, 0.04517, −0.04403. **H19:** 0.42198, 0.02115, 0.14752. **H20:** 0.18734, 0.08764, 0.00469. **Sc21:** 0.32111, 0.1628, 0.20685	Computationally optimized [50]

Alternative structures and dehydrogenation reactions of (12) have been reported; for example, H. D. Tran et al. reported that NaSc(BH$_4$)$_4$ with an orthorhombic *C222$_1$* structure [45] would be more stable than the orthorhombic *Cmcm* structure reported by Černý et al. (Table 2) [43]. The formation enthalpy of orthorhombic *Cmcm* NaSc(BH$_4$)$_4$ was independently calculated as −72.69 kJ/mol H$_2$ [46]. The theoretical calculations for NaSc(BH$_4$)$_4$ indicated an electrical insulator with a band gap of 5.055 eV [48].

KSc(BH$_4$)$_4$ was reported in 2010; this material presents similarities with NaSc(BH$_4$)$_4$ but not with LiSc(BH$_4$)$_4$ [49]. The synthesis reaction promoted by ball-milling was:

$$4KBH_4 + 2ScCl_3 \rightarrow KSc(BH_4)_4 + K_3ScCl_6 \tag{13}$$
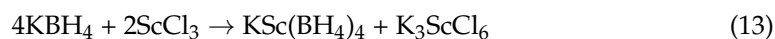
Several stoichiometric ratios between KBH$_4$ and SCl$_3$ were tested; the best ratio was 2:1 [49]. KSc(BH$_4$)$_4$ melts at ~405 K. The decomposition of KSc(BH$_4$)$_4$ at 460–500 K increases the amount of KBH$_4$ (additional to that not reacted during synthesis) [49]. The second step at 510–590 K would involve the reaction of KBH$_4$ with K$_3$ScCl$_6$, forming K(BH$_4$)$_{1-x}$Cl$_x$. The crystal structure was determined and is reported in Table 2 [49]. No further experimental reports were found on KSc(BH$_4$)$_4$.

RbSc(BH$_4$)$_4$ and **CsSc(BH$_4$)$_4$** were recently reported [50]. Both materials were produced by mechanical milling and solvent metathesis; thus, a direct comparison of the effects of the co-metathesis product was made. The synthesis reactions are [50]:

$$ScCl_3 + 3MBH_4 \rightarrow 0.5MSc(BH_4)_4 + MBH_4 + 0.5M_3ScCl_6 \tag{14}$$

$$ScCl_3 + 2MBH_4 \rightarrow 0.5MSc(BH_4)_4 + 0.5M_3ScCl_6 \tag{15}$$

$$ScCl_3 + MBH_4 + 3LiBH_4 \rightarrow MSc(BH_4)_4 + 3LiCl \tag{16}$$

where M = Rb, Cs. Pure borohydrides were extracted with dimethyl sulfide (DMS). $RbSc(BH_4)_4$ presents an orthorhombic *Pbcm* space group, while $CsSc(BH_4)_4$ is monoclinic $P2_1/c$ (Table 2) [50]. Starobrat et al. reported that, in $RbSc(BH_4)_4$, the Rb^+ and $[Sc(BH_4)_4]^{-1}$ ions create zig-zag lines of alternate ions along the c-axis [50]. Meanwhile, in $CsSc(BH_4)_4$, Cs^+ and $[Sc(BH_4)_4]^{-1}$ have three counterions as nearest neighbors [50]. Decomposition of pure and LiCl-mixed $RbSc(BH_4)_4$ is preceded by an endothermic event at 432 K, associated with a melting or phase transition. The main decomposition step was located at 510 K and was described as mainly endothermic but with an exothermic shoulder [50].

Decomposition of pure $RbSc(BH_4)_4$ was described as [50]:

$$RbSc(BH_4)_4 \rightarrow RbBH_4 + 6H_2 + B + ScB_2 \tag{17}$$
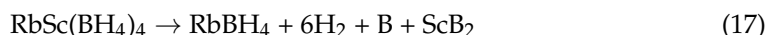
However, a minor reaction associated with the diborane evolution was described as:

$$RbSc(BH_4)_4 \rightarrow RbBH_4 + 9/2H_2 + 1/2\ B_2H_6 + ScB_2 \tag{18}$$
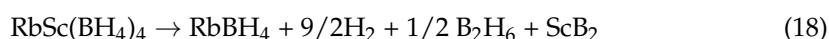
In the sample containing LiCl, a third endothermic event at 559 K was reported. Finally, $RbBH_4$ decomposed above 773 K [50].

$CsSc(BH_4)_4$ decomposition presents a melting or phase transition event at 480 K, a hydrogen release at 511 K, with minor B_2H_6 production (equations analogous to (17) and (18)), and probable formation of a ternary chloride at 532 K [50]:

$$CsSc(BH_4)_4 + 3LiCl \rightarrow CsLi_2Cl_3 + 15/2\ H_2 + ScB_x + (4-x)B + LiH \tag{19}$$
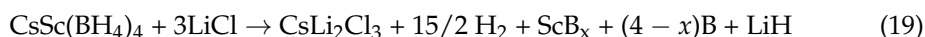
$CsBH_4$ decomposition into Cs, B, and H_2 was observed at 695 K [50].

The first reports on yttrium borohydrides date to the 1960s. Back then, the compound was obtained as a THF abduct: $Y(BH_4)_3(THF)_3$ [51,52] (and references therein). The usual reactants were YCl_3 and $LiBH_4$ in THF, but the reaction between $Y(OCH_3)_3$ with B_2H_6 in THF was also reported [51]. Later, in 2008, the metathesis synthesis of $Y(BH_4)_3$ was performed; it was assisted by ball-milling [53]:

$$YCl_3 + 3LiBH_4 \rightarrow Y(BH_4)_3 + 3LiCl \tag{20}$$

Alternatively, to avoid the formation of LiCl, **$Y(BH_4)_3$** can be produced by a gas–solid reaction promoted by mechanical milling [54,55]:

$$YH_3 + 3/2\ B_2H_6 \rightarrow Y(BH_4)_3 \tag{21}$$

$Y(BH_4)_3$ crystallizes in a cubic structure, *Pa−3 (205)* (low-temperature α-phase, Table 3); theoretical calculations give a formation enthalpy of -113 kJ/mol BH_4 and predict $Y(BH_4)_3$ to be an insulator [53]. $Y(BH_4)_3$ (+3LiCl) has a solid (α to β) phase transition, the transition temperature was reported as 483 K [56] or 453 K [54,57]. In the high-temperature polymorph, the structure is cubic *Fm-3c (226)*; the $[BH_4]^{-1}$ ion is distorted from an ideal tetrahedron [58] and it can be considered an η^2 type interaction with Y^{+3}. However, Park et al. [55] and Remhof et al. [54] did not observe the α to β phase transition in $Y(BH_4)_3$ (from reaction (21)), i.e., without LiCl.

Dehydrogenation reactions have been described in several papers. In these published results stands out the multistep nature of the dehydrogenation reaction and some differences between the dehydrogenation pathway of pure $Y(BH_4)_3$ and $Y(BH_4)_3$ + 3LiCl (i.e., upon the synthesis method and purification). The decomposition of $Y(BH_4)_3$ + 3LiCl proposed by Jaroń et al. starts at 423–433 K with a small mass release (explained in that work as a probable melting phase transition), a second step at 533–678 K, and the last stage of dehydrogenation that starts above 698 K [56]. By its part, the dehydrogenation mechanism proposed by Ranvsbæk et al. first involved the $Y(BH_4)_3$ solid α to β phase transition, followed by the β-$Y(BH_4)_3$ decomposition, starting at 463 K and forming YH_3, which then produced YH_2 at 543 K [57]. The dehydrogenation mechanism also involved the evolution

of an unidentified compound between 488 and 553 K and YB_4 as a final decomposition product [57]. The occurrence of an unidentified peak during synchrotron radiation powder X-ray diffraction (SR-PXD) characterization was also observed by Frommen et al. between 473 and 520 K for a mixture of $Y(BH_4)_3$ + 3LiCl prepared by cryogenic ball milling [58]. Yan et al. proposed $Y(B_3H_8)_3$ as the dehydrogenation intermediary's possible identity [59].

Remhof et al. [54] and Park et al. [55] observed different decomposition pathways of $Y(BH_4)_3$ without LiCl. $Y(BH_4)_3$ (from Equation (21)) started decomposing at 460 K, with a maximum rate at 523 K. No indications of solid α to β phase transformation were found, but positive indications of melting right before decomposition were revealed by time-resolved in-situ XRD [54]. Park et al. proposed that LiCl slightly shifts the peak-temperature decomposition of $Y(BH_4)_3$ and promotes the formation of YB_4 [55]. The decomposition products reported by Park et al. were YH_2, YB_4, Y, and Y_2O_3.

The decomposition pathway observed by Yan et al. in pure $Y(BH_4)_3$ (obtained by reaction (21) in ether, followed by precipitation and drying) comprises (a) phase transition, (b) melting, (c) decomposition of $Y(BH_4)_3$ into YH_3, (d) decomposition of an intermediate phase, and (e) decomposition of YH_3 into YH_2 [60]. This pathway is more similar to the $Y(BH_4)_3$ + 3LiCl dehydrogenation studies reviewed above.

Lee et al., utilizing theoretical calculations, proposed a series of dehydrogenation reactions, where the products are a combination of YH_3, YH_2, YB_4, YB_6, B, Y, and H_2 [61]. Given the experimental reaction products commented above, a possible first-step dehydrogenation reaction could be:

$$\beta\text{-}Y(BH_4)_3 \rightarrow \frac{1}{4}\,YH_3 + \frac{3}{4}\,YB_4 + 45/8\,H_2 \tag{22}$$
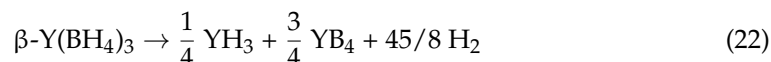
The calculated dehydrogenation temperature of (22) at P_{H2} = 0.1 MPa is ~195 K, ΔH^0 = 22.5 kJ/mol H_2 [61].

Another point to mention is the release of B-H compounds. The results are not unanimous; some reports indicate no release while others indicate the evolution of boron hydrides. On the other hand, the reported formation of YB_4 [55] is good in terms of a possible rehydrogenation. Partial rehydrogenation was achieved at 35 MPa at 523 K and 573 K [60].

LiY(BH$_4$)$_4$ and **NaY(BH$_4$)$_4$** were obtained by ball-milling of Li, Na, and Y-borohydrides, heating at 473 K and 453 K for the $LiY(BH_4)_4$ and $NaY(BH_4)_4$, respectively, and then quenching [62]. Another option is the use of weakly coordinating anions in weakly coordinating solvents such as CH_2Cl_2, i.e., equivalent to reactions (5) and (6) [63]. $LiY(BH_4)_4$ and $NaY(BH_4)_4$ are isostructural with the tetragonal *P-42c* $LiSc(BH_4)_4$, and orthorhombic *C222$_1$* $NaSc(BH_4)_4$ (Table 3) [62]. Their values of ionic conductivities are 1.26×10^{-6} and 6.92×10^{-7} S cm^{-1} at room temperature, $LiY(BH_4)_4$ and $NaY(BH_4)_4$, respectively [62]. Dai et al., employing first-principles calculations, indicated that the formation of $KY(BH_4)_4$ is thermodynamically feasible; meanwhile, the formation of analogous materials with Li and Na is not possible [64]. $LiY(BH_4)_4$ and $NaY(BH_4)_4$ are, in fact, metastable materials that decompose during days or weeks at room temperature or upon heating to 402 K or 388 K, respectively [62].

KY(BH$_4$)$_4$ was produced by the reaction between $Y(BH_4)_3$ (produced by reaction (20)) in a previous step, without elimination of LiCl) and KBH_4 [65]:

$$Y(BH_4)_3 + KBH_4 \rightarrow KY(BH_4)_4 \tag{23}$$
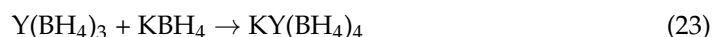
Reaction (23) was promoted by mechanical milling under a careful regime of alternating periods of 3 min milling/2–3 min resting. $KY(BH_4)_4$ is isostructural with $NaY(BH_4)_4$ (Table 3), and forms a complex anion $[Y(BH_4)_4]^{-1}$ of a slightly distorted tetrahedral geometry [65]. Furthermore, $[BH_4]^{-1}$ ions have η^3 interactions with Y [65]. The dehydrogenation of $KY(BH_4)_4$ is also a multistep process: (a) the first step is melting at 453 K; (b) from 463–483 K, an unidentified phase is detected; (c) the presence of KBH_4 is confirmed and increases upon heating at higher temperatures (493 K); (d) a probable decomposition of

YH$_3$ into YH$_2$ occurs at 543 K; and (e) two more TGA/DCS peaks are detected at 611 K and 632 K [65].

The mixture of NaBH$_4$ and Y(BH$_4$)$_3$ (with LiCl) produced NaY(BH$_4$)$_2$Cl$_2$ upon heating at 438 K [65]. One year later, in 2012, a detailed study of NaY(BH$_4$)$_2$Cl$_2$ was published [66]. The synthesis reaction promoted by mechanical milling is [66]:

$$2NaBH_4 + YCl_3 \rightarrow NaY(BH_4)_2Cl_2 + NaCl \tag{24}$$
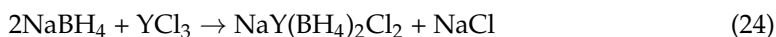
However, side reactions produced Na$_2$YCl$_6$ and Na(BH$_4$)$_{1-x}$Cl. NaY(BH$_4$)$_2$Cl$_2$ crystallizes in the monoclinic *P2/c* space group symmetry. DFT optimization of the geometry indicates that the [BH$_4$]$^{-1}$ ions interacted via η^3 with Y and η^1 with Na. NaY(BH$_4$)$_2$Cl$_2$ decomposed at ~573 K without a significant release of borane gases [66].

Binary Y-borohydrides **RbY(BH$_4$)$_4$**, **CsY(BH$_4$)$_4$**, **Rb$_3$Y(BH$_4$)$_6$**, and **Cs$_3$Y(BH$_4$)$_6$**, and the ternary materials **Rb$_2$LiY(BH$_4$)$_6$** and **Cs$_2$LiY(BH$_4$)$_6$**, were reported recently (Table 3) [67–69]. RbY(BH$_4$)$_4$ and CsY(BH$_4$)$_4$ were produced by mechanical milling of Y(BH$_4$)$_3$ and the corresponding Rb or Cs-borohydride [67]. However, the Y(BH$_4$)$_3$ was not purified and contained LiCl. Thus, the ball-milled powders were a mixture of the bimetallic borohydrides, Cl-substituted borohydrides (in Cs materials), and LiCl. Diffraction analysis resulted in a monoclinic *P2$_1$/c* RbY(BH$_4$)$_4$, but the Y-Rb sublattice can be symmetrized to orthorhombic *Pnma*. The CsY(BH$_4$)$_4$ structure was refined as a *I4$_1$/a* space group [67]. Decompositions of RbY(BH$_4$)$_4$ and CsY(BH$_4$)$_4$ were multistep processes that involved the formation of Cl-substituted bimetallic borohydrides: Rb$_2$Li[Y(BH$_4$)$_{6-x}$Cl$_x$] and Cs$_2$Li[Y(BH$_4$)$_{6-x}$Cl$_x$], i.e., the LiCl was not inert. The quickest decomposition step of RbY(BH$_4$)$_4$/LiCl occurred at 544 K, and above 523 K for CsY(BH$_4$)$_4$/LiCl [67].

Table 3. Crystal structures of Y-borohydrides.

Material and Hydrogen Content [wt.%]	Structural Parameters [Å, °]	Atomic Positions	Reference and Comments
α-Y(BH$_4$)$_3$ 9.06	Space group: cubic *Pa-3* (205) a = b = c = 10.894 α = β = γ = 90	**Y:** 0.2165, 0.2165, 0.2165. **B:** 0.1920, 0.2475, 0.9671. **H1:** 0.2900, 0.2540, 0.0241. **H2:** 0.1030, 0.2245, 0.0340. **H3:** 0.1737, 0.3481, 0.9181. **H4:** 0.2018, 0.1626, 0.8923	Theoretical calculation (predicted DFT) [53]. Isostructural to Gd(BH$_4$)$_3$ and Dy(BH$_4$)$_3$
	Space group: cubic *Pa-3* (205) a = b = c= 10.8522(7) α = β = γ = 90	**Y:** 0.2187(5), 0.2187(5), 0.2187(5). **B:** 0.1908(5), 0.2455(8), 0.9659(6). **D1:** 0.2849(6), 0.2525(8), 0.0272(7). **D2:** 0.1024(7), 0.2215(8), 0.0334(6). **D3:** 0.1781(7), 0.3450(7), 0.9189(7). **D4:** 0.1920(7), 0.1626(7), 0.8961(7)	Experimental [58]
β-Y(BH$_4$)$_3$ 9.06	Space group: cubic *Fm-3c* (226) a = b = c = 11.0086(1) α = β = γ = 90	**Y:** 0, 0, 0. **B:** 0, 0, 0.25. **D1:** 0, 0.4075(1), 0.3104(1)	Experimental, heat treatment in D at 10MPa and 475 K [58]
LiY(BH$_4$)$_4$ 10.39	Space group: tetragonal *P-42c* (112) a = b = 6.2360(9); c = 12.491(3) α = β = γ = 90	**B:** 0.7453, 0.7453, 0.6535. **H1:** 0.7642, 0.7596, 0.7527. **H2:** 0.8643, 0.8647, 0.6063. **H3:** 0.5562, 0.7854, 0.6331. **H4:** 0.7818, 0.5566, 0.6307. **Li:** 0, 0, 0.25. **Y:** 0.5, 0.5, 0.25.	[62]
NaY(BH$_4$)$_4$ 9.42	Space group: orthorhombic *C222$_1$* (20) a = 8.5263(4), b = 12.1357(5), c = 9.0535(4) α = β = γ = 90_	**B1:** 0.4983, 0.2701, −0.0300. **B2:** 0.7375, 0.0357, 0.7498. **H11:** 0.5007, 0.3256, 0.0800. **H12:** 0.4682, 0.1735, 0.0018. **H13:** 0.6262, 0.2717, −0.0945. **H14:** 0.6025, 0.3000, 0.6200. **H21:** 0.3559, 0.4813, 0.7445. **H22:** 0.7652, 0.1337, 0.7245. **H23:** 0.6732, 0.0308, 0.8723. **H24:** 0.6408, 0.0026, 0.6589. **Na1:** −0.0604, 0, 0. **Y1:** 0, 0.3478, 0.25.	[62]
m-KY(BH$_4$)$_4$ 8.61	Space group: monoclinic *C2/c* (15) a = 14.8947(18), b = 7.8012(10), c = 8.1130(10) α = γ = 90.00, β = 110.167(2)	**Y:** 0.5, 0.7966(5), 0.25. **K:** 0.25, 0.25, 0. **B1:** 0.1338(13), 0.881(2), 0.767(2). **H11:** 0.078(10), 0.90(5), 0.625(7). **H21:** 0.104(16), 0.94(4), 0.872(10). **H31:** 0.21(2), 0.95(7), 0.78(2). **H41:** 0.15(4), 0.733(13), 0.79(2). **B2:** 0.0792(11), 0.5812(18), 0.108(3). **H12:** 0.146(5), 0.58(4), 0.238(9). **H22:** 0.102(10), 0.62(3), −0.011(10). **H32:** 0.02(2), 0.68(4), 0.123(18). **H42:** 0.05(3), 0.44(2), 0.082(15)	460 K [68]

<div align="center">**Table 3.** *Cont.*</div>

| Material and Hydrogen Content [wt.%]	Structural Parameters [Å, °]	Atomic Positions	Reference and Comments
o-KY(BH₄)₄ 8.61	Space group: orthorhombic *Cmcm* (63) a = 8.59314(10), b = 12.59917(15), c = 9.78460(12) $\alpha = \beta = \gamma = 90$	**K:** 0, 0, 0.5. **Y:** 0.5, 0.13211(7), 0.75. **B1:** 0.5, 0.2416(4), 0.9513(6). **H11:** 0.6074(10), 0.2595(4), 0.8887(8). **H13:** 0.5, 0.2924(6), 1.0464(11). **H14:** 0.5, 0.1550(9), 0.9813(6). **B2:** 0.7244(5), 0.0127(4), 0.75. **H21:** 0.8318(11), −0.0390(6), 0.75. **H22:** 0.7602(6), 0.0990(9), 0.75. **H23:** 0 0.6529(9), −0.0045(4), 0.8443(9)	420 K [68]
o-RbY(BH₄)₄ 6.90	Space group: orthorhombic *Pnma* (62) a = 12.3406(3), b = 8.2482(2), c = 10.5934(3) $\alpha = \beta = \gamma = 90$	**Rb:** 0.1816(3), 0.25, 0.6609(5). **Y:** 0.0415(3), 0.25, 0.1771(6). **B1:** 0.056(3), 0.027(3), 0.315(3). **H11:** 0.06(4), −0.084(12), 0.386(10). **H12:** 0.06(3), −0.022(14), 0.211(7). **H13:** 0.13(4), 0.11(7), 0.330(14). **H14:** −0.02(3), 0.10(8), 0.336(13). **B2:** 0.212(3), 0.25, 0.070(4). **H21:** 0.214(19), 0.25, 0.181(7). **H22:** 0.167(7), 0.367(6), 0.033(11). **H23:** 0.302(9), 0.25, 0.03(2). **B3:** 0.389(4), 0.25, 0.454(4). **H31:** 0.364(14), 0.25, 0.346(8). **H32:** 0.440(5), 0.367(6), 0.476(10). **H33:** 0.310(10), 0.25, 0.517(15)	400 K [68]
c-Rb₃Y(BH₄)₆ 5.57	Space group: cubic *Fm-3* (202) a = b = c = 11.5998(3) $\alpha = \beta = \gamma = 90$	**Rb:** 0.31, 0.25, 0.25. **Y1a (Y):** 0.04, 0, 0. **Y1b (Rb):** 0.04, 0, 0. **Y2a (Rb):** 0.5, 0.5, 0.5. **Y2b (Y):** 0.5, 0.5, 0.5. **B:** 0.5, −4.930381e−032, 0.269(6) **H:** 0.580(18), 0.00000017(4), 0.325(14)**H:** 0.5, −0.080(18), 0.212(14)	490 K, cubic [68]
Cs₃Y(BH₄)₆ 4.19	Space group: cubic *Fm-3* (202) a = b = c = 12.2541(2) $\alpha = \beta = \gamma = 90$	**Cs:** 0.31, 0.25, 0.25. **Y1a (Y):** 0.029(8), 0, 0. **Y1b (Cs):** 0.029(8), 0, 0. **Y2a (Cs):** 0.452(3), 0.5, 0.5. **Y2b (Y):** 0.452(3), 0.5, 0.5. **B:** 0.5, 0, 0.254(11). **H:** 0.575(14) 0.00000016(3) 0.308(15). **H:** 0.5, −0.075(14), 0.201(15)	553 K [68]
Rb₂LiY(BH₄)₆ 6.80	Space group: cubic *Fm-3* (202) a = b = c = 11.44541(7) $\alpha = \beta = \gamma = 90$	**Rb:** 0.25, 0.25, 0.25. **Y1a (Y):** 0, 0, 0. **Y1b (Li):** 0, 0, 0. **Li2a (Li):** 0.5, 0.5, 0.5. **Li2b (Y):** 0.5, 0.5, 0.5. **B:** 0.5, 0, 0.2605(7). **H:** 0.584(3), 0.000000176(7), 0.320(2). **H:** 0.5, −0.084(3), 0.201(2)	415 K [68]
Cs₂LiY(BH₄)₆ 5.37	Space group: cubic *Fm-3* (202) a = b = c = 11.25215(19) $\alpha = \beta = \gamma = 90$	**Cs:** 0.25, 0.25, 0.25. **Y:** 0, 0, 0. **Li:** 0.5, 0.5, 0.5. **B:** 0.5, 0, 0.2508(2). **H:** 0.5824(5), 0.0000001720(11), 0.3091(4). **H:** 0.5, −0.0824(5), 0.1925(4), 0.5	Room temperature [68]

4.2. Group 4: Titanium, Zirconium, and Hafnium

Ti(BH₄)₃ is an unstable, volatile material that decomposes spontaneously at room temperature [70,71]. The first attempt to produce it involved the reaction between a bed of LiBH₄ (in excess) and vapors of TiCl₄, and it was performed by Hoekstra and Katz in 1949 [72]. Since then, it has been observed that Ti^{+4} reduced to Ti^{+3}, and, thus, the impracticability of a tetra-borohydride of titanium has been apparent [72]:

$$2TiCl_4 + 8LiBH_4 \rightarrow 2Ti(BH_4)_3 + 8LiCl + B_2H_6 + H_2 \tag{25}$$

The reaction in organic solvents (tetrahydrofuran or ether) between LiBH₄ and TiCl₄ ended in the formation of adducts such as Ti(BH₄)₃·2THF or Ti(BH₄)₃·2O(C₂H₅)₂ [73]. In fact, several phosphines of titanium borohydrides (similarly produced to the latter compounds) are stable materials that can be used as a catalyst for polymerization and hydrogenation of olefins [21,74]. The only report on the synthesis of Ti(BH₄)₃ in the solid-state was published by Fang et al. in 2009 [75]. They proposed the in-situ formation of Ti(BH₄)₃ after ball-milling of 3LiBH₄ and TiF₃ and further heating up to 403 K. Fang et al. also recommend not using TiCl₃, as the result is the decomposition of LiBH₄ in the milling process [75]. The tested materials released over 5 wt% of hydrogen at about 343–363 K. In the same work, the identification of Ti(BH₄)₃ was achieved by in-situ infrared spectroscopy during heating. During these in-situ measurements, the emergence of IR bands around 1500–1600 and 2500 cm⁻¹ at about 353 K, and further depleting at roughly 363 K, were

critical to detect the formation of $Ti(BH_4)_3$. Further decomposition of $Ti(BH_4)_3$ led to B, TiH_2, and H_2; the proposed complete reaction is: [75]

$$3LiBH_4 + TiF_3 \rightarrow Ti(BH_4)_3 + 3LiF \rightarrow 3B + TiH_2 + 5H_2 + 3LiF \qquad (26)$$
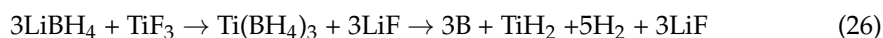
Later in 2014, Callini et al. reported the formation of $Ti(BH_4)_3$ by milling or mixing (few details were reported) an excess of $LiBH_4$ and $TiCl_3$ [35]. In that work, the formation of $Ti(BH_4)_3$ occurred on the surface of the mixtures; then, the compound was expelled to the gas phase. The decomposition of $Ti(BH_4)_3$ started at room temperature, and essentially ended at 333 K. The decomposition was observed as follows [35]:

$$Ti(BH_4)_3 \rightarrow B_2H_6 + TiH_2 + B + 2H_2 \qquad (27)$$
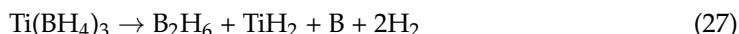
Interestingly, the stabilization of $Ti(BH_4)_3$ was achieved recently by its confinement in a Zr-based MOF ($Zr_6O_4(DBC)_6$, DBC =1,4-benzenedicarboxylate)) [76]. In such a condition, $Ti(BH_4)_3$ is reported to decompose through an intermediary stage at 350–430 K without diborane release. Instead, pentaborane (B_5H_9) is a dehydrogenation product that recombines at higher temperatures to produce higher boranes [76]. The stabilization was attributed to the occupation of few (1–2) molecules of $Ti(BH_4)_3$ in the Zr-based MOF pores of comparable size. This stabilization reduces the interaction between $Ti(BH_4)_3$ molecules in the gas phase and increases the interaction of $Ti(BH_4)_3$ with the Zr-MOF due to strong host–guest connections [76].

No experimental results on the solid-state molecular structure of $Ti(BH_4)_3$ have been reported; instead, its molecular structure in the gas phase was reported in 1991 [71] and confirmed by Ab-initio studies in 1993 [77]. The $Ti(BH_4)_3$ molecule poses a C_{3h} symmetry with a planar $Ti-B_3$ skeleton, and the $[BH_4]^{-1}$ ions are η^3 ligands [71] (Table 4). Dain et al. also suggested, based on vapor pressure measurements, the existence of a $Ti(BH_4)_3$ dimer having bridging and terminal borohydroborate groups [71]. However, no experimental confirmation has been reported.

Table 4. Molecular parameters of Ti-borohydride.

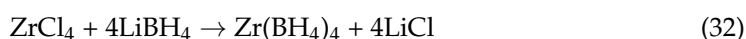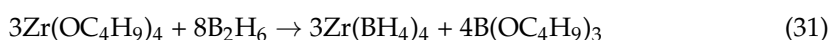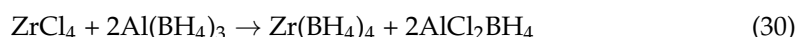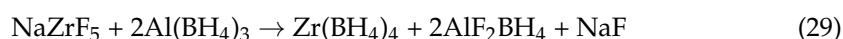| Material and Hydrogen Content [wt.%]	Symmetry	Atomic Positions [Å]	Comments
$Ti(BH_4)_3$ 13.09	*C3h*	**Ti:** 0, 0, 0. **B1:** 0.14648, 1.91483, −0.00744. **B2:** −1.61184, −0.84502, 0.00457. **B3:** 1.53773, −0.97338, 0.00253. **H1:** −1.10173, 1.64998, −0.00544. **H2:** 0.67735, 1.51811, 1.08297. **H3:** 0.67563, 1.50978, −1.09559. **H4:** −0.78907, −1.82032, 0.00764. **H5:** −1.61691, −0.23520, 1.12541. **H6:** −1.61875, −0.24383, −1.12091. **H7:** 1.97099, 0.22681, −0.00244. **H8:** 1.01724, −1.27698, 1.1273. **H9:** 1.01546, −1.28564, −1.11902. **H10:** 0.22774, 3.07799, −0.01194. **H11:** −2.65980, −1.35621, 0.00740. **H12:** 2.50443, −1.62533, 0.00429	Atomic positions were generated by symmetry arguments from selected bond distances reported in [71]

In a recent review on several materials for hydrogen storage (including metal hydrides, alloys, high entropy systems, borohydrides, etc.), $Rb_3Ti(BH_4)_5$ and $Cs_3Ti(BH_4)_5$ are enlisted [24] (and references within). The original sources are two theses which are rather

difficult to access. Both materials were prepared by mechanical milling (not many details are given in the review) [24]:

$$3MBH_4 + M'Cl_n + nLiBH_4 \rightarrow M_3M'(BH_4)_{3+n} + nLiCl, \tag{28}$$
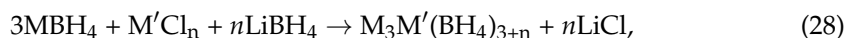
where M = Rb, Cs and M´ = Ti. $Rb_3Ti(BH_4)_5$ and $Cs_3Ti(BH_4)_5$ crystalize in tetragonal *I4/mcm* space group. The cell dimensions are a = 9.214(3) Å, and c = 16.130(5) Å in $Rb_3Ti(BH_4)_5$. For $Cs_3Ti(BH_4)_5$, the cell dimensions are a = 9.644(8) Å, and c = 16.426(15) Å [24].

Zr(BH₄)₄ was first reported in 1949 (reaction (29)) [72]. Later, $Zr(BH_4)_4$ was prepared by reactions (30), (31), and (32) in ether or THF [78]. However, the separation of the products proved difficult [79,80]. After that, the solid-state reaction (32) was implemented [81].

$$NaZrF_5 + 2Al(BH_4)_3 \rightarrow Zr(BH_4)_4 + 2AlF_2BH_4 + NaF \tag{29}$$

$$ZrCl_4 + 2Al(BH_4)_3 \rightarrow Zr(BH_4)_4 + 2AlCl_2BH_4 \tag{30}$$

$$3Zr(OC_4H_9)_4 + 8B_2H_6 \rightarrow 3Zr(BH_4)_4 + 4B(OC_4H_9)_3 \tag{31}$$

$$ZrCl_4 + 4LiBH_4 \rightarrow Zr(BH_4)_4 + 4LiCl \tag{32}$$

Recently, the preparation of $Zr(BH_4)_4$ by ball milling (Equation (32) and the homologous reaction with $NaBH_4$ [79]) and recovering by means of sublimation at low temperature (243 K) was reported [82–85]. $Zr(BH_4)_4$ is a volatile compound at room temperature, and its gas-phase structure is monomeric η^3, with a tetrahedral arrangement and a rotational barrier of the $[BH_4]^{-1}$ ions of 13.9 kJ/mol [79,81]. The sublimation heat is between 55.9 and 56.9 kJ/mol [86]. $Zr(BH_4)_4$ displays d-orbital covalency [87].

The crystal structure of $Zr(BH_4)_4$ was determined at 100 K as cubic space group *P-43m* (Table 5); in the solid-state, $[BH_4]^{-1}$ coordination to Zr is also η^3 (Figure 3) [83]. Crystals of $Zr(BH_4)_4$ melt at 302–305 K [72,79]. Igoshkin et al., employing molecular dynamics calculations, located a phase transition (solid to liquid or amorphous) at 400 K [86]. According to Gennari et al., the decomposition overlaps with melting (355 K) to give ZrB_2, B_2H_6, and H_2 as reaction products [79]. For their part, Nakamori et al. reported thermal decomposition at ~460 K [30]. To be commented on is that B_2H_6 formation was detected even during ball-milling synthesis [79].

Table 5. Crystal structures of Zr-borohydrides.

Material and Hydrogen Content [wt.%]	Structural Parameters [Å, °]	Atomic Positions	Reference and Comments
$Zr(BH_4)_4$ 10.71	Space group: cubic *P-43m* (215)a = b = c = 5.8387(4) $\alpha = \beta = \gamma = 90$	**Zr:** 1, 1, 1. **B:** 0.7714(2), 0.7714(2), 0.7714(2). **H1:** 0.668(3), 0.668(3), 0.668(3). **H2:** 0.956(4), 0.748(2), 0.748(2)	At 100 K [83]

Similar to other transition metal elements, Zr can form ions of the type $[Zr(BH_4)_5]^{-1}$ [88]:

$$LiBH_4 + Zr(BH_4)_4 \rightarrow LiZr(BH_4)_5 \tag{33}$$
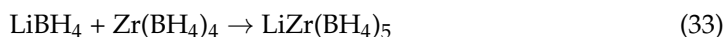
However, **LiZr(BH₄)₅** is unstable and decomposes into the initial borohydrides at ~253 K.

In a DOE annual progress report, **Na₂Zr(BH₄)₆** is briefly mentioned [89]: "unlike $Zr(BH_4)_4$, $(Na_2Zr(BH_4)_6)$ is non-volatile and undergoes rapid elimination of 2–3 wt% H_2 at 40–110 °C with no detectable B_2H_6 contamination". Other attempts to stabilize $Zr(BH_4)_4$ include: (a) formation of combined coordination compounds, with NH_3 as a ligand [84,85]; (b) formation of coordination compounds with other ligands [90]; and (c) the formation of a composite with cross-linked poly(4-vinylpyridine), which is a non-hygroscopic material that is stable for months [91].

Hf(BH$_4$)$_4$ and Zr(BH$_4$)$_4$ present similarities in chemistry and properties, such as crystal structure, bonding, and possible use as thin-film precursors. Hf(BH$_4$)$_4$ was also first produced in 1949 by a reaction analogous to reaction (29)) [72]. Later, the equivalent of reaction (32) in the solid-state was demonstrated [87,92]. Hf(BH$_4$)$_4$ is also a volatile compound at room temperature, and its gas-phase structure is monomeric η^3, with tetrahedral arrangement and high vapor pressure (~2 kPa at RT) [11,72,81,92]. The crystal structure of Hf(BH$_4$)$_4$ was determined at 110 K: cubic space group *P-43m* in the solid-state (Table 6); [BH$_4$]$^{-1}$ coordination to Hf is η^3, with d-orbital covalency [87,93]. As in the case of Zr, Hf can form a complex ion, [Hf(BH$_4$)$_5$]$^{-1}$ [88]:

$$LiBH_4 + Hf(BH_4)_4 \overset{ether, 195K}{\rightarrow} LiHf(BH_4)_5, \tag{34}$$

which is unstable at low temperature and decomposes (~253 K) to produce the precursor materials [88]. The decomposition of Hf(BH$_4$)$_4$ produces HfB$_2$, B$_2$H$_6$, and H$_2$ [11]. A possible use of Hf(BH$_4$)$_4$, Zr(BH$_4$)$_4$, and Ti(BH$_4$)$_3$ is as precursors for metal borides thin films; the proved advantages are a low temperature of the CVD process and a high conductivity in the thin films [11,94,95].

Table 6. Crystal structures of Hf-borohydrides.

Material and Hydrogen Content [wt.%]	Structural Parameters [Å, °]	Atomic Positions	Reference and Comments
Hf(BH$_4$)$_4$ 6.78	Space group: cubic *P-43m* (215)a = b = c = 5.8387(4) α = β = γ = 90	**Hf:** 0, 0, 0. **B:** 0.226(2), 0.226, 0.226. **H1:** 0.340(5), 0.340, 0.340. **H2:** 0.258(2), 0.258, 0.019(2)	At 100 K [93]

4.3. Group 5, Vanadium, Niobium and Tantalum

Few reports on vanadium borohydrides were located during the preparation of this review. In 2011, Yang et al. reported the formation of **V(BH$_4$)$_3$** by employing mechanical milling of NaBH$_4$ and VCl$_3$ [96].

$$3NaBH_4 + VCl_3 \rightarrow V(BH_4)_3 + 3NaCl \tag{35}$$
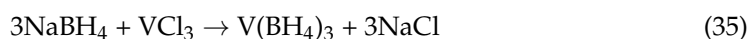
It is worth mentioning that the temperature in Yang´s ball millings was carefully controlled at 258 K and 293 K by means of a cooling jacket [96]. In the same work, characterization by XRD after-milling did not give clear evidence of the formation of V(BH$_4$)$_3$; however, changes in the dehydrogenation pathway compared to pure NaBH$_4$ served as an indirect proof [96]. The same low crystallinity of the milled products was observed by Korablov et al. in mixtures of LiBH$_4$-VCl$_2$ and NaBH$_4$-VCl$_2$ [97]. Dehydrogenation of V(BH$_4$)$_3$ by Yang et al. occurred in a three-step process, with main weight losses at 343 K, 416 K, and 518 K [96]. The dehydrogenation enthalpy was calculated as 25.4 kJ/mol V(BH$_4$)$_3$ [96]. In the report by Korablov et al., a new vanadium borohydride that decomposed at ~463 K was assumed [97].

A bi-cationic borohydride of Vanadium was reported as NaV(BH$_4$)$_4$·3DME (DME = 1,2-dimethoxyethane) [98]:

$$5NaBH_4 + VCl_4 \overset{DME}{\rightarrow} NaV(BH_4)_4\cdot3DME + 4NaCl + B_2H_6 + H_2 \tag{36}$$

$$4NaBH_4 + VCl_3 \overset{DME}{\rightarrow} NaV(BH_4)_4\cdot3DME + 3NaCl \tag{37}$$
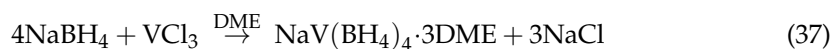
NaV(BH$_4$)$_4$·3DME decomposes at 353–378 K to produce H$_2$, B$_2$H$_6$, and DME [98]. Alternatively, Jensen et al. reported the reactions of VOCl$_3$, VCl$_4$, or VCl$_3$ with NaBH$_4$ in an organic solvent that produced [Na(DME)][V(BH$_4$)$_4$] [99]. Treatment of that compound with PMe$_3$, or the reaction of LiBH$_4$ with VCl$_3$(PMe$_3$)$_2$, produced V(BH$_4$)$_3$(PMe$_2$)$_3$ [99,100].

The analogous reaction between $VCl_2(dmpe)_2$ and $NaBH_4$ produced $V(BH_4)_2(dmpe)_2$ (dmpe = 1,2-Bis(dimethylphosphino)ethane) [100]. In the different reactions considered in all these reports, $[V(BH_4)_4]^{-1}$ and $V(BH_4)_3$ seem to become stabilized with solvents and other ligands. Theoretical calculations indicate that $NaV(BH_4)_4$ and $LiV(BH_4)_4$ (i.e., $[V(BH_4)_4]^{-1}$) would be stable [101,102].

In 1961, Nöth indicated that the reactions between alkali borohydrides ($LiBH_4$, $NaBH_4$) and halides of Hf, Th, V, Nb, Ta, Cr, Mo, W, and U, were not reported at that time [103]. Until now (2021), no homoleptic Nb-borohydrides have been reported. Compared to Nb-alanates, for which a relatively wide variety of materials have been reported [104] (and references within), the lack of homoleptic Nb-borohydrides is exceptional. Alanates of the same metal are in general less stable than the corresponding borohydrides. Concerning Ta, no reports on borohydrides of this metal were located during the preparation of this review.

4.4. Group 6: Chromium, Molybdenum and Tungsten

Some old reports on Cr(II) heteroleptic complexes with THF (2 solvent molecules) [105], TMDEA (Tetramethylethylenediamine), or Py (pyridine) [106] have been found. In particular, $Cr(BH_4)_2 \cdot 2THF$ was produced between 231 and 253 K, being unstable at room temperature [105]. Nakamori et al. reported the reaction between $LiBH_4$ and chromium chloride; however, no clear indication of the formation of chromium borohydride was presented in the data from infrared spectroscopy and hydrogen release by thermal desorption [107]. A theoretical report indicates that a hypothetical $Cr(BH_4)_4$ is unstable, but $[Cr(BH_4)_4]^{-1}$ might be stabilized by a bulky cation [102]. In fact, $Rb_3Cr(BH_4)_5$ and $Cs_3Cr(BH_4)_5$ were produced recently by mechanical milling (Equation (28) with M' = Cr), and they crystalized in tetragonal $P4_2/mbc$ [24]. The cell size of $Rb_3Cr(BH_4)_5$ was reported as a = 9.182(3) Å and c = 16.209(6) Å; while the cell size of $Cs_3Cr(BH_4)_5$ corresponds to a = 9.578(4) Å and c = 16.544(12) Å [24].

To the best of our knowledge, no experimental reports of homoleptic Mo and W borohydrides have been published.

4.5. Group 7: Manganese, Technetium and Rhenium

Manganese borohydrides have generated a large interest in recent years (mainly from 2010 to 2015) due to their high hydrogen content (9.53 wt.%), a certain balance between stability and low dehydrogenation temperature, and their similarities with $Mg(BH_4)_2$ in chemistry and crystal structures. **$Mn(BH_4)_2$** can be produced by a metathesis reaction between $2MBH_4$ and $MnCl_2$ (M = Li, Na or K) in organic solvents with further solvent extraction, or by solid-state metathesis promoted by ball milling, with or without further purification, using solvents such as $S(CH_3)_2$ [108,109]. These methods give different yields and purities [108,110]. Particularly, the presence of a second metathesis product (i.e., LiCl or NaCl) could be important; reports suggest the possibility of partial substitution of $[BH_4]^-$ by Cl^- ions [111,112]. Details of the synthesis technique are important: in the preparation using THF, the solvated material, $Mn(BH_4)_2 \cdot (THF)_3$, was obtained [113]; attempts to remove the solvent led to decomposition. However, another researcher successfully used THF and $NaBH_4$ plus $MnCl_2$ as precursors [114]. Solvent-free $Mn(BH_4)_2$ can also be obtained by using anhydrous ether [111,114]. Using a mixture of toluene/$S(CH_3)_2$, followed by the extraction of the manganese borohydride with $S(CH_3)_2$, and, finally, proper drying, the synthesis of $Mn(BH_4)_2$ can be considered reproducible [109]. This last procedure seems to be the most reliable for obtaining pure $Mn(BH_4)_2$. In the ball-milling preparation, the ratio between milling time and pauses seems very important to achieve the desired product [115]. Additionally, this synthesis method can lead to the formation of nanometric materials (~10–20 nm) [116] (and references within). A formation enthalpy of −58.89 kJ/f.u. (f.u. = formula unit) and a half-metallic nature of $Mn(BH_4)_2$ were determined through first-principle calculations [117]. Additionally, a low thermodynamic barrier for the metathesis reaction between $LiBH_4$ and $MnCl_2$ was observed [118].
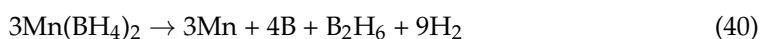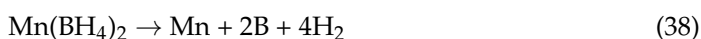
Several polymorphs of $Mn(BH_4)_2$ have been reported (Figure 5, Table 7) [109,111,115]. The α-$Mn(BH_4)_2$ phase belongs to the trigonal *P3₁12* space group symmetry, where Mn atoms are surrounded by four $[BH_4]^-$ ions in a distorted tetrahedral fashion [115], similar to *P3₁12* $Mg(BH_4)_2$ [115,119]. Drying of $Mn(BH_4)_2 \cdot 1/2S(CH_3)_2$ (after synthesis in toluene/$2S(CH_3)_2$) under vacuum at room temperature for three days produced γ-$Mn(BH_4)_2$ (cubic *Id-3a*), which is a nanoporous material similar to the zeolite-like γ-$Mg(BH_4)_2$ [109]. Some $Mg(BH_4)_2$ polymorphs are porous and can store small molecules in them [119]; thus, similar behavior can be expected from $Mn(BH_4)_2$. High-pressure polymorphs of Mn-borohydrides are: (i) δ-$Mn(BH_4)_2$, which consists of two interpenetrating $Mn(BH_4)_2$ frameworks without voids, and (ii) δ'-$Mn(BH_4)_2$ [111]. The transition δ-$Mn(BH_4)_2$ to α-$Mn(BH_4)_2$ occurred upon heating at 340–382 K [111]. The possibility of a metastable $Mn(BH_4)_2$ phase with tetragonal *P-4n2* symmetry in the pressure range 0–1.5 GPa was also reported [111].
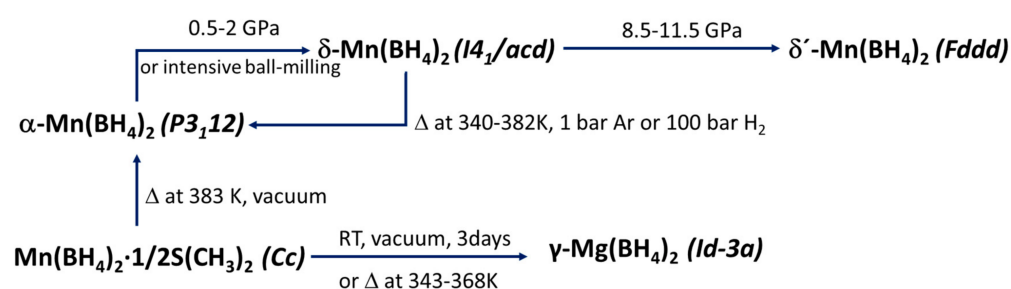
Figure 5. The interrelation of the phases of $Mn(BH_4)_2$, constructed with information from refs. [109,111,120].

The dehydrogenation temperature of α-$Mn(BH_4)_2$ (without LiCl) was established between 413 and 433 K, depending on pressure conditions (vacuum and 1 bar Ar, respectively) [109]. Hydrogen release at higher temperatures is usually due to the presence of residual precursors, i.e., $LiBH_4$ or $NaBH_4$ [112,118,121]. Tomanov et al. reported a slightly wider range of dehydrogenation temperatures, between 403 and 473 K (without NaCl) [111]. The dehydrogenation reaction of α-$Mn(BH_4)_2$ can occur even at 100 bar hydrogen pressure [111]. Meanwhile, in a ball-milled sample of α-$Mn(BH_4)_2$ (+LiCl), manganese borohydride was found to melt at 450 K [115]. Varin et al. demonstrated good dehydrogenation kinetics under isothermal conditions (373–473 K) of mixtures of $Mn(BH_4)_2$ + LiCl (from ball-milled $2LiBH_4$ + $MnCl_2$) [118]. The activation energy was between 70 and 59 kJ/mol, depending upon the milling conditions and the molar ratio of the precursors $LiBH_4$ and $MnCl_2$ [118]. A material stored at room temperature registered a release of 0.5 wt.% within a period of 80 days [118].

There is no consensus on the nature of the dehydrogenation products, particularly about the evolution of diborane and related compounds. Several dehydrogenation reactions have been proposed [112,118,121]:

$$Mn(BH_4)_2 \rightarrow Mn + 2B + 4H_2 \tag{38}$$

$$Mn(BH_4)_2 \rightarrow MnB_2 + 4H_2 \tag{39}$$

$$3Mn(BH_4)_2 \rightarrow 3Mn + 4B + B_2H_6 + 9H_2 \tag{40}$$

Regarding the diborane evolution, the terms used to describe the release range from practically undetectable to substantial amounts [109,116,122]. Liu et al. observed a peak of B_2H_6 evolution at 421 K [112], which is practically simultaneous to the hydrogen release. Recently, the addition of filamentary Ni, graphene, or $LiNH_2$ (5 wt.%) reduced the B_2H_6 release [123].

Several authors agreed about the amorphous nature of the solid products of the dehydrogenation process, particularly in manganese borides. In this way, an interesting X-

ray absorption spectroscopy study was performed by Guda et al. [124]. In this study, the Mn K-edge spectra of dehydrogenated samples are better described by the existence of Mn_2B, MnB, and MnB_4 than MnB_2 and Mn_3B_4 compounds. The authors proposed the formation of the former borides and metallic Mn as the main dehydrogenation products [124]. However, in a recent report, Pankin et al. indicated that metallic Mn does not exceed 5% [121]. Unfortunately, the only attempt to re-hydrogenate at 473 K and 100 bar H_2 (flowing at 100 mL/min in DSC) did not succeed [112].

Frequently, in addition to the formation of $Mg(BH_4)_2$, other compounds were obtained, such as bimetallic or solvated materials $K_2Mn(BH_4)_4$ or $M(Et_2O)_2Mn_2(BH_4)_5$ (M = Li, Na) [110,123]. Extraction of the solvent collapses the latter materials to $Mn(BH_4)_2$ and MBH_4 (M = Li, Na) [110]. The solvated materials of ($M(Et_2O)_2Mn_2(BH_4)_5$ and (M = Li, Na)) are insulators, with band gaps of 2.1 and 1.9 eV, respectively [110]. Dehydrogenation of $M(Et_2O)_2Mn_2(BH_4)_5$ (M = Li, Na) involves the evolution of the solvent at 383 K, and the decomposition of $Mn(BH_4)_2$ at 433 K [110].

Bimetallic and trimetallic Mn-borohydrides can be of interest. **$LiMn(BH_4)_3$** was reported by Choudhury et al. in 2009. This material was produced by mechanical milling [125]:

$$3LiBH_4 + MnCl_2 \rightarrow LiMn(BH_4)_3 + 2LiCl \tag{41}$$
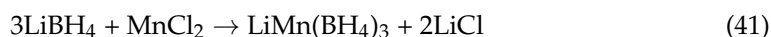
Being an amorphous material, its existence was demonstrated utilizing infrared spectroscopy [125–127]. $LiMn(BH_4)_3$ melts at about 367 K and undergoes dehydrogenation between 408 and 428 K [125]. As with other borohydrides, diborane release is a matter of controversy, from pure H_2 [125] to 4 mol% [126]. Doping with transition metals (nano-Ni, Co, Fe, Ti Zn, Cu, Pd) [125] or Ti-compounds, such as TiF_3, TiC, TiN, and TiO_2, leads to a small reduction in the activation energy and the dehydrogenation temperature, particularly with Ni and TiF_3 [125,126]. Activation energy is reduced from 130.64 kJ/mol to 111.55 kJ/mol in the Ni-doped material [125]. For the TiF_3 doped $LiMn(BH_4)_3$ material, activation energy was reported as 114 kJ/mol. The reason for the reduction in activation energy by TiF_3 is the partial formation of $Ti(BH_4)_3$, which decomposes at room temperature [126]. This supports the in-situ formation of $Ti(BH_4)_3$ observed by Fang et al. in 2009 [75]. Unfortunately, dehydrogenated $LiMn(BH_4)_3$ seems to be irreversible towards hydrogen uptake [125–127].

Severa et al. mentioned that **$Na_2Mn(BH_4)_4$** may be formed during ball milling of $NaBH_4$ with $MnCl_2$ [114]. However, more research about the existence and properties of this material should be performed.

$K_2Mn(BH_4)_4$ was produced as a minor product in a metathesis type reaction in Et_2O [110], but this material can also be obtained by ball milling of KBH_4-$MnCl_2$ or $Mn(BH_4)_2$ and KBH_4 [108]:

$$4KBH_4 + 2Mn(BH_4)_2 \rightarrow 2K_2Mn(BH_4)_4 \tag{42}$$
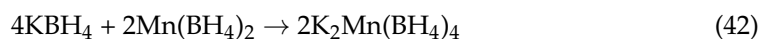
$K_2Mn(BH_4)_4$ has a monoclinic $P2_1/n$ symmetry (Table 7), and the $[Mn(BH_4)_4]^{-2}$ environment was described as a penta-capped trigonal prism [108]. The decomposition of $K_2Mn(BH_4)_4$ (420 K) produced KBH_4 and $KMn(BH_4)_3$; the crystal structure of the latter material was not solved unambiguously but proposed as tetragonal $P4/mbm$ [108]. DFT calculations on $[Mn(BH_4)_4]^{-2}$ indicate bidentate $[BH_4]^{-1}$ interaction with Mn [114].

$CsMn(BH_4)_3$ was briefly mentioned in a recent report; it crystallizes in the monoclinic Cc space group symmetry [69]. **$Rb_3Mn(BH_4)_5$** and **$Cs_3Mn(BH_4)_5$** were produced by mechanical milling (Equation (28) with M′ = Mn), and they crystalized in tetragonal $I4/mcm$ [24]. The cell size is a = 9.2963 (19) Å, c = 16.101(3) Å for $Rb_3Mn(BH_4)_5$, and a = 9.716(2) Å, c = 16.354 4) Å for $Cs_3Mn(BH_4)_5$ [24].

As with other interesting borohydrides, the formation of reactive mixtures or composites with $Mn(BH_4)_2$ is the subject of current research. Mixtures of $Mn(BH_4)_2 + M(BH_4)_x$, M = Li, Na, Mg, and Ca can be prepared by ball-milling from pure borohydrides. For M = Mg, a solid solution was also formed. $Mn(BH_4)_2$ and $Mg(BH_4)_2$ can form a solid

solution of $Mg_xMn_{(1-x)}(BH_4)_2$ in the range x = 0–0.8 from the mixing of $MgCl_2$, $MnCl_2$, and $LiBH_4$ [128]. This solid solution crystallized in the trigonal form of $Mn(BH_4)_2$, and it has the advantage of reducing the dehydrogenation temperature as compared with $Mg(BH_4)_2$ (425–450 K), while keeping a hydrogen content close to $Mg(BH_4)_2$ [128]. $Mg_xMn_{(1-x)}(BH_4)_2$ can decompose with very slow kinetics at room temperature [128]. During decomposition, up to 7.5 mol.% of diborane can be released [128].

Table 7. Crystal structures of Mn-borohydrides.

Material and Hydrogen Content [wt.%]	Structural Parameters [Å, °]	Atomic Positions	References and Comments
α-Mn(BH₄)₂ 9.53	Space group: trigonal $P3_112$ (151) a = 10.4349(1), c = 10.835(2) α = β = 90, γ = 120	**Mn1:** 0.23130(50), 0.91807(72), 0.12532(40). **Mn2:** 0.56272(32), 2x, 0.6666667. **B1:** 0.0403(34), 0.6990(30), 1.0056(58). **H11:** −0.0824(33), 0.6582(70), 1.0014(67). **H12:** 0.0712(79), 0.6455(79), 0.9292(92). **H13:** 0.0685(66), 0.6689(49), 1.0980(89). **H14:** 0.1041(50), 0.8233(31), 0.9937(44). **B2:** 0.4708(31), 2x, 0.1666667. **H21:** 0.4285(44), 1.0140(63), 0.206(41). **H22:** 0.393(40), 0.8688(61), 0.0914(60). **B3:** 2y, 0.10206, 0. **H31:** 0.1323(30), 0.1145(36), −0.0717(24). **H32:** 0.2766(30), 0.0642(23), −0.0463(37). **B4:** 0.1329(17), 1-x, 0.3333333. **H41:** 0.0199(28), 0.8265(39), 0.3754(44). **H42:** 0.1250(54), 0.7875(42), 0.2588(29). **B5:** 0.7056(23), 1-x, 0.8333333. **H51:** 0.7531(36), 0.4149(28), 0.8590(98). **H52:** 0.716(11), 0.232(10), 0.9146(22)	[115]
δ-Mn(BH₄)₂ 9.53	Space group: tetragonal $I4_1/acd$ (142) a = 7.85254(6), b = 7.85254(6), c = 12.14548(17) α = β = γ = 90	**Mn:** 0, 0.25, 0.125. **B:** 0.0197(17), 0, 0.25, **H1:** −0.0833(17), −0.01726, 0.17047. **H2:** 0.1247(17), 0.86217, 0.24890	[111]
δ′-Mn(BH₄)₂ 9.53	Space group: orthorhombic $Fddd$ (70) a = 12.638(15), b = 9.321(10), c = 9.205(17) α = β = γ = 90	**Mn:** −0.08981, 0.125, 0.125, **B1:** 0.52633, 0.44943, 0.21955. **H11:** 0.55862, 0.32065, 0.21651. **H12:** 0.31244, 0.30784, 0.26337. **H13:** 0.17630, 0.20909, 0.29581. **H14:** 0.53619, 0.49567, 0.09304	[111]
γ-Mn(BH₄)₂ 9.53	Space group: cubic Ia-$3d$ (230) a = b = c = 16.2094(13) α = β = γ = 90	**Mn:** $\frac{1}{4}$, 1/8, $\frac{1}{2}$. **B1:** 0.3090(11), 0.0590(11), 3/8. **H1:** 0.2849(11), 0.0199(11), 0.43730. **H2:** 0.2966(11), 0.1347(11), 0.38560	[109]
K₂Mn(BH₄)₄ 8.38	Space group: monoclinic $P2_1/c$ (14) a = 8.1375(7), b = 9.8456(7), c = 12.7420(12) α = 90, β = 100.552(6), γ = 90	**K1:** 0.2813(8), 0.3548(5), 0.5547(6). **K2:** 0.1974(11), 0.5047(7), 0.1980(5). **Mn1:** 0.7793(6), 0.2180(3), 0.4143(5). **B1:** 0.495(3), 0.676(3), 0.638(2). **H11:** 0.454(6), 0.74(2), 0.56(1). **H12:** 0.458(9), 0.73(2), 0.71(1). **H13:** 0.64(1), 0.66(1), 0.653(4). **H14:** 0.43(2), 0.57(2), 0.63(1). **B2:** 0.503(3), 0.270(2), 0.811(2). **H21:** 0.558(6), 0.241(5), 0.735(3). **H22:** 0.578(5), 0.213(6), 0.886(3). **H23:** 0.361(6), 0.239(7), 0.799(3). **H24:** 0.516(9), 0.389(2), 0.826(4). **B3:** 0.866(3), 0.357(3), 0.578(2). **H31:** 0.948(8), 0.354(7), 0.51(1). **H32:** 0.76(1), 0.436(8), 0.556(6). **H33:** 0.95(1), 0.388(8), 0.660(6). **H34:** 0.808(9), 0.248(5), 0.587(5). **B4:** 0.210(3), 0.524(2), 0.918(2). **H41:** 0.195(7), 0.449(3), 0.844(4). **H42:** 0.345(6), 0.513(8), 0.97(1). **H43:** 0.11(2), 0.498(9), 0.971(6). **H44:** 0.19(1), 0.637(7), 0.886(6)	[108]
Li₃MnZn₅(BH₄)₁₅ 9.67	Space group: hexagonal $P6_3/mcm$ (193) a = 15.391(3), c = 8.590(2) α = β = 90, γ = 120	**Zn1:** 1/3, 2/3, $\frac{1}{4}$. **Zn2:** 0.2861(4), 0, $\frac{1}{4}$. **Li/Mn:** 0.6089(7), 0, $\frac{1}{4}$. **Li:** 0, 0, 0. **B1:** 0.131(1), 0, $\frac{1}{4}$. **H11:** 0.089(2), 0, 0.358(2). **H12:** 0.139(2), −0.069(2), $\frac{1}{4}$. **B2:** 0.332(2), 0, 0.002(2). **H21:** 0.296(2), 0, −0.113(2). **H22:** 0.405(2), 0, −0.021(2). **H23:** 0.279(2), −0.069(2), 0.071(2). **B3:** 0.525(1), 0.344(2), $\frac{1}{4}$. **H31:** 0.443(2), 0.284(2), $\frac{1}{4}$. **H32:** 0.532(2), 0.420(2), 1/4. **H33:** 0.563(2), 0.336(2), 0.142(2)	Refined from synchrotron radiation powder diffraction data at room temperature [129]

For the rest of the $Mn(BH_4)_2$ + $M(BH_4)_x$, M = Li, Na, and Ca composites, the decomposition of the components is not significantly affected by each other. Only small
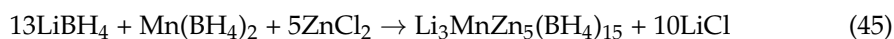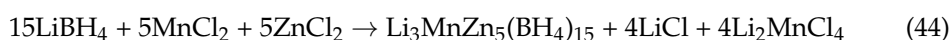
differences in the onset dehydrogenation temperature of $Mn(BH_4)_2$ were observed: 381 K in the mixture with $LiBH_4$, 379 K with $NaBH_4$, and 356 K with $Ca(BH_4)_2$ [120].

The composites of $Mn(BH_4)_2 + MH_x$, M = Li, Na, and Ca, exhibit the same dehydrogenation mechanism; the decomposition of $Mn(BH_4)_2$ overlapped with the formation of $M(BH_4)_x$ [120]:

$$Mn(BH_4)_2 + \frac{2}{3x}MH_x \rightarrow Mn + yB + 3H_2 + \frac{2}{3x}M(BH_4)_x \tag{43}$$
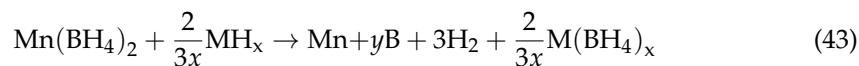
For the mixture of $Mn(BH_4)_2/MgH_2$, no formation of $Mg(BH_4)_2$ was observed, and the dehydrogenation of the components appears to be independent of each other: 373–394 K for $Mn(BH_4)_2$ and 503–615 K for MgH_2 [120].

$Li_3MnZn_5(BH_4)_{15}$ (Table 7) can be produced by mechanical milling of $LiBH_4$ and some salts [129]:

$$15LiBH_4 + 5MnCl_2 + 5ZnCl_2 \rightarrow Li_3MnZn_5(BH_4)_{15} + 4LiCl + 4Li_2MnCl_4 \tag{44}$$

$$13LiBH_4 + Mn(BH_4)_2 + 5ZnCl_2 \rightarrow Li_3MnZn_5(BH_4)_{15} + 10LiCl \tag{45}$$

Reaction (45) can be preferred over the reaction (44) due to a competing reaction to form $LiZn_2(BH_4)_5$ in the last one. Decomposition of $Li_3MnZn_5(BH_4)_{15}$ occurs at 385 K to produce $LiZn(BH_4)_5$, $LiBH_4$, and $Mn(BH_4)_2$ [129].

No reports on technetium and rhenium borohydrides have been published.

4.6. Group 8: Iron, Ruthenium, and Osmium

$Fe(BH_4)_2$ has a total hydrogen content of 9.42 wt.%. Schaeffer et al. prepared the mixture of $LiBH_4$ and $FeCl_3$ in ether at 228 K [130]. After the evaporation of the solvent, the filtrate was consistent with $Fe(BH_4)_2$, and the reduction of Fe(III) to Fe (II) was proposed [130]:

$$3LiBH_4 + FeCl_3 \rightarrow Fe(BH_4)_2 + \frac{1}{2}H_2 + \frac{1}{2}B_2H_6 + 3LiCl \tag{46}$$
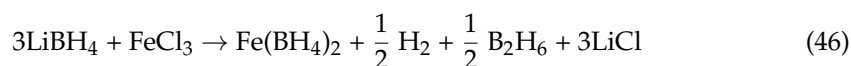
However, reaction (46) was not easily reproducible. The competing reaction of the reduction of Fe(III) to Fe (II), consuming 1 mol of $LiBH_4$, was proposed to occur:

$$LiBH_4 + FeCl_3 \rightarrow FeCl_2 + 2H_2 + B + LiCl \tag{47}$$
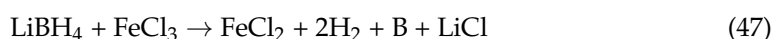
$Fe(BH_4)_2$ was reported to decompose upon heating between 263 K and 273 K; possible decomposition reactions are [130]:

$$Fe(BH_4)_2 \rightarrow Fe + H_2 + B_2H_6 \tag{48}$$

$$Fe(BH_4)_2 \rightarrow Fe + 2B + 4H_2 \tag{49}$$
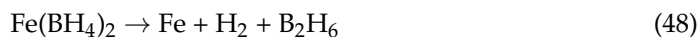
In turn, Varin et al. mixed $2LiBH_4 + FeCl_2$ by means of milling in "soft conditions" (2–30 min at room temperature, under ultra-high purity H_2 atmosphere and magneto ball-milling) [131,132]; infrared spectroscopy and X-ray diffraction results indicated the formation of a disordered $Fe(BH_4)_2$ that can decompose easily [131,132]. Recently, $Rb_3Fe(BH_4)_5$ and $Cs_3Fe(BH_4)_5$ were produced by mechanical milling (Equation (28), M′ = Fe), and they crystalized in tetragonal *I4/mcm* [24]. The cell parameters of $Rb_3Fe(BH_4)$ are a = 9.171 (4) Å, and c = 15.833(6)Å, while the cell size of $Cs_3Fe(BH_4)_5$ involves a = 9.619(11) Å, and c = 16.014 (19) Å [24].

To the best of our knowledge, no reports on ruthenium and osmium borohydrides have been published.

4.7. Group 9: Cobalt, Rhodium, and Iridium

In 1956, Stewart and Scheaffer indicated that the reaction of $CoBr_2$ and $LiBH_4$ in ether at liquid nitrogen temperature produced a greyish-white precipitate. This precipitate was presumed to be cobalt borohydride; this material turned black (decomposed) in a few minutes when warmed to room temperature, accompanied by the release of hydrogen and the formation of LiBr and CoB_2 [133]. No characterization of the greyish-white precipitate was reported. Recently, a DFT screening of ternary alkali-transition metal borohydrides indicated that **$KCo(BH_4)_3$** and **$NaCo(BH_4)_3$** would be more stable than **$Co(BH_4)_2$**. Both binary Co-borohydrides were remarked as promising materials [101].

To the best of our knowledge, no reports on homoleptic rhodium and iridium borohydrides have been published.

4.8. Group 10: Nickel, Palladium, and Platinum

To the best of our knowledge, no reports on homoleptic borohydrides of nickel, palladium, and platinum have been published. However, heteroleptic (with chelates type-ligands) Ni-borohydrides are stable and can be used as catalysts [134].

4.9. Group 11: Copper, Silver, and Gold

Essentially, no experimental advances of the group 11 borohydrides have been reported since the 1960s. **$CuBH_4$** was first reported by Wiberg; this material was produced by the metathesis reaction between CuCl and $LiBH_4$ in a THF-ether (1:1) solution at 253 K [135]. However, $CuBH_4$ decomposes in solution at 261–273 K, producing CuH, B, B_3H_6, and H_2 [135,136]. An alternative is the use of $CuCl_2$ in ether at 228K [136]:

$$CuCl_2 + 2LiBH_4 \rightarrow CuBH_4 + \frac{1}{2}B_2H_6 + \frac{1}{2}H_2 + 2LiCl \tag{50}$$
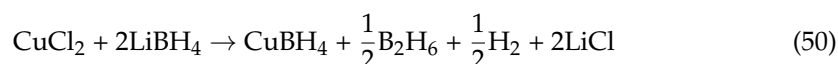
$AgBH_4$ can be produced by the following reaction in ether at 193 K [137]:

$$AgClO_4 + LiBH_4 \rightarrow AgBH_4 + LiClO_4 \tag{51}$$

$AgBH_4$ decomposed at 243 K to produce Ag, H_2, and BH_3; Wiberg proposed that Ag can catalyze the decomposition of BH_3 to B and H_2 [137].

$AuBH_4$ was proposed to be unstable by Wiberg, i.e., it will not form even at low temperature [138], but it was mentioned that $Au(BH_4)_3$ could be prepared by the reaction between $AuCl_3$ and $LiBH_4$ in ether at 153 K [139] (and ref. 39 within), but that it decomposed upon an increase in temperature. Unfortunately, no other references to $Au(BH_4)_3$ have been located. Theoretical calculations supported the statement of Wiberg; $AuBH_4$ is not stable, while $CuBH_4$ and $AgBH_4$ would be stable with a rapid exchange of the tridentate and bidentate coordination of the $[BH_4]^{-1}$ ion [139].

4.10. Group 12: Zinc, Cadmium, and Mercury

$Zn(BH_4)_2$ (8.48 wt.% hydrogen content) was first reported by Wiberg and Henle in 1952 [140]. $Zn(BH_4)_2$ was prepared by the metathesis reaction between $ZnCl_2$ and $LiBH_4$ in ether at room temperature [140]. Since then, it has become clear that $Zn(BH_4)_2$ decomposes at about 358 K to produce Zn, B, and H_2 [140]. Other synthesis routes in the organic solvent THF were published in 1969 [141]:

$$2ZnBr_2 + 2KBH_4 \rightarrow Zn(BH_4)_2 + K_2ZnBr_4 \tag{52}$$

$$3Zn(OCH_3)_2 + 4(BH_3)_2 \rightarrow 3Zn(BH_4)_2 + 2B(OCH_3)_3 \tag{53}$$
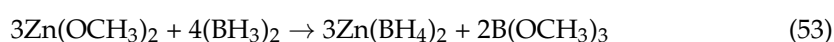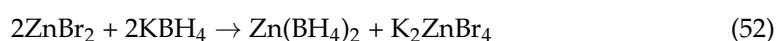
Later, the preparation of $Zn(BH_4)_2$ by mechanical milling gained popularity. Beyond possible hydrogen storage applications, $Zn(BH_4)_2$ can be used in the reduction reaction of aldehydes and ketones [142] or as a source of B_2H_6 [143]. Choudhury et al. calculated that $Zn(BH_4)_2$ is an insulator material with a band gap of 3.529 eV [144].

The crystal structure of $Zn(BH_4)_2$ has only been calculated theoretically, with some degree of controversy (Table 8). Nakamori et al. determined the $Zn(BH_4)_2$ crystal structure as triclinic *P-1* (Figure 6) [30]. Choudhury et al., utilizing DFT calculations, determined that the orthorhombic *Pmc2₁* ($Mg(BH_4)_2$ model) structure is the most stable at 0 K and finite temperatures [144]. For their part, Doan Huan et al. calculated that a tetragonal *I4₁22* $Zn(BH_4)_2$ structure would be the most stable [145]. In another DFT calculation, Aidhy and Wolverton indicated that the tetragonal *I4m2* and orthorhombic *F222* structures of $Zn(BH_4)_2$ are near in energy, and have the lowest energies compared with other proposed structures [146]. The results of several stable structures point to the possible existence of polymorphism and low energies associated with transitions between them [145]. However, no experimental confirmation of the crystal structure of $Zn(BH_4)_2$ has been reported up to now. As in the case of Sc-borohydride, Zn-borohydride can be mistaken by a solvated product in wet synthesis, or as a bi-metallic borohydride in mechanically milled materials [147].

(a)　　　　　　　　　　　　　　　　　　　　(b)
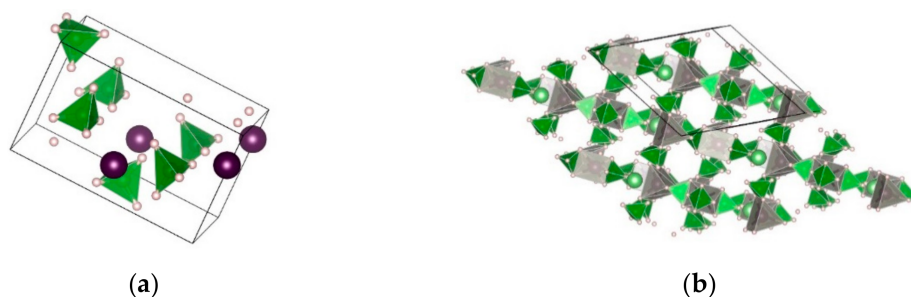
Figure 6. Crystal structure of (**a**) $Zn(BH_4)_2$ and (**b**) $LiZn(BH_4)_5$. The structures become complex with the formation of double metal borohydrides. Detailed crystallographic information can be found in Table 8.

$Zn(BH_4)_2$ (with 2NaCl, from mechanical milling synthesis) melts at 358 K, followed by the dehydrogenation reaction, which is registered 358–413 at K [148]. However, a considerable evolution of diborane was recorded. Thus, the dehydrogenation reaction was described as [148,149]:

$$Zn(BH_4)_{2\ (solid)} \rightarrow Zn(BH_4)_{2\ (liquid)} \rightarrow Zn + B_2H_6 + H_2 \qquad (54)$$
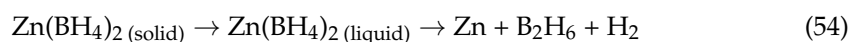
Due to the formation of B_2H_6 at low temperature, $Zn(BH_4)_2$ can be used as a diborane source for other reactions. For example, Friedrich et al. used diborane from $Zn(BH_4)_2$ into LiH to test the regeneration of $LiBH_4$ in soft T and P conditions [143]. Srinivasan et al. did not limit the formation of B_2H_6 in their discussion of results, and proposed the possible formation of B_4H_{10}, B_5H_9, and B_6H_{12} [150]. Srinivasan et al. demonstrated that 1.5 mol% nano-Ni particles reduced the formation of diborane [149,150]. Other additives such as $TiCl_3$, TiF_3, nano-Fe, Ti, nano-Ti [150], or carbon nanotubes [151] have demonstrated a small-to-moderate reduction in the decomposition temperature of $Zn(BH_4)_2$.

Interestingly, in Mg-$Zn(BH_4)_2$ and MgH_2-$Zn(BH_4)_2$ (materials composed of two layers, and 1:1 mixtures, respectively) doped with Nb_2O_5, a reaction between Mg-$Zn(BH_4)_2$ and MgH_2-$Zn(BH_4)_2$ occurred below 373K [152]. The authors proposed a reaction between MgH_2 and B_2H_6 due to the appreciable reduction in diborane evolution and the change from the endothermic decomposition of $Zn(BH_4)_2$ to the exothermic decomposition of Mg-$Zn(BH_4)_2$ and MgH_2-$Zn(BH_4)_2$ [152]. These reactions have the characteristics of a reactive hydride composite. Conversely, $Zn(BH_4)_2$ was tried as an additive for MgH_2, with no significant improvement for MgH_2 dehydrogenation kinetics [153,154].

The formation enthalpy of $Zn(BH_4)_2$ was calculated as -66.003 kJ/mol H_2 at 300 K, while the dehydrogenation enthalpy (Zn, B, and H_2 as the products) was calculated as 59.90 kJ/mol H_2 at 0 K [144]. Such formation/dehydrogenation enthalpy is above the target of 20–50 kJ/mol H_2. Thus, cation and anion substitution have been tried as strategies

to tailor the formation or dehydrogenation thermodynamics. Bimetallic compounds have been reported in research on Zn-borohydrides as early as 1950–1969 [141]:

$$ZnCl_2 + 3NaBH_4 \rightarrow NaZn(BH_4)_3 + 2NaCl \tag{55}$$
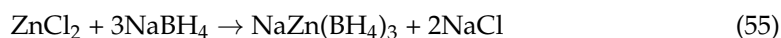
NaZn(BH$_4$)$_3$ has a monoclinic space group symmetry *P2$_1$/c* (Table 8), where the Zn atoms present a distorted tetrahedral coordination, and metal atoms and [BH$_4$]$^-$ groups form a 3D framework [147]. It must be mentioned that different stoichiometric ratios can also produce **MZn(BH$_4$)$_3$ (M = Li, Na)** (Table 8) [147,155]. A by-product, M$_2$ZnCl$_4$, plays an important role in dehydrogenation reaction [147].

LiZn$_2$(BH$_4$)$_5$ was produced by the reaction between LiBH$_4$ (or Li^{11}BD$_4$) and ZnCl$_2$ utilizing mechanical milling (either cryogenic or room temperature milling) [156]. The LiZn$_2$(BH$_4$)$_5$ structure consists of two interpenetrating 3D frameworks of complex [Zn$_2$(BH$_4$)$_5$]$^{-1}$ ions and Li ions, with no bonds between the two different 3D frameworks, similar to some MOFs structures (Figure 6) [156].

NaZn$_2$(BH$_4$)$_5$ can also be produced by mechanical ball milling, with the generalized reaction of Li- and Na- Zn-borohydrides being [147,155,157]:

$$5MBH_4 + 2ZnCl_2 \rightarrow MZn_2(BH_4)_5 + 4MCl, \text{ (M = Li or Na)} \tag{56}$$
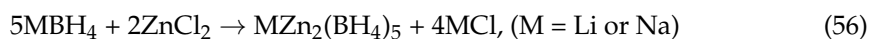
MZn$_2$(BH$_4$)$_5$ (M = Li or Na) has a 3D framework structure, with two interpenetrating frameworks composed of an alkali-metal cation and a complex anion [Zn$_2$(BH$_4$)$_5$]$^-$, and built from two triangularly coordinated Zn atoms (Table 8) [147,155,157].

A first-principle study (DFT + PEGS (prototype electrostatic ground state)) indicated that LiZn(BH$_4$)$_3$ would have a triclinic *C1* space group symmetry [146]. LiZn(BH$_4$)$_3$ is calculated to be more stable (about -8 kJ/mol cation) as compared to the parent borohydrides of Li and Zn [146], but unstable towards decomposition to LiBH$_4$ and LiZn$_2$(BH$_4$)$_5$ (from DFT along with grand canonical linear programming method) [158]. In turn, LiZn$_2$(BH$_4$)$_5$ is calculated to decompose in a rather complex pathway [158]:

$$LiZn_2(BH_4)_5 \rightarrow 2Zn + 1/5\ LiBH_4 + 2/5\ Li_2B_{12}H_{12} + 36/5\ H_2 \tag{57}$$

$$\rightarrow 2Zn + 1/6\ LiH + 5/12\ Li_2B_{12}H_{12} + 89/12\ H_2 \tag{58}$$

$$\rightarrow 11/6\ Zn + 1/6\ LiZn + 5/12\ Li_2B_{12}H_{12} + 15/2\ H_2 \tag{59}$$

$$\rightarrow Zn + 5B + LiZn + 10H_2 \tag{60}$$
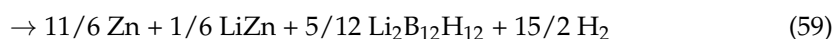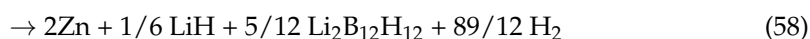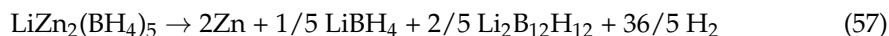
Ravnsbæk et al. agreed about the complex nature (coupled reactions) of dehydrogenation reactions and summarized them as [147]:

$$2MZn_2(BH_4)_3 + M_2ZnCl_4 \rightarrow 5Zn + 4MCl + 3B_2H_6 + 3H_2 \text{ M = Li (at 400 K), Na (at 368 K)} \tag{61}$$
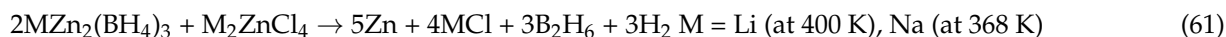
The same type of DFT + PEGS calculations on the analogous Na-Zn borohydrides indicated that NaZn(BH$_4$)$_3$ is unstable towards the decomposition of Na and Zn-borohydrides, while NaZn$_2$(BH$_4$)$_5$ would be more stable than the parent borohydrides [146]. Xia et al. suppressed the production of diborane by infiltrating NaZn(BH$_4$)$_3$ in SBA-15 (prepared by wet-ball milling, dissolution in THF, infiltration, and drying) [159]. Additionally, a slight reduction in the dehydrogenation peak temperature was observed in the infiltrated material compared to the pure material (385 K versus 393 K, respectively) [159]. Under those circumstances, the decomposition of NaZn(BH$_4$)$_3$ produced NaBH$_4$, Zn, B, and H$_2$ [159].

Table 8. Crystal structures of Zn-borohydrides.

| Material and Hydrogen Content [wt.%]	Structural Parameters [Å, °]	Atomic Positions	References and Comments
$Zn(BH_4)_2$ 8.48	Space group: triclinic *P-1* (2) a = 6.877, b = 5.440, c = 7.842 α = 89.5, β = 76.15, γ = 89.98	**Zn:** 0.2498, 0.0001, 0.9998. **B1:** 0.0567, 0.8903, 0.7939. **B2:** 0.5497, 0.1754, 0.8166. **H1:** 0.0997, 0.8534, 0.6382. **H2:** 0.5892, 0.2640, 0.6710. **H3:** 0.1789, 0.7718, 0.8612. **H4:** 0.3316, 0.7331, 0.0999. **H5:** 0.1031, 0.2267, 0.1397. **H6:** 0.3863, 0.2679, 0.9011. **H7:** 0.0498, 0.1135, 0.8210. **H8:** 0.4481, 0.0506, 0.1928	Theoretical [30]
	Space group: orthorhombic *Pmc2_1* (26) a = 4.118, b = 4.864, c = 7.916 α = β = γ = 90	**Zn:** 0, 0.28459, 0.0089. **B1:** 0.5, −0.06481, 0.4706. **B2:** 0, −0.46194, 0.24842. **H1:** 0.5, −0.30735, 0.42745. **H2:** 0.27449, −0.0050, −0.42983. **H3:** 0, 0.39706, 0.37973. **H4:** 0, 0.21066, −0.24017. **H5:** 0.25820, −0.48360, −0.32151. **H6:** 0.5, 0.08396, 0.3488	Optimized structure [144]
$LiZn(BH_4)_3$ 10.35	Space group: monoclinic *P2_1/c* (14) a = 10.59, b = 14.74, c = 8.66 α = γ = 90, β = 111.056	**Zn1:** 0.76982, 0.11283, 0.7512. **Zn2:** 0.40867, 0.26754, 0.60812. **Li1:** 0.08413, 0.12904, 0.25099. **Li2:** 0.77464, 0.09463, 0.25701. **B1:** 0.51747, 0.39654, 0.64566. **B2:** 0.24290, 0.26206, 0.72420. **B3:** 0.84715, 0.05769, 1.01282. **B4:** 0.84433, −0.00056, 0.57012. **B5:** 0.53022, 0.13104, 0.62602. **B6:** 0.87262, 0.25874, 0.80977. **H11:** 0.48781, 0.46308, 0.70437. **H12:** 0.60520, 0.40322, 0.58737. **H13:** 0.41470, 0.3777, 0.52066. **H14:** 0.5496, 0.33635, 0.75538. **H21:** 0.12228, 0.25280, 0.65129. **H22:** 0.27910, 0.33967, 0.71248. **H23:** 0.29189, 0.19988, 0.6632. **H24:** 0.27506, 0.25791, 0.37092. **H31:** 0.81526, 0.01114, 0.88397. **H32:** 0.78587, 0.12997, 0.9924. **H33:** 0.96820, 0.07003, 1.05745. **H34:** 0.81149, 0.00813, 1.10142. **H41:** 0.76794, −0.04277, 0.62085. **H42:** 0.79042, 0.00405, 0.4204. **H43:** 0.95622, −0.03529, 0.61027. **H44:** 0.87034, 0.07826, 0.62903. **H51:** 0.43883, 0.07855, 0.59858. **H52:** 0.50460, 0.19684, 0.52625. **H53:** 0.61326, 0.09429, 0.5739. **H54:** 0.57432, 0.15595, 0.77025. **H61:** 0.95757, 0.20272, 0.87941. **H62:** 0.77207, 0.22980, 0.69158. **H63:** 0.91771, 0.31006, 0.73238. **H64:** 0.83042, 0.29690, 0.90608	DFT optimization [155]
$LiZn_2(BD_4)_5$ 9.51 (calculated as H)	Space group: orthorhombic *Cmca* (64) a = 8.6031(13), b = 17.8876(4), c = 15.3598(3) α = β = γ = 90	**Zn1:** 0, 0.6440(10), 0.7665(11). **Zn2:** 0, 0.4252(12), 0.6300(16). **Li1:** 0, 0.138(6), 0.434(6). **B1:** 0, 0.2580(4), 0.3166(5). **D11:** 0, 0.1912(4), 0.3101(17). **D12:** 0, 0.2807(10), 0.3903(5). **D13:** 0.1153(7), 0.2798(7), 0.2804(7). **B2:** 0, 0.3513(4), 0.0903(5). **D21:** 0, 0.2971(5), 0.0442(8). **D22:** 0, 0.4090(5), 0.0505(9). **D23:** 0.1136(7), 0.3488(10), 0.1355(5). **B3:** 0, 0.5320(4), 0.7016(4). **D31:** 0, 0.4746(5), 0.7421(9). **D32:** 0, 0.5264(14), 0.6238(5). **D33:** 0.1145(7), 0.5662(5), 0.7223(9). **B4:** 0.2284(8), 0.3825(4), 0.5882(4). **D41:** 0.1551(14), 0.4234(6), 0.5415(7). **D42:** 0.3368(10), 0.4186(7), 0.6142(11). **D43:** 0.1591(14), 0.3629(10), 0.6520(6). **D44:** 0.2550(19), 0.3297(5), 0.5424(8)	295 K, ^{11}B [156]
$NaZn(BH_4)_3$ 9.10	Space group: triclinic P1 (1) a = 7.125, b = 7.246, c = 4.688 α = 99.254 β = 91.097 γ = 71.422	**Li:** −0.353, 0.225, −0.465. **Zn:** −0.022, −0.471, 0.277. **B:** −0.139, −0.150, 0.339. **B:** 0.257, 0.353, 0.442. **B:** −0.241, 0.396, 0.047. **H:** −0.052, −0.034, 0.428. **H:** −0.045, −0.248, 0.112. **H:** −0.134, −0.247, −0.46. **H:** −0.31, −0.086, 0.276. **H:** 0.343, 0.18, 0.356. **H:** 0.251, 0.439, 0.229. **H:** 0.092, 0.359 −0.465. **H:** 0.328, 0.438, −0.363. **H:** −0.282, 0.485, 0.298. **H:** −0.069, 0.374, −0.041. **H:** −0.242, 0.227, 0.036. **H:** −0.355, 0.495, −0.107	PEGS + DFT calculations [146]

<center>**Table 8.** *Cont.*</center>

Material and Hydrogen Content [wt.%]	Structural Parameters [Å, °]	Atomic Positions	References and Comments
$NaZn_2(BH_4)_5$ 8.84	Space group: monoclinic $P2_1/c$ (14) a = 9.397(2), b = 16.635(3), c = 9.1359(16) $\alpha = \gamma = 90$, $\beta = 112.658(19)$.	**Na1:** 0.245(6), 0.436(3), 0.117(8). **Zn1:** 0.2873(16), 0.7660(11), 0.643(3). **Zn2:** 0.8412(17), 0.6268(8), 0.395(2). **B1:** 0.5212, 0.3234, 0.2606. **B2:** 0.7102, 0.0954, 0.3551. **B3:** 0.0844, 0.6934, 0.5422. **B4:** 0.7766, 0.5874, 0.6112. **B5:** 0.7766, 0.9126, 0.6654. **H11:** 0.3982, 0.3357, 0.1991. **H12:** 0.5824, 0.3869, 0.2912. **H13:** 0.5530, 0.2145, 0.6707. **H13:** 0.5530, 0.2855, 0.3823. **H21:** 0.6098, 0.1394, 0.3049. **H22:** 0.8140, 0.1363, 0.4070. **H23:** 0.7076, 0.4452, 0.7476. **H23:** 0.7076, 0.0548, 0.4600. **H31:** 0.9880, 0.7394, 0.4940. **H32:** 0.0428, 0.6250, 0.5214. **H33:** 0.1548, 0.7038, 0.6833. **H33:** 0.1548, 0.7962, 0.9715. **H41:** 0.8304, 0.5354, 0.5677. **H42:** 0.8574, 0.6148, 0.7372. **H43:** 0.7370, 0.6415, 0.5129. **H44:** 0.6750, 0.5617, 0.6206. **H51:** 0.8304, 0.9646, 0.7627. **H52:** 0.8574, 0.8852, 0.6202. **H53:** 0.7370, 0.8585, 0.7241. **H54:** 0.6750, 0.9383, 0.5544	[147]
$KZn(BH_4)_3$ 8.12	Space group: trigonal R3 (146) a = b = 7.6291(8), c = 10.977(2)$\alpha = \gamma = 90$, $\beta = 120$	**K:** 0, 0, 0.49936. **Zn:** 0, 0, 0.00309. **B:** 0.31006, 0.05088, 0.01153. **H1:** 0.19196, 0.98384, 0.10009. **H2:** 0.44232, 0.21786, 0.03989. **H3:** 0.36275, 0.92929, 0.98755. **H4:** 0.22942, 0.06605, 0.91529	Atomic parameters at T = 100 K [160]
$Li_3MgZn_5(BH_4)_{15}$ 10.17	Space group: hexagonal $P6_3/mcm$ (193) a = b = 15.371(3), c = 8.586(2) $\alpha = \gamma = 90$, $\beta = 120$	**Zn1:** 1/3, 2/3, $\frac{1}{4}$. **Zn2:** 0.2832(5), 0, $\frac{1}{4}$. **Li/Mg:** 0.598(1), 0, $\frac{1}{4}$. **Li:** 0, 0, 0. **B1:** 0.131(1), 0, $\frac{1}{4}$. **H11:** 0.089(2), 0, 0.358(2). **H12:** 0.139(2), −0.069(2), $\frac{1}{4}$. **B2:** 0.338(1), 0, 0.004(2). **H21:** 0.302(2), 0, −0.111(2). **H22:** 0.410(2), 0, −0.019(2). **H23:** 0.285(2), −0.069(2), 0.073(2). **B3:** 0.5286(6), 0.346(2), $\frac{1}{4}$. **H31:** 0.447(2), 0.286(2), $\frac{1}{4}$. **H32:** 0.535(2), 0.423(2), $\frac{1}{4}$. **H33:** 0.566(2), 0.338(2), 0.143(2)	At RT. Occupation of the Li/Mg site Li: occ = 0.66(2), Mg: (1 − occ) = 0.34(2) Occupation of the Li site Li: 3*occ − 1 = 1 [129]

KZn(BH₄)₃ was prepared by the ball-milled assisted reaction between $ZnCl_2$ and KBH_4 [160]:

$$ZnCl_2 + 3KBH_4 \rightarrow KZn(BH_4)_3 + 2KCl \tag{62}$$
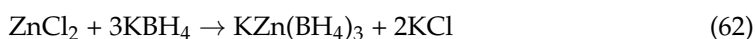
Then, a side-reaction might also occur:

$$ZnCl_2 + 2KCl \rightarrow K_2ZnCl_4 \tag{63}$$

In Equation (63), a partial substitution of Cl^- by $[BH_4]^{-1}$ ($K_2ZnCl_{4-x}(BH_4)_x$) was registered and linked to the dehydrogenation reaction [160].

$KZn(BH_4)_3$ presents a trigonal space group symmetry *R3* (Table 8); the Zn atom is coordinated with three $[BH_4]^{-1}$ groups in a triangular planar configuration, suggesting the existence of an anionic complex $[Zn(BH_4)_3]^{-1}$ located inside a rhombohedron of K atoms [160].

$KZn(BH_4)_3$ decomposes at ~385 K to produce a gas mixture of H_2 and diborane, and another double cation borohydride [160]:

$$2KZn(BH_4)_3 \rightarrow K_2Zn(BH_4)_4 + Zn + B_2H_6 + H_2 \tag{64}$$
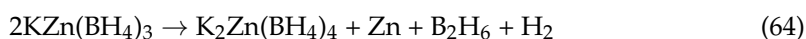
Further heating leads to multistep dehydrogenation reactions, involving an exchange of Cl^- and $[BH_4]^{-1}$ ions. For $K_2ZnCl_{4-x}(BH_4)_x$, an increase in $[BH_4]^{-1}$ content was registered, first at ~385 K but, upon further heating, $[BH_4]^{-1}$ content decreased [160].

In general, in the double cation M-Zn- borohydrides ($MZn(BH_4)_3$ and $M_2Zn(BH_4)_4$, M = Li, Na and K), their synthesis by ball-milling, and the dehydrogenation reactions present many similarities.

Mg₍₁₋ₓ₎Znₓ(BH₄)₂ (solid solution) was prepared by the mechanical milling of $Mg(BH_4)_2$ and $ZnCl_2$ at room and liquid-N_2 temperatures [161,162]. Decomposition was reported to

start at 373–398 K with the release of hydrogen and diborane [161,162]. Careful control of the milling conditions and stoichiometry are important for the successful formation of the solid solution $Mg_{(1-x)}Zn_x(BH_4)_2$, dehydrogenation temperature, and products [161,162]. Cryogenic ball-milling offered a slight advantage in the preferential release of hydrogen over diborane [162]. A periodic DFT study of $Mg_{(1-x)}Zn_x(BH_4)_2$ (x = 0.2–0.3) indicates an energetically favorable mixing of Zn and Mg borohydrides and a decomposition enthalpy of about 30 kJ/mol H_2 [163]. The DFT studies were performed by systematically replacing Mg atoms with Zn atoms in the α-$Mg(BH_4)_2$ structure (both metals present +2 oxidation state and similar ionic size, r_{Mg} = 0.065 nm and r_{Zn} = 0.074 nm [146]). $Mg_{0.8}Zn_{0.2}(BH_4)_2$ was claimed to be a promising composition [163].

Trimetallic borohydrides **$Li_3MZn_5(BH_4)_{15}$, M = Mg, and Mn**, were produced by mechanical milling [129], reactions (44) and (45). In both cases, the formation of $LiZn_2(BH_4)_5$ as a by-product was observed. $Li_3MZn_5(BH_4)_{15}$, M = Mg and Mn, also crystalizes in a hexagonal $P6_3/mcm$ structure that contains channels built up from face-sharing $(BH_4)_6$ octahedra [129]. The $Li_3MZn_5(BH_4)_{15}$ materials, M = Mg and Mn, are interesting as solid-state electrolytes, and their decomposition (at 368–393 K for Mg, and 385 K for Mn) produces the related borohydrides $LiBH_4$, $Mg(BH_4)_2$, $Mn(BH_4)_2$ and $LiZn_2(BH_4)_5$. These latter borohydrides decompose at higher temperatures [129].

Chlorine-substituted Zn-borohydrides, such as $LiZn(BH_4)_2Cl$ and $Zn(BH_4)Cl$, were observed as early as 1952, with the latter compound decomposing at 393 K to produce $ZnCl_2$, metallic Zn, B, and H_2 [140]. $KZn(BH_4)Cl_2$ was reported in 2011, and it decomposes at about 383 K to produce K_2ZnCl_4, metallic Zn, boranes $((BH_3)_n)$, and H_2 [164].

$Cd(BH_4)_2$ was first reported in 1952 by Wiberg et al. [165]. At the time, cadmium borohydride was produced in ether:

$$CdCl_2 + 2LiBH_4 \rightarrow Cd(BH_4)_2 + 2LiCl \tag{65}$$
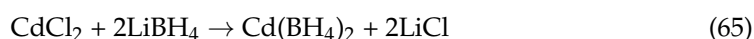
In ether, $Cd(BH_4)_2$ can also be obtained as [166]:

$$3Cd(OCH_3)_2 + 4B_2H_6 \rightarrow 3Cd(BH_4)_2 + 2B(OCH_3)_3 \tag{66}$$
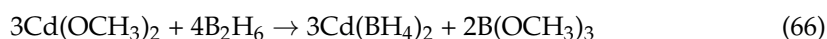
Later, in 2013, the reaction (65) without solvents was reported, i.e., ball milling synthesis [167,168]. Two polymorphs were identified: α-$Cd(BH_4)_2$ and β-$Cd(BH_4)_2$ [167,168]. The temperature of the polymorph transition was located at ~328 K [167]. The formation of the polymorphs demonstrated a dependency on the milling temperature: the material prepared by cooling the milling vial (with liquid nitrogen) was mainly α-$Cd(BH_4)_2$, while room temperature milling was associated with the formation of β-$Cd(BH_4)_2$ [168]. However, one side reaction was observed in the solid-state preparation reaction that reduced the quantity of $Cd(BH_4)_2$ formation [168]:

$$LiBH_4 + CdCl_2 \rightarrow 0.5Cd(BH_4)_2 + 0.5Li_2CdCl_4 \tag{67}$$
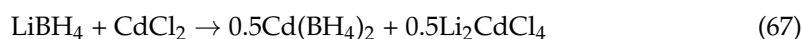
The decomposition of $Cd(BH_4)_2$ was observed at room temperature [165], and even at lower temperatures [169]. Thus, cadmium borohydride is an unstable material. In a more detailed study, $Cd(BH_4)_2$ decomposed at 348 K with fast kinetics and produced B_2H_6 and H_2 in a mole ratio of 1:1 [168]:

$$Cd(BH_4)_2 \rightarrow Cd + B_2H_6 + H_2 \tag{68}$$
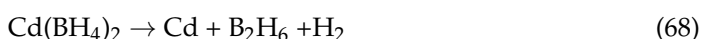
The formation of cation- and anion-substituted $Cd(BH_4)_2$ has been observed since the first reports [165] in organic solvents, such as ether or DMF (dimetylformamide) [170]:

$$CdCl_2 + 2LiBH_4 \rightarrow LiCdCl(BH_4)_2 + LiCl \tag{69}$$

$$CdCl_2 + 3LiBH_4 \rightarrow LiCd(BH_4)_3 + 2LiCl \tag{70}$$
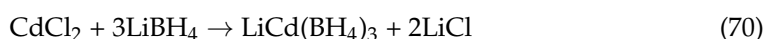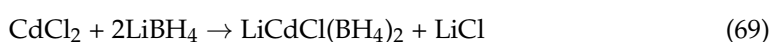
Reactions (65) and (69) in ether, and particularly reaction (70), can also occur in the systems MBH_4/CdX_2, M = Li, Na and X = Cl, Br, I [166,170]. The complex ions $[CdCl(BH_4)_2]^{-1}$ and $[Cd(BH_4)_3]^{-1}$ were observed during the solvent synthesis, and the formation of adducts was demonstrated [169–171]. The addition of an equivalent of $LiBH_4$ to $LiCd(BH_4)_3$ in diglyme can produce a precipitate soluble in THF [171]:

$$LiCd(BH_4)_3 + LiBH_4 \leftrightarrow Li_2Cd(BH_4)_4 \tag{71}$$
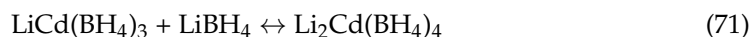
The **$Li_2Cd(BH_4)_4$** precipitated as an adduct with four molecules of diglyme [171]. The ball milling of $MBH_4/CdCl_2$, M = Li, Na, K, in several molar ratios (1:1 to 4:1) only succeeded in producing **$KCd(BH_4)_3$** and **$K_2Cd(BH_4)_4$** [167]. The last product, $K_2Cd(BH_4)_4$, is composed of tetrahedral $[Cd(BH_4)_4]^{-2}$ ions and eight-coordinated K^+ cations. $KCd(BH_4)_3$ has a structure that can be considered a framework intermediate between those of α-$Cd(BH_4)_2$ and β-$Cd(BH_4)_2$ [167]. Decomposition of the K-Cd borohydrides was proposed to be sequential [167]:

$$2KCd(BH_4)_3 \rightarrow K_2Cd(BH_4)_4 + Cd + B_2H_6 + H_2, \sim353 \text{ K} \tag{72}$$

$$K_2Cd(BH_4)_4 \rightarrow 2KBH_4 + Cd + B_2H_6 + H_2, \sim358 \text{ K} \tag{73}$$

For the last element in group 12, i.e., Hg, Nöth mentioned that the reaction of $LiBH_4$ with $HgCl_2$ at 195 K produced a reduction in Hg without the formation of mercury borohydride [166].

5. Main-Group Borohydrides

5.1. Group 13: Aluminum, Gallium, Indium, and Thallium

$Al(BH_4)_3$ is an "old" borohydride which has been known since 1939 [172,173]. Its standard formation enthalpy is 301.6 kJ/mol liquid $Al(BH_4)_3$ [174]. It is a very hazardous and volatile liquid at room temperature (melting point ~208 K), with an average heat of vaporization of 29.9 kJ/mol [173] that detonates on contact with air containing traces of moisture [175]. $Al(BH_4)_3$ can be produced by reactions (74) and (75) [172,173,175], and recovered by proper condensing (cooling) of the volatile product:

$$Al_2(CH_3)_6 + 4B_2H_6 \rightarrow 2B(CH_3)_3 + 2Al(BH_4)_3, 178\text{-}353 \text{ K} \tag{74}$$

$$AlX_3 + 3MBH_4 \rightarrow Al(BH_4)_3\uparrow + 3MX, X = \text{Cl or Br}, M = \text{Li, Na or K} \tag{75}$$
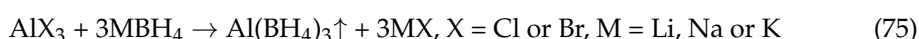
$Al(BH_4)_3$ was used to prepare other borohydrides (Th, U, Hf, Ti, etc.) in the 1940s [72]. Many years later, the low temperature α- and β-$Al(BH_4)_3$ crystalline structures were discovered (Table 9) [176]: α-$Al(BH_4)_3$ presents a monoclinic space group $C2/c$, while β-$Al(BH_4)_3$ presents an orthorhombic space group of $Pna2_1$. Both polymorphs are composed of discrete molecular $Al(BH_4)_3$ units. The α- to β-$Al(BH_4)_3$ phase change occurs between 180 and 195 K [176]. In 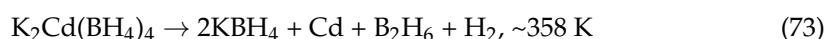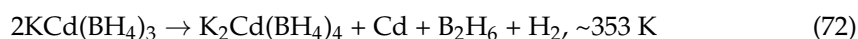the gas phase, $Al(BH_4)_3$ presents a D_{3h} symmetry with a planar Al-B_3 skeleton and η^2-$[BH_4]^{-1}$ ligands [176–180]. The heats of formation were calculated in 2006 by first principles, as −132 kJ/mol and −131 kJ/mol (without zero-point correction) for α- and β-$Al(BH_4)_3$, respectively [181]. The calculations also demonstrated the non-metallic nature of α-$Al(BH_4)_3$, with a calculated band gap of 6.0 eV [181]. Decomposition of $Al(BH_4)_3$ was predicted to be a spontaneous process above approximately 400 K, occurring with the release of B_2H_6 [70], but the experimentally observed decomposition occurred at room temperature [172,173]. In 2016, Harrison et al. proposed reducing diborane production, at least theoretically, by including a second cation, as in $Al_{1-x}Sc_x(BH_4)_3$ [182].

Thermal stabilization was achieved by the formation of double cation borohydrides of Al with group 1 alkali metals, i.e., the formation of $[Al(BH_4)_4]^{-1}$ ions [183,184]. $MAl(BH_4)_4$, M = Li, Na, K, Rb, and Cs, can be produced by the following reaction [184]:

$$Al(BH_4)_3 + MBH_4 \rightarrow MAl(BH_4)_4 \tag{76}$$

Table 9. Crystal structures of Al-borohydrides.

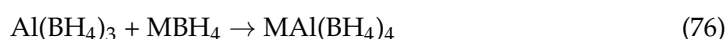| Material and Hydrogen Content [wt.%]	Structural Parameters [Å, °]	Atomic Positions	References and Comments
α-Al(BH$_4$)$_3$ 16.91	Space group: monoclinic *C2/c* (15) a = 21.917(4), b = 5.9860(12), c = 21.787(4) α = 90, β = 111.90(3), γ = 90	**Al:** 0.3795(2), 0.5901(7), 0.8361(2). **B1:** 0.3206(8), 0.3030(32), 0.8238(9). **H1A:** 0.3757(22), 0.2993(63), 0.8366(46). **H1B:** 0.3013(20), 0.4814(73), 0.8173(47). **H1C:** 0.3027(47), 0.2727(183), 0.8584(38). **H1D:** 0.3046(48), 0.2249(160), 0.7796(31). **B2:** 0.3866(8), 0.7476(31), 0.7508(8). **H2A:** 0.4169(33), 0.5987(109), 0.7778(30). **H2B:** 0.3557(34), 0.8117(91), 0.7806(28). **H2C:** 0.3642(41), 0.7334(182), 0.7017(23). **H2D:** 0.4205(40), 0.8679(136), 0.7655(48). **B3:** 0.4304(8), 0.7262(30), 0.9308(8). **H3A:** 0.3763(23), 0.7595(127), 0.9008(25). **H3B:** 0.4537(21), 0.6121(126), 0.9038(25). **H3C:** 0.4382(48), 0.6799(171), 0.9768(28). **H3D:** 0.4517(46), 0.8796(97), 0.9376(49)	[176] CCDC (Cambridge Crystallographic Data Centre) identification number 230830
β-Al(BH$_4$)$_3$ 16.91	Space group: orthorhombic *Pna2* (33) a = 18.021(3), b = 6.138(2), c = 6.1987(14) α = β = γ = 90	**Al:** 0.86775(6), 0.1592(2), 0.20350(9). **B1:** 0.7780(5), 0.0040(15), 0.0503(15). **H1:** 0.8398(18), −0.0226(76), 0.0215(80). **H1B:** 0.7744(19), 0.1321(67), 0.1790(80). **H1C:** 0.7576(29), −0.1277(74), 0.1214(93). **H1D:** 0.7568(32), 0.0678(98), −0.0833(79). **B2:** 0.9113(5), 0.0203(17), 0.4915(15). **H2:** 0.9320(23), −0.0107(69), 0.3238(56). **H2B:** 0.8667(21), 0.1458(67), 0.4853(78). **H2C:** 0.9534(26), 0.0912(84), 0.5627(93). **H2D:** 0.8887(32), −0.1166(69), 0.5420(101). **B3:** 0.9122(5), 0.4460(15), 0.0629(21). **H3A:** 0.8716(23), 0.4427(57), 0.1979(76). **H3B:** 0.9300(25), 0.2732(53), 0.0287(83). **H3C:** 0.9542(26), 0.5038(87), 0.1428(94). **H3D:** 0.8912(33), 0.4975(103), −0.0728(77)	[176] CCDC (Cambridge Crystallographic Data Centre) identification number 230829
Li$_4$Al$_3$(BH$_4$)$_{13}$ 17.37	Space group: cubic *P-43n* (218) a = b = c = 11.3640(3) Å α = β = γ = 90	**Li:** 0.1315(11), 0.1315(11), 0.1315(11). **B1:** 0, 0, 0. **H11:** 0.9424(5), 0.9424(5), 0.9424(5). **Al:** $\frac{1}{4}$, $\frac{1}{2}$, 0. **B2:** 0.1731(5), 0.6680(5), 0.4547(4). **H21:** 0.1892(15), 0.6358(15), 0.3636(8). **H22:** 0.1595(15), 0.7671(6), 0.4548(15). **H23:** 0.0876(10), 0.6266(14), 0.4893(15). **H24:** 0.2463(11), 0.6455(15), 0.5176(12)	At 100 K Rietveld refinement [186]
KAl(BH$_4$)$_4$ 12.85	Space group: orthorhombic Fddd (70) a = 9.7405(3), b = 12.4500(4), c = 14.6975(4) α = β = γ = 90	**K:** 0.125, 0.125, 0.125. **Al:** 0.375, 0.375, 0.375. **B:** 0.7760(4), 0.6939(3), 0.7263(3). **H1:** 0.6927(10), 0.7372(10), 0.6864(8). **H2:** 0.7559(12), 0.7164(11), 0.7984(5). **H3:** 0.7654(12), 0.6077(5), 0.7198(8). **H4:** 0.8767(8), 0.7204(8), 0.7007(8)	[185]

Reaction (76) was obtained by transferring the liquid Al(BH$_4$)$_3$ into the vessel that contains solid MBH$_4$, and further purification was achieved by evaporation of the newly formed aluminum borohydride [185]. **Li$_4$Al$_3$(BH$_4$)$_{13}$** was always produced as a side product of reaction (76) when using LiBH$_4$ [184]. Li$_4$Al$_3$(BH$_4$)$_{13}$ can be considered a decomposition product of **LiAl(BH$_4$)$_4$** because, upon the heating of LiAl(BH$_4$)$_4$ at 333 K, the following reaction occurs [184]:

$$4\text{LiAl(BH}_4)_4 \rightarrow \text{Li}_4\text{Al}_3(\text{BH}_4)_{13} + \text{Al(BH}_4)_3 \tag{77}$$

Li$_4$Al$_3$(BH$_4$)$_{13}$ can also be produced by the following reaction (under ball-milling with careful temperature and pressure monitoring) [186]:

$$3\text{AlCl}_3 + 13\text{LiBH}_4 \rightarrow \text{Li}_4\text{Al}_3(\text{BH}_4)_{13} + 9\text{LiCl} \tag{78}$$
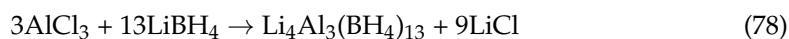
The crystal structures of LiAl(BH$_4$)$_4$ and Li$_4$Al$_3$(BH$_4$)$_{13}$ are monoclinic *P2$_1$/c* and cubic *P-43n*, respectively (Table 9) [184]. The crystal structure of Li$_4$Al$_3$(BH$_4$)$_{13}$ is composed of

the complex cation $[(BH_4)Li_4]^{+3}$ and the $[Al(BH_4)_4]^{-1}$ anion [186]. The decomposition of $Li_4Al_3(BH_4)_{13}$ occurred at 363 K, producing more $Al(BH_4)_3$ and $LiBH_4$ [184,186,187].

NaAl(BH$_4$)$_4$ was briefly mentioned by Dovgaliuk et al.; this material crystallized in the monoclinic space group *C2/c* and decomposed at 363 K to produce the parent Na and Al borohydrides [184]. **KAl(BH$_4$)$_4$** can be produced by direct contact of K and Al borohydrides at room temperature [185,188]:

$$KBH_{4\,(s)} + Al(BH_4)_{3\,(l)} \rightarrow KAl(BH_4)_{4\,(s)} \tag{79}$$

Reaction (79) was reported to occur slowly for several days under high precautions due to the reactivity of $Al(BH_4)_3$ [188]. $KAl(BH_4)_4$ crystallized in the orthorhombic *Fddd* space group, where the $[Al(BH_4)_4]^{-1}$ anion forms distorted tetrahedra [185].

Thermal decomposition of $KAl(BH_4)_4$ begins at 427 K, with a separation into the original borohydrides and an enthalpy of 36 kJ/mol [188]. Then, the decomposition of $Al(BH_4)_3$ was proposed to occur as [188]:

$$Al(BH_4)_{3\,(g)} \rightarrow AlH(BH_4)_{2\,(s)} + 0.5B_2H_{6\,(g)} \tag{80}$$

$$AlH(BH_4)_{2\,(s)} \rightarrow AlH_2(BH_4)_{(s)} + 0.5B_2H_{6\,(g)} \tag{81}$$

$$AlH_2(BH_4)_{\,(s)} \rightarrow Al_{(s)} + 0.5B_2H_{6\,(g)} + 1.5H_2 \tag{82}$$

$$0.5B_2H_{6\,(g)} \rightarrow (BH)_{n\,(s)} + H_2 \tag{83}$$
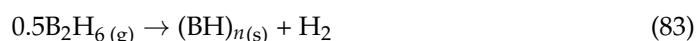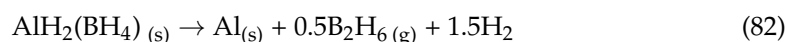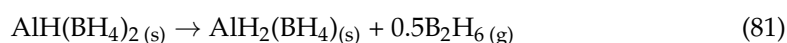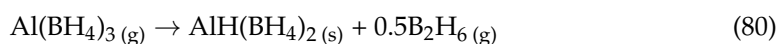
For their part, Dovgaliuk et al. proposed a one-step dehydrogenation of $KAl(BH_4)_4$ at 433 K (maximum DSC peak) [185]:

$$2KAl(BH_4)_4 \rightarrow KBH_4 + KAl_2B_3 + 2B_2H_6 + 8H_2 \tag{84}$$
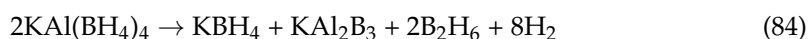
Reaction (84) was proposed based on the combined results of several characterization techniques [185]. The decomposition product KAl_2B_3 is an amorphous material [185]. Decomposition of KBH_4 must occur at higher temperatures. No re-hydrogenation was achieved up to 10 MPa hydrogen pressure and 593 K [185].

RbAl(BH$_4$)$_4$ *(orthorhombic Fddd)* and **CsAl(BH$_4$)$_4$** (tetragonal *I4$_1$/amd*) were also briefly mentioned by Dovgaliuk et al.; these materials decomposed at 433 K and 423 K, respectively [184].

Homoleptic gallium borohydride does not exist. However, the related compounds, **GaH(BH$_4$)$_2$** and **GaH$_2$(BH$_4$)**, were reported in [189,190]. $GaH(BH_4)_2$ can be produced in the absence of solvent at 228 K with an excess of $LiBH_4$ [189,191,192]:

$$GaCl_3 + 3LiBH_4 \rightarrow GaH(BH_4)_2 + 3LiCl + \frac{1}{2}B_2H_6, \, 228\,K \tag{85}$$

or

$$HGaCl_2 + 2LiBH_4 \rightarrow GaH(BH_4)_2 + 2LiCl, \, 228\,K \tag{86}$$
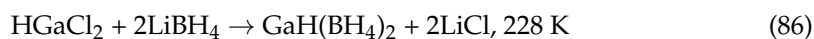
These reactions are globally similar to the $GaH_2(BH_4)$ synthesis [190]:

$$\frac{1}{2}(H_2GaCl)_2 + LiBH_4 \rightarrow GaH_2(BH_4) + LiCl, \, 250\,K, \tag{87}$$
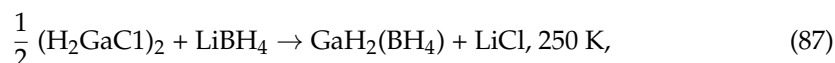
$GaH(BH_4)_2$ is volatile (melting point at approximately 203 K and vapor pressure of 10 mmHg at 228 K [189]), unstable, and decomposes above 228 K [189]. $GaH_2(BH_4)$ is also unstable and decomposes upon heating [190]. Decomposition products of both compounds are Ga, H_2, and B_2H_6 [189,190].

In(BH$_4$)$_3$ was reported in 1957, and this borohydride was obtained by the reaction in ether at 228 K [193]:

$$InR_3 + (3 + 3/n)BH_3 \rightarrow In(BH_4)_3 + (3/n)BH_{3-n}R_n, \, R = methyl \tag{88}$$
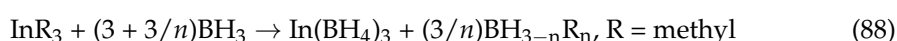
This reaction is slow (2 days). Another option (less efficient) is the following reaction in ether at 248 K [193]:

$$InCl_3 + 3LiBH_4 \rightarrow In(BH_4)_3 + 3LiCl \tag{89}$$
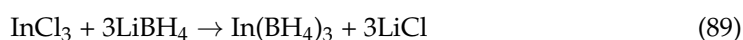
In(BH$_4$)$_3$ crystalized as In(BH$_4$)$_3$·3THF at 233 K and as In(BH$_4$)$_3$·2THF at 243 K, and decomposed at 263 K to produce metallic indium, hydrogen, and borane [193].

TlBH$_4$ was reported in 1957 [194]; no additional reports have been located. TlBH$_4$ was synthesized by the reaction between thallium ethylate and lithium borohydride in ether at room temperature [194]:

$$TlOR + LiBH_4 \rightarrow TlBH_4 + LiOR \tag{90}$$

Purification of the TlBH$_4$ was not possible, and decomposition of the whole mixture, TlBH$_4$ + LiOR, was registered at 423 - 443 K [194]. The homoleptic borohydride of Tl(III) cannot be prepared, even at a low temperature; instead, TlCl(BH$_4$)$_2$ was produced at 163 K [195]:

$$TlCl_3 + 2LiBH_4 \rightarrow TlCl(BH_4)_2 + 2LiCl \tag{91}$$
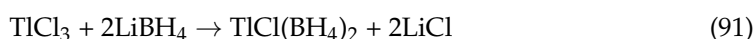
TlCl(BH$_4$)$_2$ decomposed at 178 K producing hydrogen, borane, and TlCl [195].

5.2. Group 14: Lead

CsPb(BH$_4$)$_3$ and **CsPb(BH$_4$)$_2$Cl** were briefly described in a recent report [69]. CsPb(BH$_4$)$_3$ is a semiconducting borohydride with an experimental band gap of ~1.5 eV at RT. CsPb(BH$_4$)$_3$ releases 4.3 wt%. hydrogen at 360 K [69].

6. Rare Earth Metal Borohydrides

In 1959, a report described the reactions between RE(OCH$_3$)$_3$, RE = Y, Sm, Eu, Gd, Td, Dy, Ho, Er, Tm, Yb, and Lu, with diborane in THF [51]. The products were solvated borohydrides, RE(BH$_4$)$_3$. As stated in the introductory section, the synthesis of these borohydrides currently follows a new approach in the sense of combining mechanical milling with solvent extraction, solvent and reactant function of precursors, or the use of mixtures of solvents to extract products selectively. As the products are frequently solvated, the release of solvent molecules such as S(CH$_3$)$_2$ has been confirmed by TGA/DSC or in-situ diffraction characterization. However, some materials cannot be dried without decomposing. Additionally, the emission of some B$_2$H$_6$ is also observed during heating to temperatures close to those of solvent release. Besides decomposition, the release of B$_2$H$_6$ could be related to occluded impurities from the synthesis process. Stadie et al. demonstrated that the elimination of solvents and B-H impurities with supercritical N$_2$ processing (roughly, exposing to liquid N$_2$ at 110 K and 2 MPa and degassing several times) practically eliminated B$_2$H$_6$ release from Mg(BH$_4$)$_2$ [196]. Another issue to be noticed is that the metathesis reaction between RECl$_3$ and LiBH$_3$ frequently leads to the formation of mixtures of RE(BH$_4$)$_3$, LiRE(BH$_4$)$_4$ and LiRE(BH$_4$)$_3$Cl [197]. The relative amount of these products might depend on synthesis conditions, such as the excess of reactants or milling time and temperature [198].

6.1. Lanthanides

La(BH$_4$)$_3$ was produced by mechanical milling of anhydrous LaCl$_3$ and LiBH$_4$ using different milling times (1 to 48 h) [199]. Zhang et al. indicated that a similar reaction with LaF$_3$ was not as responsive as with LaCl$_3$ [199]. The dehydrogenation of these mixtures indicated a multistep process; the main dehydrogenation event occurred at approximately 523 K for the LaCl$_3$ precursor and 573 K for LaF$_3$ [199]. The difference was explained by the formation of La(BH$_4$)$_3$ in the first case and the in-situ reaction between LiBH$_4$ and LaF$_3$ in the second case [199]. In both cases, the dehydrogenation products were LaH$_2$, LaB$_6$, H$_2$, and LiCl or LiF, respectively. Standard dehydrogenation enthalpies were estimated as 48.2 and 49.3 kJ/mol H$_2$, respectively [199]. Partial hydrogen uptake of the dehydrogenated

materials was observed (at 623 K or 723 K, 10 MPa, 24 h) [199]. Recently, pure La(BH$_4$)$_3$ was produced by the reaction of (pre-milled) LaCl$_3$ and LiBH$_4$ in toluene with further solvent extraction with S(CH$_3$)$_2$ [200]. Using EtO$_2$ as a solvent or by means of ball-milling, the mixed compound LiLa(BH$_4$)$_3$Cl was produced [200]. La(BH$_4$)$_3 \cdot n$S(CH$_3$)$_2$ released S(CH$_3$)$_2$ upon heating between 333 and 382 K and hydrogen at 531 K [200]. In general, LiLa(BH$_4$)$_3$X, X = Cl, Br, and I, can be produced and possess high Li-conductivity [201].

NaLa(BH$_4$)$_4$ was obtained by the reaction between pure La(BH$_4$)$_3$ and NaBH$_4$, induced by ball-milling [202]. However, the same procedure using LiBH$_4$ does not give LiLa(BH$_4$)$_4$ [202]. Any remaining La(BH$_4$)$_3$ and NaBH$_4$ continue to react between 355 and 463 K and 0.1 MPa argon pressure to form more NaLa(BH$_4$)$_4$ [202]. NaLa(BH$_4$)$_4$ crystallizes in orthorhombic space group *Pbcn* (Table 10) [202]. NaLa(BH$_4$)$_4$ decomposed in several steps, starting at 413–483 K with the release of the remaining solvent (dimethyl sulfide) and some diborane (as read from the TGS-DSC-MS plot in ref. [202]). The subsequent (proper) dehydrogenation reactions can be summarized as [202]:

$$\text{NaLa(BH}_4)_4 \rightarrow \text{La(BH}_4)_3 + \text{NaBH}_4, \text{ 463-483K} \tag{92}$$

$$\text{La(BH}_4)_3 \rightarrow \frac{1}{2}\text{LaH}_2 + \frac{1}{2}\text{LaB}_6 + 11/2\ \text{H}_2, \text{ 538-623 K} \tag{93}$$
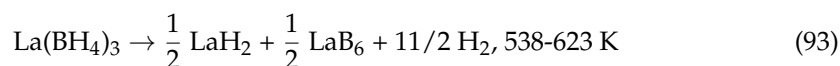
Partial reversibility was achieved by the re-formation of NaBH$_4$ at 10 MPa hydrogen pressure, and up to 723 K [202].

K$_3$La(BH$_4$)$_6$ was produced by the same procedure as NaLa(BH$_4$)$_4$, i.e., the addition reaction between La(BH$_4$)$_3$ and 3KBH$_4$, assisted by ball-milling [202]. K$_3$La(BH$_4$)$_6$ and NaLa(BH$_4$)$_4$ behave in a similar way [202]. K$_3$La(BH$_4$)$_6$ crystallized in a monoclinic *P2$_1$/n* (Table 10), double-perovskite structure (Figure 7), and also decomposed at 532–563 K into the precursor borohydrides (La(BH$_4$)$_3$ and KBH$_4$) [202].
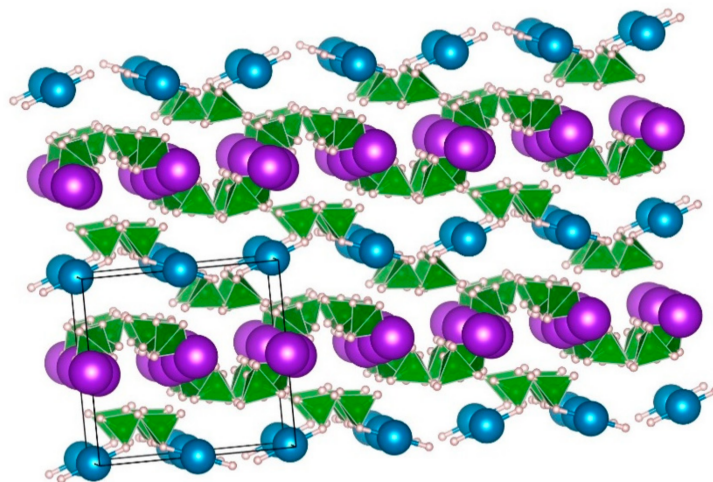
Figure 7. Crystal structure of K$_3$La(BH$_4$)$_6$. Detailed crystal structure can be found in Table 10.

At these temperatures, the decomposition of La(BH$_4$)$_3$ is immediate (Equation (93)) [202]. Between 573 and 673 K, a reaction between LaH$_2$ (the decomposition product of La(BH$_4$)$_3$) and KBH$_4$ occurred:

$$\frac{1}{2}\text{LaH}_2 + 3\text{KBH}_4 \rightarrow 3\text{KH} + 1/2\text{LaB}_6 + 5\text{H}_2 \tag{94}$$
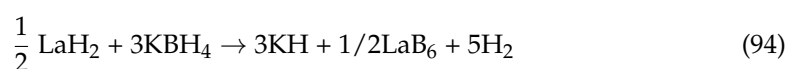
Partial reversibility was also observed in this case, with the hydrogenation reaction being attributed to the reverse reaction of (94) at 10 MPa H$_2$-pressure and 723 K [202].

Li$_3$K$_3$La$_2$(BH$_4$)$_{12}$ was observed due to the contamination with small quantities of LiBH$_4$ during the synthesis of K$_3$La(BH$_4$)$_6$ [202]. The crystal structure of Li$_3$K$_3$La$_2$(BH$_4$)$_{12}$ was reported in [202] (Table 10). Li$_3$K$_3$La$_2$(BH$_4$)$_{12}$ is a ionic Li$^+$ conductor (6 × 10^{-7} S/cm) [203].

Table 10. Crystal structures of La-borohydrides.

Material and Hydrogen Content [wt.%]	Structural Parameters [Å, °]	Atomic Positions	Comments
NaLa(BH$_4$)$_4$ 7.29	Space group: orthorhombic *Pbcn* (60) a = 6.79865, b = 17.31073, c = 7.26547 α = β = γ = 90.00	**Na:** 0.50044, 0.07200, 0.75028. **La:** 0.00006, 0.17197, 0.24971. **B:** 0.26676, 0.43014, 0.88057. **H1:** 0.34758, 0.36477, 0.88347. **H2.** 0.24611, 0.45458, 1.03337. **H3:** 0.10366, 0.42625, 0.80070. **H4:** 0.37496, 0.47548, 0.79356. **B:** 0.75157, 0.19400, 0.51886. **H1:** 0.63613, 0.20423, 0.38704. **H2:** 0.70323, 0.13930, 0.60198. **H3:** 0.74575, 0.25066, 0.62265. **H4:** 0.92434, 0.18235, 0.45697	[202]. NaLa(BH$_4$)$_4$ is isostructural to NaCe(BH$_4$)$_4$ and NaPr(BH$_4$)$_4$ [204]
K$_3$La(BH$_4$)$_6$ 7.01	Space group: monoclinic *P2$_1$/n* (14) a = 7.93840, b = 8.35246, c = 11.57068 α = γ = 90, β = 90.18977	**K1:** 0.5, 0.5, 0.5. **K2:** 0.47777, 0.05175, 0.25048. **La:** 0, 0, 0.5. **B1:** 0.34697, 0.83332, 0.0777. **H1:** 0.40173, 0.79562, 0.16487. **H2:** 0.28607, 0.95646, 0.08622. **H3:** 0.45213, 0.83873, 0.01072. **H4:** 0.24803, 0.74232, 0.04903. **B2:** 0.16081, 0.32239, 0.07051. **H1:** 0.09016, 0.29934, 0.15464. **H2:** 0.23328, 0.43994, 0.07762. **H3:** 0.25285, 0.21998, 0.05400. **H4:** 0.06681, 0.33015, −0.00418. **B3:** 0.63098, 0.43325, 0.22717. **H1:** 0.72435, 0.37192, 0.28787. **H2:** 0.55241, 0.52310, 0.27813. **H3:** 0.70283, 0.49845, 0.15596. **H4:** 0.54446, 0.33942, 0.18673	[202]
Li$_3$K$_3$La$_2$(BH$_4$)$_{12}$ 8.14	Space group: cubic *Ia-3d* (230) a = 17.60563, b = 17.60563, c = 17.60563 α = β = γ = 90	**K:** 0.25, 0.8750, 0.5. **Li:** 0.3750, 0, 0.25. **La:** 0.5, 0, 0. **B:** 0.4, 0.7, 0.28. **H1:** 0.36161, 0.75067, 0.28790. **H2:** 0.45847, 0.71997, 0.26308. **H3:** 0.40365, 0.66722, 0.33496. **H4:** 0.37619, 0.66215, 0.23408	[202]

Ce(BH$_4$)$_3$ was also produced by mechanical milling of anhydrous CeCl$_3$ and LiBH$_4$ for different milling times (1 to 48 h) [199]. The behavior of Ce(BH$_4$)$_3$ is very similar to La(BH$_4$)$_3$ [199]: CeF$_3$ was not as reactive as LaCl$_3$, and dehydrogenation of these mixtures indicates a multistep process; the main dehydrogenation event occurred at approximately 498 K for the CeCl$_3$ precursor and 563 K for CeF$_3$. The difference was also explained by the formation of Ce(BH$_4$)$_3$ in the first case, and the in-situ reaction between LiBH$_4$ and CeF$_3$ in the second case [199]. In both cases, the dehydrogenation products were CeH$_2$, CeB$_6$, H$_2$, and LiCl or LiF. Standard dehydrogenation enthalpies were estimated as 23.2 and 25.6 kJ/mol H$_2$, respectively [199]. A partial hydrogen uptake of the dehydrogenated materials was observed (623 K or 723 K, 10 MPa, 24 h) [199]. Gennari et al. reported the production of Ce(BH$_4$)$_3$ by the mechanical ball-milling of CeCl$_3$ + 3LiBH$_4$ [205]. Ce(BH$_4$)$_3$ (plus LiCl) desorbed hydrogen in three endothermic events at approximately 503, 533, and 533 K (as read from DSC curves in [205]). The proposed global dehydrogenation products are CeH$_2$, B or CeB$_6$, and H$_2$, with Ce$_2$(B$_{12}$H$_{12}$)$_3$ as an intermediary [205]. Ce(BH$_4$)$_3$ was also produced in the same way as La(BH$_4$)$_3$, i.e., in toluene with further solvent extraction with S(CH$_3$)$_2$ [200]. Ce(BH$_4$)$_3$, as La(BH$_4$)$_3$, crystalizes in rhombohedral (r-) (Figure 3) and cubic

(c-) polymorphs, Table 11 [200]. $Ce(BH_4)_3$ released ~6 wt% between 473 K and 573 K, with an endothermic peak at 524 K, and simultaneous H_2 and B_2H_6 release [200]. **LiCe(BH$_4$)$_3$Cl** was produced as a by-product, and it is reported to have Li-ion conductivity [200].

Table 11. Crystal structures of Ce-borohydrides.

Material and Hydrogen Content [wt.%]	Structural Parameters [Å, °]	Atomic Positions	Comments
r-Ce(BH$_4$)$_3$ 6.55	Space group: trigonal *R-3c* (167) a = b = 7.3745(1), c = 20.1567(2) α = β = 90, γ = 120	**Ce:** 0, 0, 0. **B:** 0.632(2), 0, $\frac{1}{4}$. **H1:** 0.461(2), −0.094(5), 0.261(2). **H2:** 0.759(2), 0.026(5), 0.288(2)	[200]. Isostructural to r-La(BH$_4$)$_3$
c-Ce(BH$_4$)$_3$ 6.55	Space group: cubic *Fm-3c* (226) a = b = c = 11.7106(6) α = β = γ = 90	**Ce:** 0, 0, 0. **B:** 0, 0, $\frac{1}{4}$. **H:** 0, 0.4075(1), 0.3104(1)	[200]. Isostructural to c-La(BH$_4$)$_3$
NaCe(BH$_4$)$_4$ 7.25	Space group: orthorhombic *Pbcn* (60) a = 6.8028(5), b = 17.5181(13), c = 7.2841(5) α = β = γ = 90	**Na1:** 0.50044, 0.0720, 0.75028. **Ce2:** 0.00006, 0.17197, 0.24971. **B3:** 0.26676, 0.43014, 0.88057. **H14:** 0.34758, 0.36477, 0.88347. **H15:** 0.24611, 0.45458, 0.03337. **H16:** 0.10366, 0.42625, 0.80070. **H17:** 0.37496, 0.47548, 0.79356. **B8:** 0.75157, 0.1940, 0.51886. **H19:** 0.63613, 0.20423, 0.38704. **H110:** 0.70323, 0.13930, 0.60198. **H111:** 0.74575, 0.25066, 0.62265. **H112:** 0.92434, 0.18235, 0.45697	[204]
Li$_3$K$_3$Ce$_2$(BH$_4$)$_{12}$ 8.11	Space group: cubic *Ia-3d* (230) a = 17.60756(4), b = 17.60756(4), c = 17.60756(4) α = β = γ = 90	**Ce:** 0.5, 0, 0. **K:** 0.25, 0.8750, 0.5. **B:** 0.39971, 0.70333, 0.28374. **H13:** 0.3513, 0.68574, 0.32305. **H14:** 0.40777, 0.76754, 0.28684. **H15:** 0.45434, 0.67373, 0.30222. **H16:** 0.38538, 0.68622, 0.22287. **Li:** 0.3750, 0, 0.25	[203]

NaCe(BH$_4$)$_4$ was produced by mechanical milling of $Ce(BH_4)_3$ and $NaBH_4$, and the milling was performed with careful control of the milling time and pauses [204]. $Ce(BH_4)_3$ was produced first as described above, and then used to produce $NaCe(BH_4)$. The $NaCe(BH_4)_4$ is isostructural to $NaLa(BH_4)_4$ [204] (Table 11). Heating of the ball-milled mixture of $Ce(BH_4)_3$ and $NaBH_4$ induced the supplementary addition reaction between the (initially unreacted) $Ce(BH_4)_3$ and $NaBH_4$ at approximately 373 K [204]. The maximum amount of $NaCe(BH_4)_4$ occurred at 446–460 K [204]. However, the presence of two unknown compounds that might be solvates of Ce-borohydride was reported [204]. The release of solvents $(S(CH_3)_2)$, B_2H_6, and H_2 occurred over a narrow temperature range, 453–498 K, with a second release of B_2H_6 and H_2 at 523 K (as read from TGA-DSC-MS plots) [204]. The decomposition of $NaCe(BH_4)_4$ is understood to first form Ce- and Na-borohydrides [204].

K$_3$Ce(BH$_4$)$_6$ ($P2_1/n$ [22]) was briefly mentioned as a by-product of the synthesis of $Li_3K_3Ce_2(BH_4)_{12}$ [203]. **Li$_3$K$_3$Ce$_2$(BH$_4$)$_{12}$** is an ionic Li$^+$ conductor; its bulk conductivity was reported to be nearly seven orders of magnitude higher (3×10^{-7} S/cm) than in $Li_3Tb_3Te_2O_{12}$ (Table 11) [203]. Its conductivity is explained by a "paddle-wheel" (combined size and ionic dynamical disorder) effect of the $[BH_4]^{-1}$ on Li$^+$ [203]. Li substitution by Na, K, or Rb, Ce substitution by Ca, Sr or Eu, or $[BH_4]^{-1}$ substitution by Cl$^-$ could modify the conductivity properties [203]. As stated in the introductory section, borohydrides might be an option in batteries, providing high ionic conductivity at room temperature. Thus, ionic conductivity is studied and data are reported recently [206]. However, we must perform a brief parenthesis to link ion conductivity (ion mobility) to dehydrogenation properties.

Wu proposed that tuning the mobility of small ions can help to improve the hydrogen storage properties of metal hydride materials, as do particle size reduction, catalyst, or destabilization [207]. Luo et al. proposed that ionic conductivity is influenced by ionic radius and structure [206]. Wu describes that materials with a perovskite structure might accelerate hydrogen mobility [207], while Davies et al. [208] and Anderson et al. [209] suggest that halide substitution in amide materials improves ionic conductivity and hydrogen release properties. Unfortunately, not enough data on borohydrides are available to perform a correlation.

Rb$_3$Ce(BH$_4$)$_6$ (monoclinic *P2$_1$/n*) was briefly mentioned in a recent report [69].

The formation of reactive hydride composites of Ce-Li was studied by Gennari et al. [210]. They produced, using mechanical milling, the following mixture [210]:

$$6LiBH_4 + CeCl_3 \rightarrow Ce(BH_4)_3 + 3LiCl + 3LiBH_4 \tag{95}$$

The mixture decomposed in a multistep pathway starting at 493 K and going up to 673 K [210]. The mixture presented partial reversibility at 673 K and 6 MPa. After the second dehydrogenation, the products included CeB$_6$, CeH$_2$, CeB$_4$, LiH, and H$_2$, with the first two being confirmed by X-ray diffraction [210].

Pr(BH$_4$)$_3$ was reported recently; this material was produced by the reaction of pre-milled PrH$_3$ with S(CH$_3$)BH$_3$ in toluene, with further extraction/purification with DMS and drying [31]. LiPr(BH$_4$)$_3$Cl can also be produced during the synthesis of Pr(BH$_4$)$_3$ when using LiBH$_4$ and PrCl$_3$ as precursors [211]. Pr(BH$_4$)$_3$ presents different phases when heated under hydrogen pressure (4 MPa): α-, β-, β′-, β″-, and r- Pr(BH$_4$)$_3$ (Table 12). α-Pr(BH$_4$)$_3$ is stable at room temperature and isostructural to α-Y(BH$_4$)$_3$ and α-Gd(BH$_4$)$_3$. β-Pr(BH$_4$)$_3$ appeared along with α-Pr(BH$_4$)$_3$ during the drying of Pr(BH$_4$)$_3$·S(CH$_3$)$_2$, i.e., from the solvated material. β-Pr(BH$_4$)$_3$ is a high-pressure polymorph (4 MPa H$_2$ pressure and 463 K) [31]. At ~449 K, β-Pr(BH$_4$)$_3$ transformed to β′-Pr(BH$_4$)$_3$, with contraction of the unit cell. At 463 K, a further contraction of the β′-phase occurred, producing β″-Pr(BH$_4$)$_3$ [31]. Further heating produces the disappearance of α-Pr(BH$_4$)$_3$ and the emergence of r-Pr(BH$_4$)$_3$. The decomposition of Pr(BH$_4$)$_3$ was registered at 520 K, with practically no B$_2$H$_6$ evolution; the reaction is [31]:

$$2Pr(BH_4)_3 \rightarrow PrB_6 + PrH_2 + 11H_2 \tag{96}$$
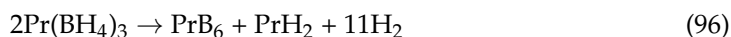
NaPr(BH$_4$)$_4$ was produced by the addition reaction between NaBH$_4$ and halide-free Pr(BH$_4$)$_3$. The addition reaction was carried out by ball-milling, with careful control of the milling time/pause [204]. NaPr(BH$_4$)$_4$ crystallizes in an orthorhombic unit cell (*Pbcn*), and is isostructural to NaLa(BH$_4$)$_4$ (Table 12) [204]. In-situ diffraction studies during heating of the NaBH$_4$ and Pr(BH$_4$)$_3$ mixture, i.e., NaPr(BH$_4$)$_4$, demonstrated the formation of two unidentified crystalline materials and the decrease in intensity of NaPr(BH$_4$)$_4$ XRD reflections at about 463 K (as read from an in-situ synchrotron radiation x-ray diffraction pattern) [204]. Further heating led to the decomposition of the unidentified materials. Partial reversibility (low hydrogenation levels over several cycles) was achieved in this material [204].

Table 12. Crystal structures of Pr-borohydrides.

Material and Hydrogen Content [wt.%]	Structural Parameters [Å, °]	Atomic Positions	References and Comments
α-Pr(BH$_4$)$_3$ 6.52	Space group: cubic *Pa-3* (205) a = b = c = 11.2941(5) α = β = γ = 90	**Pr:** 0.2179, 0.2179, 0.2179. **B:** 0.1930, 0.2473, 0.9682. **H13:** 0.2909, 0.2534, 0.0243. **H14:** 0.1043, 0.2257, 0.0351. **H15:** 0.1752, 0.3475, 0.9192. **H16:** 0.2014, 0.1623, 0.8942	[31]
β-Pr(BH$_4$)$_3$ β´-Pr(BH$_4$)$_3$ β´´-Pr(BH$_4$)$_3$ 6.52	Space group: cubic *Fm-3c* (226) a = b = c = 11.458(2) a = b = c = 11.3283(6) a = b = c = 11.1438(2) α = β = γ = 90	**Pr:** 0, 0, 0. **B:** 0, 0, 0.25. **H13:** 0, 0.4069, 0.3116	[31]
r -Pr(BH$_4$)$_3$ 6.52	Space group: trigonal *R-3c* (167) a = b = 7.373(6), c = 19.89(2) α = β = 90, γ = 120	**Pr:** 0, 0, 0. **B:** 0.6202(2), 0, 0.25. **D13:** 0.4835(4), −0.1056(10), 0.2881(1). **D14:** 0.7699(3), 0.1072(8), 0.2834(1)	[31]
NaPr(BH$_4$)$_4$ 7.22	Space group: orthorhombic *Pbcn* (60) a = 6.7617(2), b = 17.4679(7), c = 7.2523(3) α = β = γ = 90.00	**Na:** 0.50044, 0.0720, 0.75028. **Pr:** 0.00006, 0.17197, 0.24971. **B:** 0.26676, 0.43014, 0.88057. **H14:** 0.34758, 0.36477, 0.88347. **H15:** 0.24611, 0.45458, 0.03337. **H16:** 0.10366, 0.42625, 0.8007. **H17:** 0.37496, 0.47548, 0.79356. **B8:** 0.75157, 0.1940, 0.51886. **H19:** 0.63613, 0.20423, 0.38704. **H110:** 0.70323, 0.13930, 0.60198. **H111:** 0.74575, 0.25066, 0.62265. **H112:** 0.92434, 0.18235, 0.45697	[204]

Nd(BH$_4$)$_3$ was produced by the reaction of pre-milled NdH$_3$ with S(CH$_3$)BH$_3$ in toluene, with further extraction/purification with DMS and drying at 453 K under vacuum [31]. α-Nd(BH$_4$)$_3$ is isostructural to the room temperature polymorphs of α-Y(BH$_4$)$_3$ and α-Gd(BH$_4$)$_3$ [31], with cubic group symmetry *Pa-3*, and a = 11.2462(2) Å [17]. β-Nd(BH$_4$)$_3$ is also a high-pressure polymorph (543 K, 9.8 MPa) and is isostructural to β-RE(BH$_4$)$_3$, RE = Ce, Sm, Ho, Y, Er, Tm, Yb (Figure 8) [31]. Nd(BH$_4$)$_3$ also undergoes phase transitions when heated under pressure β- to β′- at 447–463 K, and then to -β″— 463–543 K [31]. Non-solvated Nd(BH$_4$)$_3$ decomposed at approximately 523 K, in a reaction similar to (97) [17,31].

(a)   (b)
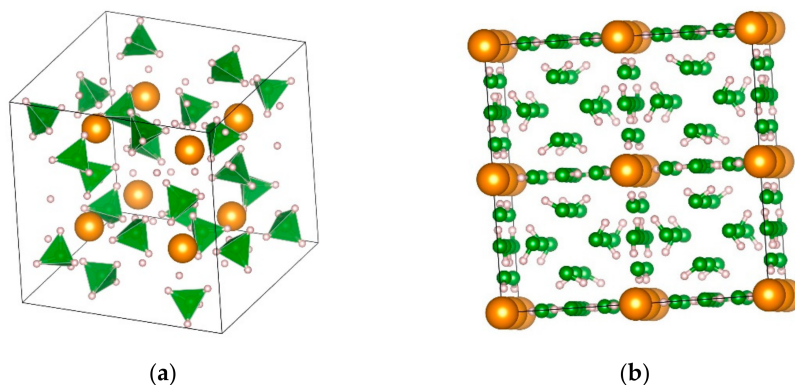
Figure 8. Crystal structure of (**a**) α-Nd(BH$_4$)$_3$ (isostructural to α-Y(BH$_4$)$_3$ and α-Gd(BH$_4$)$_3$ [31]); and (**b**) β-Nd(BH$_4$)$_3$ (isostructural to β-RE(BH$_4$)$_3$, RE = Ce, Sm, Ho, Y, Er, Tm, Yb).

No Pm-borohydrides were located during the investigation for this review.

A few reports about **Sm(BH$_4$)$_2$** were located during the preparation of this review; in one report, SmCl$_3$ reacted with LiBH$_4$ (1:3) in anhydrous diethyl ether. During the reaction, Sm^{+3} was reduced to Sm^{+2} to form Sm(BH$_4$)$_2$. Adding S(CH$_3$)$_2$, and further drying/annealing allowed the production of non-solvated Sm(BH$_4$)$_2$ material above 438 K [212]. In another report, Sm(BH$_4$)$_2$ was produced by the reaction between SmH$_2$ and THF·BH$_3$ (1M) in THF for 48 h at 338 K [213]. In another type of synthesis, ball-milling/mixing of LiBH$_4$ and SmCl$_3$ (6:1) produced two Sm-borohydrides: α-**Sm(BH$_4$)$_3$** and β-Sm(BH$_4$)$_3$ [214].

Sm(BH$_4$)$_2$ crystallized in the orthorhombic *Pbcn* space group (Table 13) [17,212]. Sm(BH$_4$)$_2$ is isostructural to Sr(BH$_4$)$_2$ and Eu(BH$_4$)$_2$ [213]. It is worth mentioning that Eu and Sm can appear as divalent and trivalent cations, and some of their corresponding borohydrides have been reported. The structure of Sm(BH$_4$)$_2$ was described as [Sm(BH$_4$)$_6$] sharing-edges octahedra (with other two octahedra), building chains in the c-direction [214]. Each chain of octahedra is connected via corner-sharing to four others; each [BH$_4$]$^{-1}$ tetrahedra is surrounded by 3 Sm atoms in a distorted trigonal planar environment [214].

Table 13. Crystal structures of Sm-borohydrides.

Material and Hydrogen Content [wt.%]	Structural Parameters [Å, °]	Atomic Positions	Comments
Sm(BH$_4$)$_2$ 4.48	Space group: orthorhombic *Pbcn* (60) a = 6.97129(14), b = 8.43870(17), c = 7.56841(14) α = β = γ = 90	**Sm:** 0, 0.15216(14), 0.25. **B:** 0.2544(14), 0.3710(18), 0.4218(14). **H1:** 0.384(4), 0.292(4), 0.369(6). **H2:** 0.153(6), 0.292(5), 0.514(7). **H3:** 0.164(7), 0.421(6), 0.300(4). **H4:** 0.316(6) 0.479(5) 0.506(7)	[212]

The decomposition of pure Sm(BH$_4$)$_2$ occurred at ~608 K, with no evidence of the formation of crystalline SmB$_6$ [212]. In the 6:1 ball-milled mixture of LiBH$_4$ and SmCl$_3$ at 473 K, the reduction of trivalent borohydride to divalent borohydride with diborane release was proposed [214]. TG measurements of the 6:1 ball-milled mixture of LiBH$_4$ and SmCl$_3$ presented two mass loss events at approximately 448 K and 598 K [214]. Crystalline Sm(BH$_4$)$_2$ from the reduced ball-milled mixture decomposed at lower temperatures than the solvent-extracted material. This difference in decomposition temperatures was explained by the presence of LiCl and other Sm-compounds that modify/destabilize the Sm-borohydrides [212]. Additionally, in the 6:1 ball-milled mixture of LiBH$_4$ and SmCl$_3$, the formation of **LiSm(BH$_4$)$_3$Cl** as a secondary reaction between LiCl and Sm(BH$_4$)$_2$ was proposed upon heating at 453 K [214].

MSm(BH$_4$)$_3$ were produced by the ball-milling of Sm(BH$_4$)$_2$ and M(BH$_4$)$_3$ where, for M = K, the bimetallic borohydride was observed right after ball milling and, for M = Rb and Cs, further heating of the milled mixture led to the formation of the bimetallic borohydrides [213]. The MSm(BH$_4$)$_3$ compounds M = K, Rb, and Cs are isostructural to MSr(BH$_4$)$_3$; i.e., they have perovskite-type structures [213]. The similarities are attributed to similar cation size [213]. **CsSm(BH$_4$)$_3$** presented two second-order polymorphic transitions, the first one at 354 K, possibly related to the formation of α′-CsSm(BH$_4$)$_3$, and the second at ~618 K, involving the formation of β- CsSm(BH$_4$)$_3$, which only exists between 635 and 655 K [213]. All of the MSm(BH$_4$)$_3$ phases, M = K, Rb, and Cs, decomposed at T > 553 K, and the proposed reaction is [213]:

$$3MSm(BH_4)_3 \rightarrow 3MBH_4 + 2SmH_2 + SmB_6 + 10H_2 \qquad (97)$$
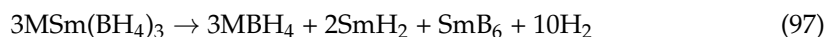
Very importantly, partial rehydrogenation has been achieved for the MSm(BH$_4$)$_3$ materials by heating at 623 K and 19 MPa hydrogen pressure; the authors mentioned that it is probable that the original double-cation borohydrides were re-formed [213].

Recently, the study of Eu-borohydrides has gained attention due to the luminescence of these compounds. **Eu(BH$_4$)$_2$** can be produced by the reaction of freshly ball-milled EuH$_2$ with triethylamine borane [215]:

$$EuH_2 + 2(C_2H_5)_3N\text{-}BH_3 \rightarrow Eu(BH_4)_2 + 2N(C_2H_5)_3 \qquad (98)$$
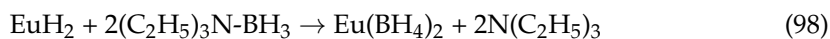
The initial mixture was kept at 373 K overnight under reflux, and then at 418 K for 5 h [215]. After that, Eu(BH$_4$)$_2$ was extracted and dried. Eu(BH$_4$)$_2$ can also be prepared using ball-milling of LiBH$_4$ and EuCl$_2$ or EuCl$_3$ with or without purification/solvent extraction [212]. Several polymorphs have been reported: *o*-Eu(BH$_4$)$_2$, which transforms to *t*-Eu(BH$_4$)$_2$ upon heating at 668 K and coexists with *c*-Eu(BH$_4$)$_2$ (Table 14) [215]. This last compound is considered (probably) metastable [215]. *t*-Eu(BH$_4$)$_2$ melts at 698 K. Humphries et al. identified an amorphization process at 461 K [212]. Eu(BH$_4$)$_2$ presents a single emission band at 463 nm [215]. Decomposition of Eu(BH$_4$)$_2$ at 668 K is reported as a complex process, with the initial thermal decomposition described as [215]:

$$2Eu(BH_4)_2 \rightarrow Eu_2(BH_4)H_3 + B_3H_9 \qquad (99)$$

Table 14. Crystal structures of Eu-borohydrides.

Material and Hydrogen Content [wt.%]	Structural Parameters [Å, °]	Atomic Positions	References and Comments
o-Eu(BH$_4$)$_2$ 4.44	Space group: orthorhombic *Pbcn* (60) a = 6.90343(16), b = 8.37272(18), c = 7.48321(16) $\alpha = \beta = \gamma = 90$	**Eu:** 0, 0.15042(20), 0.25. **B:** 0.2459(21), 0.3837(31),0.4335(21). **H1:** 0.327(11), 0.280(8), 0.352(11). **H2:** 0.138(11), 0.325(10), 0.540(10). **H3:** 0.155(12), 0.465(9), 0.332(11). **H4:** 0.363(10), 0.464(9), 0.509(13)	[212]
t-Eu(BH$_4$)$_2$ 4.44	Space group: tetragonal *P4$_1$2$_1$2* (92) a = 5.4091(6), b = 5.4091(6), c = 11.6201(17) $\alpha = \beta = \gamma = 90$	**Eu1:** 0.0627(16), 0.0624(16), 0. **B2:** 0.9401, 0.4249, 0.3648. **H3:** 0.0998, 0.4164, 0.4199. **H4:** 0.9590, 0.58450, 0.3101. **H5:** 0.9311, 0.2550, 0.3159. **H6:** 0.7705, 0.4436, 0.41330	[215]
c-Eu(BH$_4$)$_2$ 4.44	Space group: cubic *Fm-3m* (225) a = b = c = 7.0602(17) $\alpha = \beta = \gamma = 90$	**Eu1:** 0, 0, 0. **B2:** 0.25, 0.25, 0.25. **H3:** 0.15789, 0.15716, 0.34228	[215]

Eu$_2$(BH$_4$)H$_3$ melts at 698 K; its crystalline structure is reported in [215].

Another way to reduce the dehydrogenation temperature of actinide borohydrides is through the production of mixtures. For example, a ball-milled mixture of EuCl$_3$ + 6LiBH$_4$ (i.e., Eu(BH$_4$)$_2$, LiBH$_4$, and LiCl) decomposed between approximately 348 and 398 K (as observed in a TG/DSC plot) [214].

The synthesis of **Eu(BH$_4$)$_3$** was achieved only recently, by way of mechanical milling at low temperatures, 77–273 K, and a large excess of LiBH$_4$ [7]. Two polymorphs of Eu(BH$_4$)$_3$ were produced [7]:

$$EuCl_3 + 3LiBH_4 \rightarrow \alpha\text{-}Eu(BH_4)_3 + 3LiCl \qquad (100)$$

$$EuCl_3 + 12LiBH_4 \rightarrow \beta\text{-}Eu(BH_4)_3 + 3LiCl + 9LiBH_4 \qquad (101)$$

The Eu(BH$_4$)$_3$ polymorphs are unstable at room temperature, and compared to other RE(BH$_4$)$_3$ decomposition products; Eu(BH$_4$)$_3$ decomposition did not involve the formation of Eu(BH$_4$)$_2$. Wegner et al. explain this peculiarity as due to the redox potential of the Eu^{+3}/Eu^{+2} pair [7].

Other compounds with Eu and [BH$_4$]$^{-1}$ ligands have been reported, but their existence was not corroborated due to poor characterization or synthesis details. Halide substitution was reported as early as 1966; EuBr(BH$_4$) was produced by the reaction of EuBr$_2$ (reduced

in-situ from $EuBr_3$) and $LiBH_4$ in THF [216]. In a 1999 report, $NaEu(BH_4)_4 \cdot 4DME$ was used as a precursor to $Eu(BH_4)_2$ [217]. **$CsEu(BH_4)_3$** was reported recently (with few details of its synthesis); it shows intense blue luminescence centered around 485 nm, which is 20 nm red-shifted from $Eu(BH_4)_2$ [69]. **$RbEu(BH_4)_3$** was also briefly mentioned in a recent report as having luminescence properties [69].

Reports on gadolinium borohydrides indicated a rich chemistry, several different crystal structures (Table 15), and structural modifications by means of double cation or anion substituted materials. Ball-milling produced **$Gd(BH_4)_3$** (+3LiCl) presented two relevant endothermic processes upon heating: (i) at 484 K (peak temperature), a phase transition to a high-temperature $Gd(BH_4)_3$ polymorph (cubic structure with a = 11.418 Å [218]). (ii) Decomposition started at 503 K, with a peak temperature at 531 K [218]. Among the dehydrogenation products, GdB_4 [7] and GdH_2 were observed; thus, two dehydrogenation reactions were proposed [218]:

$$Gd(BH_4)_3 \rightarrow 0.25GdH_2 + 0.75GdB_4 + 5.75H_2 \tag{102}$$

$$Gd(BH_4)_3 \rightarrow GdH_2 + 3B + 5H_2 \tag{103}$$
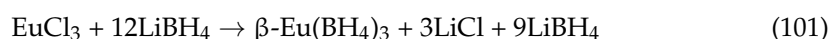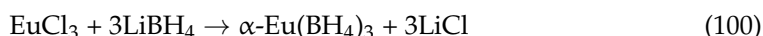
Table 15. Crystal structures of Gd-borohydrides.

Material and Hydrogen Content [wt.%]	Structural Parameters [Å, °]	Atomic Positions	Reference and Comments
α-$Gd(BH_4)_3$ 5.99	Space group: cubic *Pa-3* (205) a = b = c = 11.008 α = β = γ = 90	**Gd:** 0.2169, 0.2169, 0.2169. **B:** 0.1919, 0.2475, 0.9670. **H1:** 0.2892, 0.2539, 0.0231. **H2:** 0.1039, 0.2248, 0.0335. **H3:** 0.1736, 0.3472, 0.9186. **H4:** 0.2012, 0.1633, 0.8931	Theoretical calculation (predicted DFT). [53]
$K_2Gd(BH_4)_5$ 6.51	Space group: monoclinic *P2₁/m* (11) a = 8.7001(3), b = 12.1241(5), c = 11.9893(5) α = 90, β = 105.009(1), γ = 90	**K1:** 0.5957(9), 0.5399(6), 0.3382(7). **K2:** 0.8353(14), 0.7500, 0.6833(11). **K3:** 0, 0.5, 0. **Gd1:** −0.1357(3), 0.25, 0.6319(3). **Gd2:** −0.4610(3), 0.25, 0.0824(3). **B1:** −0.433(5), 0.25, 0.474(4). **H11:** −0.37(2), 0.25, 0.402(14). **H12:** −0.34(2), 0.25, 0.563(11). **H13:** −0.512(6), 0.172(3), 0.466(12). **B2:** 0.155(6), 0.25, 0.540(4). **H21:** 0.293(8), 0.25, 0.573(16). **H22:** 0.10(2), 0.25, 0.618(11). **H23:** 0.114(13), 0.172(3), 0.485(5). **B3:** −0.050(6), 0.25, 0.850(4). **H31:** 0.064(16), 0.25, 0.926(14). **H32:** −0.161(17), 0.25, 0.887(18). **H33:** −0.052(16), 0.172(3), 0.794(5). **B4:** 0.493(6), 0.25, 0.862(5). **H41:** 0.356(8), 0.25, 0.827(17). **H42:** 0.55(2), 0.25, 0.785(12). **H43:** 0.533(13), 0.172(3), 0.917(6). **B5:** −0.206(4), −0.515(2), 0.592(3). **H51:** −0.20(3), −0.477(12), 0.505(7). **H52:** −0.11(3), −0.48(2), 0.667(8). **H53:** −0.19(6), −0.609(7), 0.591(9). **H54:** −0.331(13), −0.50(4), 0.605(13). **B6:** −0.653(4), 0.100(2), 0.130(3). **H61:** −0.788(8), 0.116(16), 0.119(14). **H62:** −0.621(19), 0.119(9), 0.044(8). **H63:** −0.62(2), 0.009(7), 0.157(14). **H64:** −0.580(19), 0.158(14), 0.202(11). **B7:** −0.212(4), 0.108(2), 0.179(3). **H71:** −0.17(2), 0.017(6), 0.185(13). **H72:** −0.204(13), 0.145(11), 0.092(7). **H73:** −0.132(19), 0.158(11), 0.254(8). **H74:** −0.343(8), 0.111(15), 0.186(12)	[20] experimental 298 K
$KGd(BH_4)_4$ 6.31	Space group: monoclinic *P2₁/c* (14) a = 7.1051(6), b = 7.7365(6), c = 8.1049(6), α = γ = 90, β = 102.192(4)	**K1:** 0.5, 0, 0.5. **Gd1:** 0, 0.5, 0.5. **B1:** −0.107(8), 0.771(7), 0.328(7). **H11:** −0.10(6), 0.71(3), 0.46(2). **H12:** 0.01(6), 0.70(6), 0.27(4). **H13:** −0.07(11), 0.92(2), 0.34(5). **H14:** −0.26(3), 0.75(10), 0.24(4). **B2:** 0.653(8), 0.146(5), 0.900(7). **H21:** 0.56(3), 0.27(2), 0.92(3). **H22:** 0.55(3), 0.03(2), 0.86(3). **H23:** 0.76(3), 0.12(3), 1.027(18). **H24:** 0.74(3), 0.17(3), 0.80(2)	[20] experimental 450 K
$Cs_3Gd(BH_4)_6$ 3.75	Space group: cubic *F23* (196) a = b = c = 11.3000(1), α = β = γ = 90	**Cs1:** 0, 0, 0. **Cs2:** 0, 0.5, 0. **Cs3:** 0.75, 0.75, 0.75. **Gd:** 0.2503, 0.7495, 0.7483. **B:** 0.7498, 0.7499, 0.4965. **H1:** 0.8059, 0.8100, 0.5550. **H2:** 0.6900, 0.8062, 0.4380	[20] experimental 298 K

Solvated gadolinium borohydride, $Gd(BH_4)_3 \cdot S(CH_3)_2$, released $S(CH_3)_2$ upon heating at 408 K (peak temperature) [219], and then decomposed at 508 K [14]–543 K [17], with a small release of B_2H_3 [219].

Several double cation Gd-borohydrides have been reported: **$NaGd(BH_4)_4$** was formed after heat treatment of $NaBH_4$-$Gd(BH_4)_3$; it was so amorphous and unstable that it decomposed at RT in one day [204]. **$A_nGd(BH_4)_{n+3}$, A = K, and Cs**, were produced by ball-milling mediated addition reactions between KBH_4 or $CsBH_4$ and $Gd(BH_4)_3$; the

available crystallographic information is collected in Table 15 [20,69,204]. The structure of **Cs$_3$Gd(BH$_4$)$_6$** is double-perovskite-type with luminescence properties [69].

Cation- and anion-substituted LiGd(BH$_4$)$_3$Cl can be produced as a by-product of mechanical milling and further heating to 466 K of GdCl$_3$ and LiBH$_4$ [14]:

$$Gd(BH_4)_3 + LiCl \rightarrow LiGd(BH_4)_3Cl \qquad (104)$$
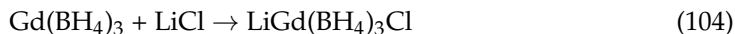
LiGd(BH$_4$)$_3$Cl possesses high Li-ion conductivity at 293 K; 3.5×10^{-4} S cm^{-1} [14]. Decomposition of LiGd(BH$_4$)$_3$Cl was reported at 534 K to form GdH$_2$, GdB$_4$, H$_2$, and LiCl. Essentially, there is no difference in dehydrogenation products as compared to other millings of GdCl$_3$/LiBH$_4$ or reactive mixtures.

The reactive mixture of Gennari et al., Gd(BH$_4$)$_3$ + 3LiBH$_4$ + 3LiCl (from mechanical milled 6LiBH$_4$ + GdCl$_3$), present similarities with the analogous mixture with Ce; dehydrogenation is a multistep process, with hydrogen desorption occurring at 493 K, 548K, and 588K [210]. Among the dehydrogenation products, crystalline GdB$_4$ and GdH$_2$ were identified [210]. The proposed dehydrogenation pathway is, first, the decomposition of Gd(BH$_4$)$_3$ to produce GdH$_2$, GdB$_4$, and H$_2$; then, GdH$_2$ reacts with LiBH$_4$ to produce additional GdB$_4$ and H$_2$, as well as LiH [210]. In line with the possible formation of LiRE(BH$_4$)$_3$Cl during the ball-milling of 6:1 mixtures of LiBH$_4$ and RECl$_3$, Olsen et al. proposed another general dehydrogenation reaction occurring in this kind of reactive mixture [214]:

$$LiRE(BH_4)_3Cl + 3LiBH_4 \rightarrow LiCl + REB_6 + 3LiH + (21/2)H_2 \qquad (105)$$

Partial rehydrogenation of the dehydrogenated Gd(BH$_4$)$_3$ + 3LiBH$_4$ + 3LiCl mixture was achieved at 673 K and 6 MPa [210].

For the late lanthanide borohydrides of RE = Tb, Dy, Ho, Er, Tb, Tm, Yb, and Lu, the synthesis is the same as that described above, i.e., pre-milled REH$_3$ reacted with dimethyl sulfide-borane in toluene at 318 K for up to seven days, followed by solvent extraction [13]. Yet, mechanical milling of LiBH$_4$ and RECl$_3$ can also be an option, with or without temperature control [7]. The α- and β-RE(BH$_4$)$_3$ polymorphs share the same cubic group symmetry, α: *Pa-3*, and β: *Fm-3* [13], with smooth size changes of the crystallographic cell upon the cation radii [7]. In the mechanical-milling route, an excess of LiBH$_4$ favors the formation of the β-RE(BH$_4$)$_3$ polymorph [7]. Wegner et al. reported that most of the RE(BH$_4$)$_3$ prepared by mechanical milling decomposed with the fasted rate at 523 K, producing very pure hydrogen [7]. The decomposition products of RE(BH$_4$)$_3$ have the formation of REB$_4$ in common, except for the Lu-containing compound, which forms LuB$_2$ [7].

Two Ho-borohydrides have been reported—**Ho(BH$_4$)$_3$** and **KHo(BH$_4$)$_4$** [220]. Ho(BH$_4$)$_3$ behaved like the usual RE(BH$_4$)$_3$ compounds described above, i.e., this material presents two polymorphs, α- and β-, whose relative amount depends on the excess of LiBH$_4$ during the ball milling [220]. The peak decomposition temperature of 523 K was preceded by two smaller endothermic peaks [220]. KHo(BH$_4$)$_4$ was prepared by means of the solid-state reaction [220]:

$$HoCl_3 + 3LiBH_4 + KBH_4 \rightarrow KHo(BH_4)_4 + 3LiCl \qquad (106)$$
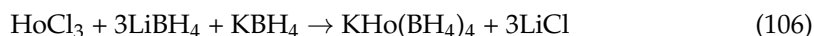
KHo(BH$_4$)$_4$ crystallizes in an orthorhombic lattice (*Cmcm*). Upon heating, this material melts at 448 K, and decomposition occurs at 531 K [220].

Er(BH$_4$)$_3$ (from ball-milling ErCl$_3$ + 3LiBH$_4$, extraction with solvent and heat treatment) decomposed at 559 K (peak temperature), with low B$_2$H$_6$ emission [211]. Rehydrogenation at 613 K, 10 MPa hydrogen pressure during 21 h did not succeed [211]. **NaEr(BH$_4$)$_4$** was formed by the assisted ball-milled reaction between NaBH$_4$ and Er(BH$_4$)$_3$ (crystal structure at Table 16) [204]. Melting was observed between 427 K and 435 K.
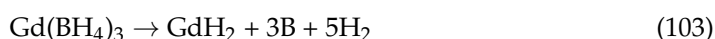
Table 16. Crystal structures of Er-borohydrides.

Material and Hydrogen Content [wt.%]	Structural Parameters [Å, °]	Atomic Positions	Comments
NaEr(BH$_4$)$_4$ 6.46	Space group: orthorhombic *Cmcm* (63) a = 8.5379(2), b = 12.1570(4), c = 9.1652(3) α= β= γ = 90	**Na11:** 0, 0, 0.5. **Er12:** 0.5, 0.1430, 0.75. **B13:** 0.5, 0.2630, 0.9630. **H14:** 0.5, 0.3200, 0.0640. **H15:** 0.5, 0.1720, 1.0020. **H16:** 0.6113, 0.2800, 0.8930. **B17:** 0.7390, 0.0410, 0.75. **H18:** 0.8660, 0.0060, 0.75. **H19:** 0.7440, 0.1360, 0.75. **H110:** 0.6730, 0.0110, 0.85368	[204]

Yb (as in the case of Sm and Eu) can form **Yb(BH$_4$)$_2$** by the reduction in **Yb(BH$_4$)$_3$** [7]:

$$2\text{Yb(BH}_4)_3 \rightarrow 2\text{Yb(BH}_4)_2 + \text{B}_2\text{H}_6 + \text{H}_2 \tag{107}$$
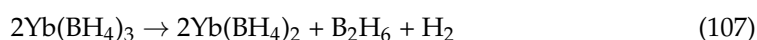
Ytterbium (II) borohydride has four reported polymorphs: α-Yb(BH$_4$)$_2$, α′-Yb(BH$_4$)$_2$, β-Yb(BH$_4$)$_2$, and γ-Yb(BH$_4$)$_2$ (Table 17) [17]. For their part, the Ytterbium (III) borohydrides α-Yb(BH$_4$)$_3$ and β-Yb(BH$_4$)$_3$ can be produced by mechanical milling of 3LiBH$_4$ and YbCl$_3$ [198]. α-Yb(BH$_4$)$_3$ is isostructural to the low temperature α-Y(BH$_4$)$_3$; however, β-Yb(BH$_4$)$_3$ is not similar to the high-temperature polymorph of Y(BH$_4$)$_3$ (Table 17) [198] because of a disordered [BH$_4$]$^{-1}$ orientation. α-Yb(BH$_4$)$_3$ and β-Yb(BH$_4$)$_3$ can coexist because the two modifications are close in energy [198]. Decomposition of Yb(BH$_4$)$_3$ occurred in two steps: the first one at 418 K and the second at 618 K (temperature of maximum gas evolution) [198]. As in other RE-borohydrides, chlorine substituted Yb-borohydrides have been reported: **LiYb(BH$_4$)$_{4-x}$Cl$_x$** and **Yb(BH$_4$)$_{2-x}$Cl$_x$** [198].

Table 17. Crystal structures of Yb-borohydrides.

Material and Hydrogen Content [wt.%]	Structural Parameters [Å, °]	Atomic Positions	Comments
α- Yb(BH$_4$)$_2$ 5.56	Space group: cubic *Pa-3* (205) a = b= c = 10.70715(15) α= β= γ = 90	**Yb:** 0.71615(5), 0. 71615(5), 0. 71615(5). **B:** −0.0391(12), 0.6968(11), 0.7536(18). **H1:** −0.104(6), 0.640(6), 0.684(6). **H2:** 0.064(3), 0.652(5), 0.753(8). **H3:** −0.079(7), 0.693(7), 0.857(3). **H4:** −0.031(6), 0.803(2), 0.720(7)	[198]
β-Yb(BH$_4$)$_2$ 5.56	Space group: cubic *Pm-3m* (221) a = b = c = 5.44223(3) α = β = γ = 90	**Yb:** 0, 0, 0. **B:** $\frac{1}{2}$, 0, 0. **H:** 0.3745(4), 0, 0.1826(3)	[198]

Mechanically milled LiYb(BH$_4$)$_4$ and NaYb(BH$_4$)$_4$ were briefly mentioned in a recent report; they presented lower Auzel´s crystal field strength properties as compared to Tb, Dy, Tm, and Ho-borohydrides [19]. **NaYb(BH$_4$)$_4$** and **KYb(BH$_4$)$_4$** were produced by a reaction analogous to (106); both compounds are isostructural to NaSc(BH$_4$)$_4$ and KY(BH$_4$)$_4$, i.e., orthorhombic *Cmcm* space group [221].

6.2. Actinides

Some of the actinide borohydrides were first synthesized during the Manhattan Project [222]. Today, the interest on actinide homoleptic borohydrides has notably decreased, yet they are summarized in this section. Actinide borohydrides, from Th to Pu, are volatile molecules near room temperature. Th(BH$_4$)$_4$, Pa(BH$_4$)$_4$, and U(BH$_4$)$_4$ are isomorphic, and their volatility increases with the increasing atomic number, whereas Np(BH$_4$)$_4$ and Pu(BH$_4$)$_4$ resemble the Zr-borohydride [223]. Additionally, Th, Pa, and U borohydrides

have double-bridged $[BH_4]^{-1}$ groups that link metal atoms in a low-symmetry polymeric structure in the crystalline phase [223,224].

Th(BH$_4$)$_4$ was produced in the Th-analogous reaction (109) at room temperature [72], and crystallized in the tetragonal $P4_32_12$ space group. It is a polymeric material, melting at 476 K [222].

Pa(BH$_4$)$_4$ was produced by the following reaction in the absence of solvent, followed by heating to 328 K, and recovered by condensation in a cold tramp at 273 K [222]:

$$PaF_4 + 2Al(BH_4)_{3\ (l)} \rightarrow Pa(BH_4)_4 + 2AlF_2BH_4 \tag{108}$$
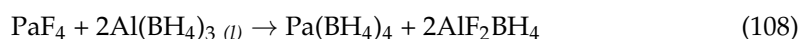
Pa(BH$_4$)$_4$ behaves like U(BH$_4$)$_4$ and Th(BH$_4$)$_4$ [222].

U(BH$_4$)$_4$ was first produced during the Manhattan Project [225]. It can be prepared by stirring UCl$_4$ and an excess of LiBH$_4$ at room temperature for two weeks [81]. Old reports indicate that the reaction of UF$_4$ with liquid Al(BH$_4$)$_3$ (Equation (109)) produces the uranium borohydride [226,227]. U(BH$_4$)$_4$, being volatile at room temperature, can be collected in a cold tramp and also purified in this way [81]. U(BH$_4$)$_4$ forms lustrous dark-green crystals; it is polymeric in the solid-state and monomeric in the gas phase [228]. U(BH$_4$)$_4$ crystallizes in the tetragonal $P4_32_12$ space group, and its melting point is 399 K [222]. U(BH$_4$)$_4$ possesses high symmetry (T_d), efficient screening of the metal atom, and the limited bridging ability of the $[BH_4]^{-1}$ ion [81]. The optical spectrum of U(BH$_4$)$_4$ can be revised at [223,227] and, relatively recently, the f-orbital covalency in U(BH$_4$)$_4$ was demonstrated [87]. U(BH$_4$)$_4$ is fairly stable at room temperature [229], but can decompose upon the action of ultraviolet photons of 253.5 nm (4.8 eV) at 295 K, with B$_2$H$_6$ being a decomposition product [228]:

$$2U(BH_4)_4 \rightarrow 2U(BH_4)_3 + B_2H_6 + H_2 \tag{109}$$

or

$$U(BH_4)_4 \rightarrow U(BH_4)_2 + B_2H_6 + H_2 \tag{110}$$
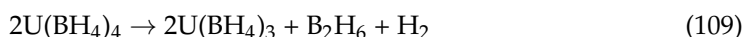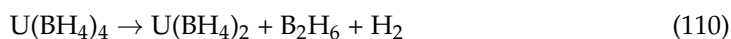
Thermal decomposition of U(BH$_4$)$_4$ was reported in 1981; Ghiassee et al. followed the decomposition of U(BH$_4$)$_4$, utilizing infrared spectroscopy in the gas phase [229]. U(BH$_4$)$_4$ decomposes thermally in two ranges of temperature: at 373 K, the proposed reaction is (109) [226,229,230]; at a temperature superior to 423 K, decomposition is rapid with the formation of a black-silver mirror [229]:

$$U(BH_4)_4 \rightarrow U + 4B + 8H_2 \tag{111}$$

Decomposition kinetics was of first-order between 403 and 443 K and of second-order between 373 and 393 K [229].

Np(BH$_4$)$_3$ is a dark green, pyrophoric, volatile, and reactive liquid that decomposes at 298 K [225], and whose physical properties resemble those of Hf and Zr borohydrides. Its optical spectrum was reported in detail in [231]. Np(BH$_4$)$_3$ was produced in a reaction type analogous to (108), but is unstable at room temperature, so that the reaction was carried out at 273 K [222]. Np(BH$_4$)$_3$ crystallizes in the tetragonal $P4_2/nmc$ space group; structural single-crystal studies were performed at 130 K. The melting point is 287 K and the boiling point is 426 K [222].

Pu(BH$_4$)$_3$ is also an unstable and volatile compound; its synthesis was similar to that of Np(BH$_4$)$_3$ [222]. Pu(BH$_4$)$_3$ melts at 287 K and decomposes roughly at 293 K [225].

7. Thermodynamics (Thermal Stability)

As with any hydrogen storage material, formation enthalpy is the best predictor of a borohydride's stability [232]. However, such information is only available for a small number of borohydrides. Because of that, other predictors have been considered.

Nakamori et al. proposed an equation that relates the Pauling electronegativity, χ_P, of the metal counter-ion with the formation enthalpy (per $[BH_4]^{-1}$ ion) [30,181]:

$$\Delta H_{boro} = 248.7\chi_P - 390.8 \tag{112}$$

However, borohydrides can form double or even triple cation compounds. Thus, an adjustment must be made to Equation (112). In a series of $ZrLi_{m-4}(BH_4)_m$, Li et al. proposed an average value of χ_P as a predictor of the dehydrogenation temperature [233]:

$$\chi_P = \frac{1.4 + 1.0(m-4)}{1 + (m-4)} \tag{113}$$

m = 0–4, in $ZrLi_{m-4}(BH_4)_m$. However, an extension to other bi-cationic borohydrides is necessary. In Figure 9, we collected the dehydrogenation temperatures of the borohydrides (in logarithmic scale) encountered during the preparation of this review, and plotted as a function of the Pauling electronegativity. For bi-cation borohydrides of the general form $M1_xM2_y(BH_4)_z$, a weighted average was used:

$$\chi_P = \frac{x * \chi_{PM1} + y * \chi_{PM2}}{x + y} \tag{114}$$

where χ_{PM1} and χ_{PM2} are the Pauling electronegativities of the respective cations in the borohydride. For visual reference, some previously reported data were included. Globally, a general tendency of reducing dehydrogenation temperature with the increase in cation electronegativity is confirmed. The red line in Figure 9 indicates the fitting of all collected data:

$$\log T = 3.1529 - 0.3859\chi_p \tag{115}$$

where χ_P is the Pauling electronegativity of the cation, or the average (Equation (114)) for bicationic borohydrides. The r-square of Equation (115) is rather low: 0.63866. However, it must be mentioned that there is no homogeneity in the way of reporting dehydrogenation temperatures; researchers have reported onset temperatures, peak temperatures, or ranges from the beginning and end of the reaction. Additionally, some (minor) fractions of the data were taken directly from the original plots in the reports; from DSC plots, for example. Moreover, data are reported from different techniques; for example, DSC, TGA, temperature-programmed desorption, and in-situ X-ray diffraction, and each technique shows differences in heating ramps or reaction atmospheres. Moreover, for the same borohydride, several temperatures of dehydrogenation have been reported, depending on different experimental parameters, particularly for the most studied Group I and II-borohydrides.

Other proposed predictors include the following: (i) The polarizing ability of the cationic bonding component [234], where the decreasing stability of the metal borohydride correlating with its increasing polarizing ability, as found in ab-inito studies [234]; and (ii) the relation between the Pauling electronegativity and the boron chemical NMR shift of metal borohydrides [235].
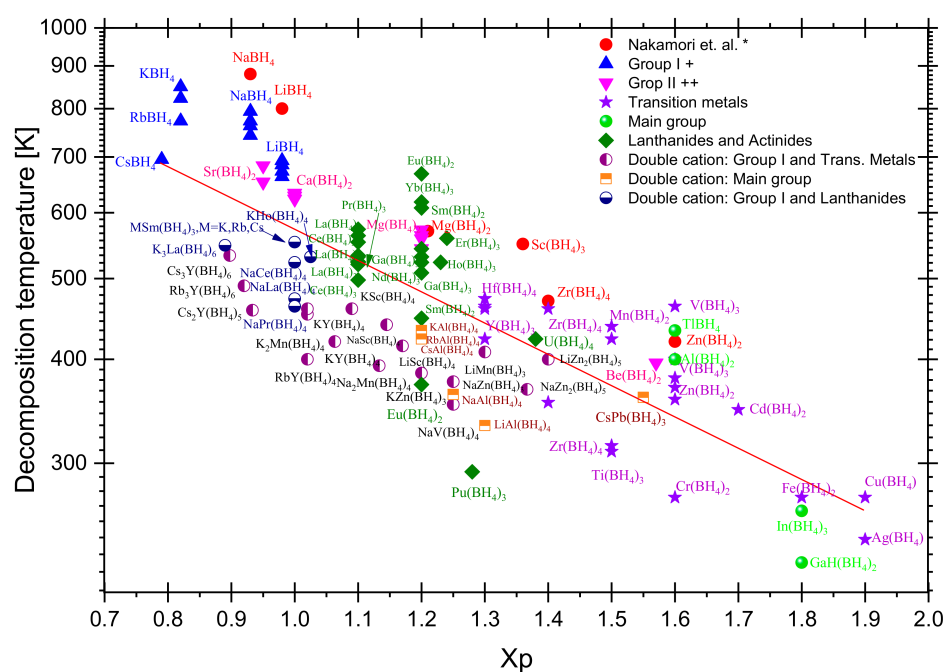
Figure 9. Compilation of dehydrogenation temperature (peak temperature whenever available, otherwise, onset temperature) versus Pauling electronegativity or weighted average Pauling electronegativity. Source data: * (red dots) Nakamori et al. (2006) [30]. + Group I borohydrides: $LiBH_4$ [236–240], $NaBH_4$ [241–246], KBH_4 [4,247–249], $RbBH_4$, and $CsBH_4$ [50]. ++ Group II borohydrides: $Be(BH_4)_2$ [250], $Mg(BH_4)_2$ [251–254], $Ca(BH_4)_2$ [255–258], and $Sr(BH_4)_2$ [215,259,260].

8. The Boron Problem

Particularly for hydrogen applications, the release of diborane and the formation of stable B-H species is a problem, as it compromises re-hydrogenation reactions. On the other hand, the release of hydrogen at low temperatures (from RT to roughly 373 K) is required for compatibility with PEM (polymer exchange membrane) fuel cell applications. However, diborane release is frequently associated with the low-temperature decomposition of borohydrides. The last facts seem entirely incompatible. Yet, along with the borohydrides listed in this review, several factors appear to influence the release of diborane. These factors include, but are not limited to, the synthesis method, purification, elimination of occluded molecules with supercritical N_2 processing [196], thermal history of the material, storage conditions, temperature and pressure of dehydrogenation, existence (intentional or not) of other materials such as salts, hydrides or other borohydrides, etc. Among the consulted papers, different researchers reported from null or undetectable to high amounts of diborane release for the same material. Thus, several authors have proposed theories to understand the factors influencing diborane release. Diborane release can be explained in three ways: (i) Diborane is released but decomposes at high temperatures (before being detected); (ii) diborane is an intermediary in the formation and decomposition of borohydrides; and (iii) diborane is not emitted. [261].

The accepted explanation of diborane emission during dehydrogenation reactions is that the amount of B_2H_6 released scales inversely with borohydride stability, which depends on the corresponding cation's electronegativity [262]. Callini et al. mentioned that the difference in electronegativity results in a charge transfer from the cation to the anion that destabilizes and distorts the $[BH_4]^{-1}$ units [262]. $[BH_4]^{-1}$ distortion can be detected and quantified utilizing infrared spectroscopy; Callini et al. proposed the stretching span (Δs) as a way to classify B_2H_6-releasing borohydrides. In this approach, the stretching span is the difference in energies of the stretching vibrations of hydrogen atoms with different bonding lengths [262]. In this model, a threshold of $\Delta s > 200$ cm^{-1} is proposed as the predictor of B_2H_6-releasing borohydrides; materials such as $LiSc(BH_4)_4$,

$Zr(BH_4)_4$, and $Al(BH_4)_3$ will release B_2H_6, while $LiBH_4$ will not [262]. Yet, $LiBH_4$ releases B_2H_6 under several reaction conditions [262]. Harrison et al. mentioned that diborane production did not follow any clear trend but, for threshold values between 1.36 and 1.55 of electronegativity of the corresponding metal in the Pauling scale, χ_P, diborane production is observed [182].

Furthermore, the dehydrogenation mechanism is frequently unresolved for transition metal borohydrides, in contrast to Group I and II borohydrides, where the formation of intermediaries such as $M_x(B_{12}H_{12})$ M = Li, K, Rb, Cs has been identified [263–265]. However, some models and reactions of B-H compounds can be used to explain the dehydrogenation reaction. In the model of Callini, the distorted $[BH_4]^{-1}$ unit is the precursor for the formation of $(H^{\delta-})_2$ and $BH_2^{\delta+}$, with the formation of diborane proposed as [262]:

$$2M^{\delta1+} + 2(BH_4)^{\delta1-} \rightarrow 2M^{\delta1+} + (H^{\delta-})_2 + BH_2^{\delta1+}BH_4^{\delta1-} \rightarrow 2M + H_2 + B_2H_6 \qquad (116)$$

Other B–H compounds or ions have been reported from the reaction between B_2H_6 and borohydrides or hydrides in the context of studying the borane chemistry [266]:

$$B_2H_6 + MBH_4 \rightarrow MB_3H_8 + H_2 \qquad (117)$$

$$B_5H_9 + MH \rightarrow M(B_5H_8) + H_2 \qquad (118)$$

$$M(B_5H_8) + \frac{1}{2}B_2H_6 \rightarrow M(B_6H_{11}) \qquad (119)$$

$$B_{10}H_{14} + MBH_4 \rightarrow MB_{11}H_{14} + 2H_2, \text{ M = Li, Na} \qquad (120)$$
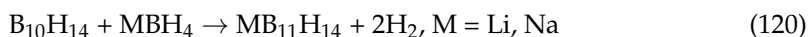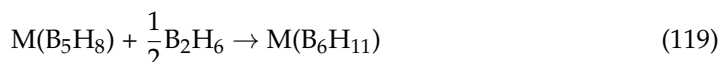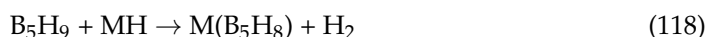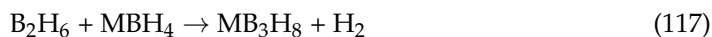
Reaction (117) requires a temperature of about 373 K to proceed at a reasonable rate [266]. Meanwhile, Equations (118)–(120) correspond to different reactions for a growing B–H cluster [266]. Those reactions were performed in solvent; however, some of these reactions might occur during heating of the metal borohydrides. Indeed, the formation of $[B_3H_8]^-$ intermediaries in Y borohydride and $[B_{12}H_{12}]^{2-}$ in Sc borohydride [235] (and references within) has been reported. Other possible intermediaries include $[B_{10}H_{12}]^{2-}$ and $[B_{11}H_{14}]^-$ [267,268]. For its part, the rapid dissociation of a $BH_4^{\bullet}$ radical into BH_3 an $H^{\bullet}$ above 250 K was predicted by means of ab-initio MO calculations [269].

It is also worth mentioning that, during the dehydrogenation of borohydrides or their composites, the formation of MB_x species seems to favor re-hydrogenation [270,271]. In turn, the increase in back pressure during dehydrogenation favors the formation of MB_x compounds [271]. Thus, a competition between the formation of metal boride compounds and B_2H_6 might be established.

Strategies for reducing the release of B-H compounds include increasing the hydrogen back-pressure during dehydrogenation [269], modification of the dehydrogenation pathway by using, for example, the formation of reactive composites [269], the use of catalysts (such as Mo(100) surface) for the decomposition of diborane [261], or other B-H intermediaries, etc.

Nano- and meso-confinement could be beneficial; until now, this was mostly employed for Group I borohydrides [272]. For example, Xia et al. reported the complete suppression of the release of B_xH_y by-products and a reduction in the decomposition temperature (a decrease of about 50 K) in SBA-15- confined $NaZn(BH_4)_3$ [159]. Stabilization of volatile $Ti(BH_4)_3$ was achieved by nano-confinement in MOF UiO-66 ($Zr_6O_4(BDC)_6$, BDC =1,4-benzenedicarboxylate) [76]. In this way, $Ti(BH_4)_3$-UiO-66 was stabilized at room temperature under an argon atmosphere and, during dehydrogenation, there was no emission of diborane [76]. Instead, the decomposition involved B_5H_9 that recombined at an increased temperature to form solid higher boranes [76].

Finally, other essential data of $[BH_4]^{-1}$ must be mentioned: the electronegativity of $[BH_4]^{-1}$ is considered as 2.13 [22,108], and its electron affinity is 3.18 eV [188], while its ionic size is 2.03 Å [22].

9. Conclusions and Perspectives

Beyond Groups I and II, borohydrides present interesting properties related to chemistry, structure, hydrogen release, and, in an emerging trend, ionic conductivity and photoluminescence. Among the materials reviewed in the present work the transition metals and lanthanide borohydrides stand out.

Several strategies have been tried to generate new bimetallic and trimetallic borohydrides with tailored decomposition temperatures and mechanisms of diborane release in materials intended for hydrogen storage. However, many of these new materials decompose into the "parent" borohydrides, and then high temperatures are required to release a substantial amount of hydrogen. Thus, decomposition of double or triple cation borohydrides into the "parent" borohydrides is not recommendable in the hydrogen storage area. Re-hydrogenation is still to be reached in most revised compounds. The ideal procedure would be a one-step decomposition into simple (and re-hydrogenable) compounds. To achieve this goal, several routes, such as the addition of catalysts, the use of different ligands (take advantage of organometallic chemistry), or the formation of ammonia–borane compounds, are still to be explored or are under exploration.

Additionally, the nanoconfinement of borohydrides into MOFs, polymers, zeolites, etc., could soon be a strategy for the development of new composite materials. Otherwise, porous borohydrides can be used for the confinement of H_2 or other small molecules.

Anion substitution is another opportunity area that should be thoroughly studied because of the possibilities for generating new materials with high ionic conductivity for battery applications. Along with this review, we observed the formation of several Cl-substituted borohydrides, i.e., their synthesis is facile and their niche application can be developed.

References

1. Lai, Q.; Sun, Y.; Wang, T.; Modi, P.; Cazorla, C.; Demirci, U.B.; Ramon, J.; Fernandez, A.; Leardini, F. How to Design Hydrogen Storage Materials? Fundamentals, Synthesis, and Storage Tanks. *Adv. Sustain. Syst.* **2019**, *1900043*, 1–64. [CrossRef]
2. Chem, G.; Lai, Q. Borohydrides as Solid-State Hydrogen Storage Materials: Past, Current Approaches and Future Perspectives. *Gen. Chem.* **2018**, *4*, 1–11. [CrossRef]
3. Laversenne, L. Synthesis and crystal structure of transition element borohydrides: M(BH$_4$)$_y$, M= Ti, Zr, Hf, Mn, Fe, Cu, Zn, Cd. In *Hydrogen Storage Materials*; Burzo, E., Ed.; Springer: Berlin/Heidelberg, Germany, 2018; pp. 297–299. [CrossRef]
4. Paskevicius, M.; Ley, M.B.; Sheppard, D.A.; Jensen, R.; Buckley, C.E. Eutectic melting in metal borohydrides. *Phys. Chem. Chem. Phys.* **2013**, *15*, 19774–19789. [CrossRef]
5. Zhang, Q.; Gao, Z.; Shi, X.; Zhang, C.; Liu, K.; Zhang, J.; Zhou, L.; Ma, C.; Du, Y. Recent advances on rare earths in solid lithium ion conductors. *J. Rare Earths* **2021**, *39*, 1–10. [CrossRef]

6. Ohno, S.; Banik, A.; Dewald, G.F.; Kraft, M.A.; Krauskopf, T.; Minafra, N.; Till, P.; Weiss, M.; Zeier, W.G. Materials design of ionic conductors for solid state batteries. *Prog. Energy* **2020**, *2*, 022001. [CrossRef]

7. Wegner, W.; Jaroń, T.; Grochala, W. Preparation of a series of lanthanide borohydrides and their thermal decomposition to refractory lanthanide borides. *J. Alloys Compd.* **2018**, *744*, 57–63. [CrossRef]

8. Luo, W.; Huang, Z.; Cai, X.; Niu, R.; Nie, R.; Feng, Q.; Wang, F.; Gan, Z. Microstructure and superconducting properties of MgB$_2$ bulks prepared from Mg + B + Mg(BH$_4$)$_2$ composites. *Supercond. Sci. Technol.* **2019**, *32*, 085006. [CrossRef]

9. Fujii, H.; Ozawa, K. Superconducting properties of PIT-processed MgB$_2$ tapes using Mg(BH$_4$)$_2$ precursor. *Supercond. Sci. Technol.* **2011**, *24*, 095009. [CrossRef]

10. Andrievski, R.A. Nanostructured titanium, zirconium and hafnium diborides: The synthesis, properties, size effects and stability. *Russ. Chem. Rev.* **2015**, *84*, 540–554. [CrossRef]

11. Yang, Y.; Jayaraman, S.; Kim, D.Y.; Girolami, G.S.; Abelson, J.R. CVD growth kinetics of HfB$_2$ thin films from the single-source precursor Hf(BH$_4$)$_4$. *Chem. Mater.* **2006**, *18*, 5088–5096. [CrossRef]

12. Kang, S.-W.; Park, Y.-J.; Kim, Y.-S.; Shin, Y.-H.; Yun, J.-Y. Real-Time Evaluation of Aluminum Borohydride Trimethylamine for Aluminum Chemical Vapor Deposition. *J. Electrochem. Soc.* **2009**, *156*, H333. [CrossRef]

13. Grinderslev, J.B.; Møller, K.T.; Bremholm, M.; Jensen, T.R. Trends in Synthesis, Crystal Structure, and Thermal and Magnetic Properties of Rare-Earth Metal Borohydrides. *Inorg. Chem.* **2019**, *58*, 5503–5517. [CrossRef] [PubMed]

14. Ley, M.B.; Boulineau, S.; Janot, R.; Filinchuk, Y.; Jensen, T.R. New Li ion conductors and solid state hydrogen storage materials: LiM(BH$_4$)$_3$Cl, M = La, Gd. *J. Phys. Chem. C* **2012**, *116*, 21267–21276. [CrossRef]

15. Lyubov, D.M.; Tolpygin, A.O.; Trifonov, A.A. Rare-earth metal complexes as catalysts for ring-opening polymerization of cyclic esters. *Coord. Chem. Rev.* **2019**, *392*, 83–145. [CrossRef]

16. Visseaux, M.; Bonnet, F. Borohydride complexes of rare earths, and their applications in various organic transformations. *Coord. Chem. Rev.* **2011**, *255*, 374–420. [CrossRef]

17. Richter, B.; Grinderslev, J.B.; Møller, K.T.; Paskevicius, M.; Jensen, T.R. From Metal Hydrides to Metal Borohydrides. *Inorg. Chem.* **2018**, *57*, 10768–10780. [CrossRef]

18. Wylezich, T.; Sontakke, A.D.; Castaing, V.; Suta, M.; Viana, B.; Meijerink, A.; Kunkel, N. One Ion, Many Facets: Efficient, Structurally and Thermally Sensitive Luminescence of Eu $^{2+}$ in Binary and Ternary Strontium Borohydride Chlorides. *Chem. Mater.* **2019**, *31*, 8957–8968. [CrossRef]

19. Wegner, W.; van Leusen, J.; Majewski, J.; Grochala, W.; Kögerler, P. Borohydride as Magnetic Superexchange Pathway in Late Lanthanide Borohydrides. *Eur. J. Inorg. Chem.* **2019**, *2019*, 1776–1783. [CrossRef]

20. Schouwink, P.; Didelot, E.; Lee, Y.S.; Mazet, T.; Černý, R. Structural and magnetocaloric properties of novel gadolinium borohydrides. *J. Alloys Compd.* **2016**, *664*, 378–384. [CrossRef]

21. Marks, T.J.; Kolb, J.R. Covalent transition metal, lanthanide, and actinide tetrahydroborate complexes. *Chem. Rev.* **1977**, *77*, 263–293. [CrossRef]

22. Černý, R.; Schouwink, P. The crystal chemistry of inorganic metal borohydrides and their relation to metal oxides. *Acta Crystallogr. Sect. B Struct. Sci. Cryst. Eng. Mater.* **2015**, *71*, 619–640. [CrossRef]

23. Paskevicius, M.; Jepsen, L.H.; Schouwink, P.; Černý, R.; Ravnsbæk, D.B.; Filinchuk, Y.; Dornheim, M.; Besenbacher, F.; Jensen, T.R. Metal borohydrides and derivatives-synthesis, structure and properties. *Chem. Soc. Rev.* **2017**, *46*, 1565–1634. [CrossRef] [PubMed]

24. Bannenberg, L.J.; Heere, M.; Benzidi, H.; Montero, J.; Dematteis, E.M.; Suwarno, S.; Jaroń, T.; Winny, M.; Orłowski, P.A.; Wegner, W.; et al. Metal (boro-) hydrides for high energy density storage and relevant emerging technologies. *Int. J. Hydrog. Energy* **2020**, *45*, 33687–33730. [CrossRef]

25. Zanella, P.; Crociani, L.; Masciocchi, N.; Giunchi, G. Facile High-Yield Synthesis of Pure, Crystalline Mg(BH$_4$)$_2$. *Inorg. Chem.* **2007**, *46*, 9039–9041. [CrossRef] [PubMed]

26. Remhof, A.; Yan, Y.; Friedrichs, O.; Kim, J.W.; Mauron, P.; Borgschulte, A.; Wallacher, D.; Buchsteiner, A.; Hoser, A.; Oh, K.H.; et al. Towards room temperature, direct, solvent free synthesis of tetraborohydrides. *J. Phys. Conf. Ser.* **2012**, *340*. [CrossRef]

27. Hagemann, H.; Černý, R. Synthetic approaches to inorganic borohydrides. *Dalt. Trans.* **2010**, *39*, 6006. [CrossRef] [PubMed]

28. Bauer, R. Notizen: Zur Kenntnis der Magnesiumboranat-Bildung. *Z. Naturforsch. B* **1962**, *17*, 277–278. [CrossRef]

29. Jaroń, T.; Orłowski, P.A.; Wegner, W.; Fijałkowski, K.J.; Leszczyński, P.J.; Grochala, W. Hydrogen Storage Materials: Room-Temperature Wet-Chemistry Approach toward Mixed-Metal Borohydrides. *Angew. Chemie* **2015**, *127*, 1252–1255. [CrossRef]

30. Nakamori, Y.; Miwa, K.; Ninomiya, A.; Li, H.; Ohba, N.; Towata, S.I.; Züttel, A.; Orimo, S.I. Correlation between thermodynamical stabilities of metal borohydrides and cation electronegativites: First-principles calculations and experiments. *Phys. Rev. B-Condens. Matter Mater. Phys.* **2006**, *74*, 1–9. [CrossRef]

31. Payandeh Gharibdoust, S.; Heere, M.; Nervi, C.; Sørby, M.H.; Hauback, B.C.; Jensen, T.R. Synthesis, structure, and polymorphic transitions of praseodymium(III) and neodymium(III) borohydride, Pr(BH$_4$)$_3$ and Nd(BH$_4$)$_3$. *Dalt. Trans.* **2018**, *47*, 8307–8319. [CrossRef]

32. Díaz-Torres, R.; Alvarez, S. Coordinating ability of anions and solvents towards transition metals and lanthanides. *Dalt. Trans.* **2011**, *40*, 10742. [CrossRef]

33. Łodziana, Z.; van Setten, M.J. Binding in alkali and alkaline-earth tetrahydroborates: Special position of magnesium tetrahydroborate. *Phys. Rev. B* **2010**, *81*, 024117. [CrossRef]

34. Besora, M.; Lledós, A. Coordination Modes and Hydride Exchange Dynamics in Transition Metal Tetrahydroborate Complexes. In *Contemporary Metal Boron Chemistry I*; Springer: Berlin/Heidelberg, Germany, 2007. [CrossRef]

35. Callini, E.; Borgschulte, A.; Hugelshofer, C.L.; Ramirez-Cuesta, A.J.; Züttel, A. The Role of Ti in Alanates and Borohydrides: Catalysis and Metathesis. *J. Phys. Chem. C* **2014**, *118*, 77–84. [CrossRef]

36. Chua, Y.S.; Chen, P.; Wu, G.; Xiong, Z. Development of amidoboranes for hydrogen storage. *Chem. Commun.* **2011**, *47*, 5116. [CrossRef]

37. Xu, Z.; Lin, Z. Transition metal tetrahydroborato complexes: An orbital interaction analysis of their structure and bonding. *Coord. Chem. Rev.* **1996**, *156*, 139–162. [CrossRef]

38. Nakamoto, K. Infrared and Raman Spectra of Inorganic and Coordination Compounds. Handbook of Vibrational Spectroscopy. *Handb. Vib. Spectrosc.* **2006**, 1872–1892. [CrossRef]

39. D'Anna, V.; Spyratou, A.; Sharma, M.; Hagemann, H. FT-IR spectra of inorganic borohydrides. *Spectrochim. Acta-Part A Mol. Biomol. Spectrosc.* **2014**, *128*, 902–906. [CrossRef] [PubMed]

40. Morris, J.H.; Smith, W.E. Synthesis and characterisation of a tetrahydrofuran derivative of scandium tetrahydroborate. *J. Chem. Soc. D Chem. Commun.* **1970**, 245a. [CrossRef]

41. Hwang, S.J.; Bowman, R.C.; Reiter, J.W.; Rijssenbeek, J.; Soloveichik, G.L.; Zhao, J.C.; Kabbour, H.; Ahn, C.C. NMR confirmation for formation of $[B_{12}H_{12}]^{2-}$ complexes during hydrogen desorption from metal borohydrides. *J. Phys. Chem. C* **2008**, *112*, 3164–3169. [CrossRef]

42. Hagemann, H.; Longhini, M.; Kaminski, J.W.; Wesolowski, T.A.; Černý, R.; Penin, N.; Sørby, M.H.; Hauback, B.C.; Severa, G.; Jensen, C.M. LiSc(BH$_4$)$_4$: A novel salt of Li and discrete Sc(BH$_4$)$_4^-$ Complex anions. *J. Phys. Chem. A* **2008**, *112*, 7551–7555. [CrossRef]

43. Černý, R.; Severa, G.; Ravnsbæk, D.B.; Filinchuk, Y.; D'Anna, V.; Hagemann, H.; Haase, D.; Jensen, C.M.; Jensen, T.R. NaSc(BH$_4$)$_4$: A novel scandium-based borohydride. *J. Phys. Chem. C* **2010**, *114*, 1357–1364. [CrossRef]

44. Kim, C.; Hwang, S.J.; Bowman, R.C.; Reiter, J.W.; Zan, J.A.; Kulleck, J.G.; Kabbour, H.; Majzoub, E.H.; Ozolins, V. LiSc(BH$_4$)$_4$ as a hydrogen storage material: Multinuclear high-resolution solid-state NMR and first-principles density functional theory studies. *J. Phys. Chem. C* **2009**, *113*, 9956–9968. [CrossRef]

45. Tran, H.D.; Amsler, M.; Botti, S.; Marques, M.A.L.; Goedecker, S. First-principles predicted low-energy structures of NaSc(BH$_4$)$_4$. *J. Chem. Phys.* **2014**, *140*. [CrossRef]

46. Huang, L.W.; Elkedim, O.; Li, X. First principles investigation of scandium-based borohydride NaSc(BH$_4$)$_4$. *J. Alloys Compd.* **2012**, *536*, S546–S549. [CrossRef]

47. Kim, K.C. Validation of the reaction thermodynamics associated with NaSc(BH$_4$)$_4$ from first-principles calculations: Detecting metastable paths and identifying the minimum free energy path. *J. Chem. Phys.* **2012**, *137*, 084111. [CrossRef] [PubMed]

48. Kim, K.C. Crystal structures and thermodynamic investigations of NaSc(BH$_4$)$_4$ from first-principles calculations. *Int. J. Quantum Chem.* **2013**, *113*, 119–124. [CrossRef]

49. Černý, R.; Ravnsbæk, D.B.; Severa, G.; Filinchuk, Y.; D'Anna, V.; Hagemann, H.; Haase, D.; Skibsted, J.; Jensen, C.M.; Jensen, T.R. Structure and characterization of KSc(BH$_4$)$_4$. *J. Phys. Chem. C* **2010**, *114*, 19540–19549. [CrossRef]

50. Starobrat, A.; Jaroń, T.; Grochala, W. Two new derivatives of scandium borohydride, MSc(BH$_4$)$_4$, M = Rb, Cs, prepared: Via a one-pot solvent-mediated method. *Dalt. Trans.* **2019**, *48*, 11829–11837. [CrossRef]

51. Zange, E. Entwicklung eines Mikroverfahrens zur Darstellung von Boranaten der schweren Lanthaniden. *Chem. Ber.* **1960**, *93*, 652–657. [CrossRef]

52. Segal, B.G.; Lippard, S.J. Transition metal hydroborate complexes. 10. Crystal and molecular structure of tris(tetrahydroborato)tris(tetrahydr *Inorg. Chem.* **1978**, *17*, 844–850. [CrossRef]

53. Sato, T.; Miwa, K.; Nakamori, Y.; Ohoyama, K.; Li, H.; Noritake, T.; Aoki, M. Experimental and computational studies on solvent-free rare-earth metal borohydrides R(BH$_4$)$_3$ (R = Y, Dy, and Gd). *Phys. Rev. B* **2008**, *3*, 1–8. [CrossRef]

54. Remhof, A.; Borgschulte, A.; Friedrichs, O.; Mauron, P.; Yan, Y.; Züttel, A. Solvent-free synthesis and decomposition of Y(BH$_4$)$_3$. *Scr. Mater.* **2012**, *66*, 280–283. [CrossRef]

55. Park, K.; Lee, H.-S.; Remhof, A.; Lee, Y.-S.; Yan, Y.; Kim, M.-Y.; Kim, S.J.; Züttel, A.; Cho, Y.W. Thermal properties of Y(BH$_4$)$_3$ synthesized via two different methods. *Int. J. Hydrog. Energy* **2013**, *38*, 9263–9270. [CrossRef]

56. Jaroń, T.; Grochala, W. Y(BH$_4$)$_3$ —an old–new ternary hydrogen store akalearning from a multitude of failures. *Dalt. Trans.* **2010**, *39*, 160–166. [CrossRef]

57. Ravnsbæk, D.B.; Filinchuk, Y.; Cern, R.; Jakobsen, H.J.; Jensen, T.R.; Esrf, S.B. Thermal Polymorphism and Decomposition of Y(BH$_4$)$_3$. *Inorg. Chem.* **2010**, 3801–3809. [CrossRef]

58. Frommen, C.; Aliouane, N.; Deledda, S.; Fonneløp, J.E.; Grove, H.; Lieutenant, K.; Llamas-Jansa, I.; Sartori, S.; Sørby, M.H.; Hauback, B.C. Crystal structure, polymorphism, and thermal properties of yttrium borohydride Y(BH$_4$)$_3$. *J. Alloys Compd.* **2010**, *496*, 710–716. [CrossRef]

59. Yan, Y.; Remhof, A.; Rentsch, D.; Lee, Y.-S.; Whan Cho, Y.; Züttel, A. Is Y$_2$(B$_{12}$H$_{12}$)$_3$ the main intermediate in the decomposition process of Y(BH$_4$)$_3$? *Chem. Commun.* **2013**, *49*, 5234. [CrossRef]

60. Yan, Y.; Li, H.W.; Sato, T.; Umeda, N.; Miwa, K.; Towata, S.I.; Orimo, S. Dehydriding and rehydriding properties of yttrium borohydride Y(BH$_4$)$_3$ prepared by liquid-phase synthesis. *Int. J. Hydrog. Energy* **2009**, *34*, 5732–5736. [CrossRef]

61. Lee, Y.S.; Shim, J.H.; Cho, Y.W. Polymorphism and thermodynamics of Y(BH$_4$)$_3$ from first principles. *J. Phys. Chem. C* **2010**, *114*, 12833–12837. [CrossRef]

62. Roedern, E.; Lee, Y.-S.; Ley, M.B.; Park, K.; Cho, Y.W.; Skibsted, J.; Jensen, T.R. Solid state synthesis, structural characterization and ionic conductivity of bimetallic alkali-metal yttrium borohydrides MY(BH$_4$)$_4$ (M = Li and Na). *J. Mater. Chem. A* **2016**, *4*, 8793–8802. [CrossRef]

63. Jaroń, T.; Wegner, W.; Fijałkowski, K.J.; Leszczyński, P.J.; Grochala, W. Facile Formation of Thermodynamically Unstable Novel Borohydride Materials by a Wet Chemistry Route. *Chem. A Eur. J.* **2015**, *21*, 5689–5692. [CrossRef]

64. Dai, J.; Chen, Y.; Xie, R.; Hu, Z.; Song, Y. Influence of alloying elements on the stability and dehydrogenation properties on Y(BH$_4$)$_3$ by first principles calculations. *Int. J. Hydrog. Energy* **2016**, *41*, 1662–1671. [CrossRef]

65. Jaroń, T.; Grochala, W. Probing Lewis acidity of Y(BH$_4$)$_3$ via its reactions with MBH$_4$ (M = Li, Na, K, NMe$_4$). *Dalt. Trans.* **2011**, *40*, 12808–12817. [CrossRef]

66. Ravnsbæk, D.B.; Ley, M.B.; Lee, Y.S.; Hagemann, H.; D'Anna, V.; Cho, Y.W.; Filinchuk, Y.; Jensen, T.R. A mixed-cation mixed-anion borohydride NaY(BH$_4$)$_2$Cl$_2$. *Int. J. Hydrog. Energy* **2012**, *37*, 8428–8438. [CrossRef]

67. Jaroń, T.; Wegner, W.; Grochala, W. M[Y(BH$_4$)$_4$] and M$_2$Li[Y(BH$_4$)$_{6-x}$Cl$_x$] (M = Rb, Cs): New borohydride derivatives of yttrium and their hydrogen storage properties. *Dalt. Trans.* **2013**, *42*, 6886. [CrossRef] [PubMed]

68. Sadikin, Y.; Stare, K.; Schouwink, P.; Brix Ley, M.; Jensen, T.R.; Meden, A.; Černý, R. Alkali metal-Yttrium borohydrides: The link between coordination of small and large rare-earth. *J. Solid State Chem.* **2015**, *225*, 231–239. [CrossRef]

69. Schouwink, P.; Ley, M.B.; Tissot, A.; Hagemann, H.; Jensen, T.R.; Smrčok, L.; Černý, R. Structure and properties of complex hydride perovskite materials. *Nat. Commun.* **2014**, *5*, 1–10. [CrossRef]

70. Łodziana, Z. Multivalent metal tetrahydroborides of Al, Sc, Y, Ti, and Zr. *Phys. Rev. B* **2010**, *81*, 144108. [CrossRef]

71. Dain, C.J.; Downs, A.J.; Goode, M.J.; Evans, D.G.; Nicholls, K.T.; Rankin, D.W.H.; Robertson, H.E. Molecular structure of gaseous titanium tris(tetrahydroborate), Ti(BH$_4$)$_3$: Experimental determination by electron diffraction and molecular orbital analysis of some Ti(BH$_4$)$_3$ derivatives. *J. Chem. Soc. Dalt. Trans.* **1991**, 967. [CrossRef]

72. Hoekstra, H.R.; Katz, J.J. The Preparation and Properties of the Group IV-B Metal Borohydrides. *J. Am. Chem. Soc.* **1949**, *71*, 2488–2492. [CrossRef]

73. Franz, K.; Fusstetter, H.; Nöth, H. Metallboranate und Boranatometallate. IX [1]; Äther-Addukte von Tris(boranato)-titan(III) und dimere Alkoxy-bis(boranato)-titan(III)-Verbindungen. *Z. Anorg. und Allg. Chemie* **1976**, *427*, 97–113. [CrossRef]

74. Jensen, J.A.; Wilson, S.R.; Girolami, G.S. Titanium(III) tetrahydroborates. Preparation and crystal structure of Ti(BH$_4$)$_3$(PMe$_3$)$_2$ containing an unusual Ti.cntdot..cntdot..cntdot.H.cntdot..cntdot..cntdot.B agostic interaction. *J. Am. Chem. Soc.* **1988**, *110*, 4977–4982. [CrossRef]

75. Fang, Z.Z.; Ma, L.P.; Kang, X.D.; Wang, P.J.; Wang, P.; Cheng, H.M. In situ formation and rapid decomposition of Ti(BH$_4$)$_3$ by mechanical milling LiBH$_4$ with TiF$_3$. *Appl. Phys. Lett.* **2009**, *94*, 1–4. [CrossRef]

76. Callini, E.; Szilágyi, P.Á.; Paskevicius, M.; Stadie, N.P.; Réhault, J.; Buckley, C.E.; Borgschulte, A.; Züttel, A. Stabilization of volatile Ti(BH$_4$)$_3$ by nano-confinement in a metal–organic framework. *Chem. Sci.* **2016**, *7*, 666–672. [CrossRef]

77. Jarid, A.; Lledos, A.; Jean, Y.; Volatron, F. Ab initio study of the coordination modes of tetrahydroborato ligands: Structure of the tris(tetrahydroborato)titanium. *Inorg. Chem.* **1993**, *32*, 4695–4699. [CrossRef]

78. Reid, W.E.; Bish, J.M.; Brenner, A. Electrodeposition of Metals from Organic Solutions. *J. Electrochem. Soc.* **1957**, *104*, 21–29. [CrossRef]

79. Gennari, F.C.; Fernández Albanesi, L.; Rios, I.J. Synthesis and thermal stability of Zr(BH$_4$)$_4$ and Zr(BD$_4$)$_4$ produced by mechanochemical processing. *Inorg. Chim. Acta* **2009**, *362*, 3731–3737. [CrossRef]

80. James, B.D.; Smith, B.E. Convenient, High-Yield Syntheses of Bis(tetrahydroborato)bis(cyclopentadienyl)zirconium(IV) and Tetrakis(tetrahydroborato)zirconium(IV). *Synth. React. Inorg. Met. Chem.* **1974**, *4*, 461–465. [CrossRef]

81. Haaland, A.; Shorokhov, D.J.; Tutukin, A.V.; Volden, H.V.; Swang, O.; McGrady, G.S.; Kaltsoyannis, N.; Downs, A.J.; Tang, C.Y.; Turner, J.F.C. Molecular structures of two metal tetrakis(tetrahydroborates), Zr(BH$_4$)$_4$ and U(BH$_4$)$_4$: Equilibrium conformations and barriers to internal rotation of the triply bridging BH$_4$ groups. *Inorg. Chem.* **2002**, *41*, 6646–6655. [CrossRef] [PubMed]

82. Volkov, V.V.; Myakishev, K.G. Mechanochemical reactions in the chemistry of boranes. *Inorg. Chim. Acta* **1999**, *289*, 51–57. [CrossRef]

83. Rude, L.H.; Corno, M.; Ugliengo, P.; Baricco, M.; Lee, Y.-S.; Cho, Y.W.; Besenbacher, F.; Overgaard, J.; Jensen, T.R. Synthesis and Structural Investigation of Zr(BH$_4$)$_4$. *J. Phys. Chem. C* **2012**, *116*, 20239–20245. [CrossRef]

84. Huang, J.; Tan, Y.; Su, J.; Gu, Q.; Černý, R.; Ouyang, L.; Sun, D.; Yu, X.; Zhu, M. Synthesis, structure and dehydrogenation of zirconium borohydride octaammoniate. *Chem. Commun.* **2015**, *51*, 2794–2797. [CrossRef] [PubMed]

85. Wu, D.F.; Ouyang, L.Z.; Huang, J.M.; Liu, J.W.; Wang, H.; Shao, H.; Zhu, M. Synthesis and hydrogen storage property tuning of Zr(BH$_4$)$_4$·8NH$_3$ via physical vapour deposition and composite formation. *Int. J. Hydrog. Energy* **2018**, *43*, 19182–19188. [CrossRef]

86. Igoshkin, A.M.; Golovnev, I.F.; Krisyuk, V.V.; Igumenov, I.K.; Mechanics, A.; Branch, S.; Branch, S. Structure of Zirconium Tetrahydroborate Zr(BH$_4$)$_4$: A Molecular Dynamics Study. *J. Struct. Chem.* **2016**, *57*, 1068–1073. [CrossRef]

87. Green, J.C.; De Simone, M.; Coreno, M.; Jones, A.; Pritchard, H.M.I.; McGrady, G.S. Electronic structure of M(BH$_4$)$_4$, M = Zr, Hf, and U, by variable photon-energy photoelectron spectroscopy and density functional calculations. *Inorg. Chem.* **2005**, *44*, 7781–7793. [CrossRef]

88. Ehemann, M.; Nöth, H. Metallboranate und Boranatometallate. IV. Boranatokomplexe M(BH$_4$)$_{4+n}$ $^{n-}$ des Zirkoniums, Hafniums und Thoriums. *Z. Anorg. und Allg. Chemie* **1971**, *386*, 87–101. [CrossRef]

89. Jensen, C.M.; Severa, G.; Zhang, S.; Culnane, L.; Langley, W.; Ayabe, R.; Humphries, T.; Setthanan, U.; McGrady, G.S. IV.A.1j Fundamental Studies of Advanced High-Capacity, Reversible Metal Hydrides. Available online: https://www.hydrogen.energy. gov/pdfs/progress08/iv_a_1j_jensen.pdf (accessed on 12 May 2021).

90. Roy, D.K.; Mondal, B.; De, A.; Panda, S.; Ghosh, S. Novel Neutral Zirconaborane [(Cp$_2$Zr)$_2$B$_5$H$_{11}$]: An arachno -B$_3$H$_9$ Analogue (Cp =η^5 -C$_5$H$_5$). *Organometallics* **2015**, *34*, 908–912. [CrossRef]

91. Tamami, B.; Goudarzian, N. Polymer supported ziroconium borohydride: A stable, efficient and regenerable reducing agent. *J. Chem. Soc. Chem. Commun.* **1994**, 1079. [CrossRef]

92. Borisenko, K.B.; Downs, A.J.; Robertson, H.E.; Rankin, D.W.H.; Tang, C.Y. Molecular structure of Hf(BH$_4$)$_4$ investigated by quantum mechanical calculations and gas-phase electron diffraction. *Dalt. Trans.* **2004**, 967–970. [CrossRef]

93. Broach, R.W.; Chuang, I.S.; Marks, T.J.; Williams, J.M. Metrical characterization of tridentate tetrahydroborate ligation to a transition-metal ion. Structure and bonding in Hf(BH$_4$)$_4$ by single-crystal neutron diffraction. *Inorg. Chem.* **1983**, *22*, 1081–1084. [CrossRef]

94. Jensen, J.A.; Gozum, J.E.; Pollina, D.M.; Girolami, G.S. Titanium, zirconium, and hafnium tetrahydroborates as "tailored" CVD precursors for metal diboride thin films. *J. Am. Chem. Soc.* **1988**, *110*, 1643–1644. [CrossRef]

95. Wayda, A.L.; Schneemeyer, L.F.; Opila, R.L. Low-temperature deposition of zirconium and hafnium boride films by thermal decomposition of the metal borohydrides (M[BH$_4$]$_4$). *Appl. Phys. Lett.* **1988**, *53*, 361–363. [CrossRef]

96. Yang, C.H.; Tsai, W.T.; Chang, J.K. Hydrogen desorption behavior of vanadium borohydride synthesized by modified mechano-chemical process. *Int. J. Hydrog. Energy* **2011**, *36*, 4993–4999. [CrossRef]

97. Korablov, D.; Ravnsbæk, D.B.; Ban, V.; Filinchuk, Y.; Besenbacher, F.; Jensen, T.R. Investigation of MBH$_4$-VCl$_2$, M = Li, Na or K. *Int. J. Hydrog. Energy* **2013**, *38*, 8376–8383. [CrossRef]

98. Makhaev, V.D.; Semenenko, K.N. Synthesis and properties of vanadium borohydride complex NaV(BH$_4$)$_4$·3DME. *Bull. Acad. Sci. USSR Div. Chem. Sci.* **1978**, *27*, 2520–2521. [CrossRef]

99. Jensen, J.A.; Girolami, G.S. Vanadium(III) tetrahydroborates. Preparation, reaction chemistry, and crystal structures of V(BH$_4$)$_3$(PMe$_3$)$_2$ and the oxo dimer [V(BH$_4$)$_2$(PMe3)$_2$]$_2$O. *Inorg. Chem.* **1989**, *28*, 2114–2119. [CrossRef]

100. Jensen, J.A.; Girolami, G.S. Vanadium tetrahydroborates: Preparation and characterization of V(■^{2}-BH$_4$)$_3$(PMe$_3$)$_2$ and the unusual unidentate BH$_4$− complex V(■^{1}-BH$_4$)$_2$(dmpe)$_2$. *J. Am. Chem. Soc.* **1988**, *110*, 4450–4451. [CrossRef]

101. Hummelshøj, J.S.; Landis, D.D.; Voss, J.; Jiang, T.; Tekin, A.; Bork, N.; Duak, M.; Mortensen, J.J.; Adamska, L.; Andersin, J.; et al. Density functional theory based screening of ternary alkali-transition metal borohydrides: A computational material design project. *J. Chem. Phys.* **2009**, *131*. [CrossRef] [PubMed]

102. Charkin, O.P. Theoretical study of tetrahydroborates and alanates L(MH$_4$)$_4$, HL(MH$_4$)$_3$, H$_2$L(MH$_4$)$_2$, and H$_3$L(MH$_4$) (L = Al, Sc, Ti, V, Cr; M = B, Al). *Russ. J. Inorg. Chem.* **2009**, *54*, 951–960. [CrossRef]

103. Nöth, H. Anorganische Reaktionen der Alkaliboranate. *Angew. Chemie* **1961**, *73*, 371–383. [CrossRef]

104. Suárez-Alcántara, K.; Tena-Garcia, J.R.; Guerrero-Ortiz, R. Alanates, a comprehensive review. *Materials* **2019**, *12*, 2724. [CrossRef]

105. Seitz, M.A.X. Preparation and Characterization of Chromium(II) Tetrahydroborate- Tetrahydrofuran (1/2). *J. Chem. Soc. Chem. Commun.* **1976**, *547*, 1976.

106. Dionne, M.; Hao, S.; Gambarotta, S. Preparation and characterization of a new series of Cr(II) hydroborates. *Can. J. Chem.* **1995**, *73*, 1126–1134. [CrossRef]

107. Nakamori, Y.; Li, H.W.; Matsuo, M.; Miwa, K.; Towata, S.; Orimo, S. Development of metal borohydrides for hydrogen storage. *J. Phys. Chem. Solids* **2008**, *69*, 2292–2296. [CrossRef]

108. Schouwink, P.; D'Anna, V.; Ley, M.B.; Lawson Daku, L.M.; Richter, B.; Jensen, T.R.; Hagemann, H.; Černý, R. Bimetallic borohydrides in the system M(BH$_4$)$_2$-KBH$_4$ (M = Mg, Mn): On the structural diversity. *J. Phys. Chem. C* **2012**, *116*, 10829–10840. [CrossRef]

109. Richter, B.; Ravnsbæk, D.B.; Tumanov, N.; Filinchuk, Y.; Jensen, T.R. Manganese borohydride; Synthesis and characterization. *Dalt. Trans.* **2015**, *44*, 3988–3996. [CrossRef] [PubMed]

110. Tumanov, N.A.; Safin, D.A.; Richter, B.; Łodziana, Z.; Jensen, T.R.; Garcia, Y.; Filinchuk, Y. Challenges in the synthetic routes to Mn(BH$_4$)$_2$: Insight into intermediate compounds. *Dalt. Trans.* **2015**, *44*, 6571–6580. [CrossRef]

111. Tumanov, N.A.; Roedern, E.; Łodziana, Z.; Nielsen, D.B.; Jensen, T.R.; Talyzin, A.V.; Černý, R.; Chernyshov, D.; Dmitriev, V.; Palasyuk, T.; et al. High-Pressure Study of Mn(BH$_4$)$_2$ Reveals a Stable Polymorph with High Hydrogen Density. *Chem. Mater.* **2016**, *28*, 274–283. [CrossRef]

112. Liu, R.; Reed, D.; Book, D. Decomposition behaviour of Mn(BH$_4$)$_2$ formed by ball-milling LiBH$_4$ and MnCl$_2$. *J. Alloys Compd.* **2012**, *515*, 32–38. [CrossRef]

113. Makhaev, V.D.; Borisov, A.P.; Gnilomedova, T.P.; Lobkovskii, É.B.; Chekhlov, A.N. Production of manganese borohydride complexes of manganese solvated with THF, and the structure of Mn(BH$_4$)$_2$ (THF)$_3$. *Bull. Acad. Sci. USSR Div. Chem. Sci.* **1987**, *36*, 1582–1586. [CrossRef]

114. Severa, G.; Hagemann, H.; Longhini, M.; Kaminski, J.W.; Wesolowski, T.A.; Jensen, C.M. Thermal desorption, vibrational spectroscopic, and DFT computational studies of the complex manganese borohydrides Mn(BH$_4$)$_2$ and [Mn(BH$_4$)$_4$]$^{2-}$. *J. Phys. Chem. C* **2010**, *114*, 15516–15521. [CrossRef]

115. Černý, R.; Penin, N.; Hagemann, H.; Filinchuk, Y. The first crystallographic and spectroscopic characterization of a 3d-Metal borohydride: Mn(BH$_4$)$_2$. *J. Phys. Chem. C* **2009**, *113*, 9003–9007. [CrossRef]

116. Bidabadi, A.S.; Korinek, A.; Botton, G.A.; Varin, R.A. High resolution transmission electron microscopy (TEM), energy-dispersive X-ray spectroscopy (EDS) and X-ray diffraction studies of nanocrystalline manganese borohydride (Mn(BH$_4$)$_2$) after mechano-chemical synthesis and thermal dehydrogenation. *Acta Mater.* **2015**, *100*, 392–400. [CrossRef]

117. Choudhury, P.; Bhethanabotla, V.R.; Stefanakos, E. Manganese borohydride as a hydrogen-storage candidate: First-principles crystal structure and thermodynamic properties. *J. Phys. Chem. C* **2009**, *113*, 13416–13424. [CrossRef]

118. Varin, R.A.; Bidabadi, A.S. The effect of milling energy input during mechano-chemical activation synthesis (MCAS) of the nanocrystalline manganese borohydride (Mn(BH$_4$)$_2$) on its thermal dehydrogenation properties. *Int. J. Hydrog. Energy* **2014**, *39*, 11620–11632. [CrossRef]

119. Zavorotynska, O.; El-Kharbachi, A.; Deledda, S.; Hauback, B.C. Recent progress in magnesium borohydride Mg(BH$_4$)$_2$: Fundamentals and applications for energy storage. *Int. J. Hydrog. Energy* **2016**, *41*, 14387–14403. [CrossRef]

120. Roedern, E.; Jensen, T.R. Thermal decomposition of Mn(BH$_4$)$_2$-M(BH$_4$)$_x$ and Mn(BH$_4$)$_2$-MH$_x$ composites with M = Li, Na, Mg, and Ca. *J. Phys. Chem. C* **2014**, *118*, 23567–23574. [CrossRef]

121. Pankin, I.A.; Guda, A.A.; Tumanov, N.A.; Filinchuk, Y.; Lomachenko, K.A.; Bugaev, A.L.; Guda, S.A.; Shapovalov, V.V.; Lamberti, C.; Soldatov, A.V. Experimental and theoretical study of hydrogen desorption process from Mn(BH$_4$)$_2$. *J. Alloys Compd.* **2018**, *735*, 277–284. [CrossRef]

122. Varin, R.A.; Zbroniec, L.; Polanski, M.; Filinchuk, Y.; Černý, R. Mechano-chemical synthesis of manganese borohydride (Mn(BH$_4$)$_2$) and inverse cubic spinel (Li$_2$MnCl$_4$) in the (nLiBH$_4$ + MnCl$_2$) (n = 1, 2, 3, 5, 9 and 23) mixtures and their dehydrogenation behavior. *Int. J. Hydrog. Energy* **2012**, *37*, 16056–16069. [CrossRef]

123. Varin, R.A.; Bidabadi, A.S.; Polanski, M.; Biglari, M.; Stobinski, L. The effects of filamentary Ni, graphene and lithium amide (LiNH$_2$) additives on the dehydrogenation behavior of mechano-chemically synthesized crystalline manganese borohydride (Mn(BH$_4$)$_2$) and its solvent filtration/extraction. *Mater. Res. Bull.* **2018**, *100*, 394–406. [CrossRef]

124. Guda, A.A.; Pankin, I.A.; Bugaev, A.L.; Lomachenko, K.A.; Guda, S.A.; Dmitriev, V.P.; Soldatov, A.V. X-ray absorption spectroscopy determination of the products of manganese borohydride decomposition upon heating. *Bull. Russ. Acad. Sci. Phys.* **2015**, *79*, 139–143. [CrossRef]

125. Choudhury, P.; Srinivasan, S.S.; Bhethanabotla, V.R.; Goswami, Y.; McGrath, K.; Stefanakos, E.K. Nano-Ni doped Li-Mn-B-H system as a new hydrogen storage candidate. *Int. J. Hydrog. Energy* **2009**, *34*, 6325–6334. [CrossRef]

126. Fang, F.; Li, Y.T.; Song, Y.; Zha, J.; Zhao, B.; Sun, D.L. LiMn(BH$_4$)$_3$/2LiCl Composite Synthesized by Reactive Ball-Milling and Its Dehydrogenation Properties. *Acta Phys. Chim. Sin.* **2011**, *27*, 1537–1542. [CrossRef]

127. Varin, R.A.; Zbroniec, L. The effects of ball milling and nanometric nickel additive on the hydrogen desorption from lithium borohydride and manganese chloride (3LiBH$_4$ + MnCl$_2$) mixture. *Int. J. Hydrog. Energy* **2010**, *35*, 3588–3597. [CrossRef]

128. Černý, R.; Penin, N.; D'Anna, V.; Hagemann, H.; Durand, E.; Růžička, J. Mg$_x$Mn$_{(1-x)}$(BH$_4$)$_2$ (x = 0-0.8), a cation solid solution in a bimetallic borohydride. *Acta Mater.* **2011**, *59*, 5171–5180. [CrossRef]

129. Černý, R.; Schouwink, P.; Sadikin, Y.; Stare, K.; Smrčok, L.; Richter, B.; Jensen, T.R. Trimetallic borohydride Li$_3$MZn$_5$(BH$_4$)$_{15}$ (M = Mg, Mn) containing two weakly interconnected frameworks. *Inorg. Chem.* **2013**, *52*, 9941–9947. [CrossRef]

130. Schaeffer, G.W.; Roscoe, J.S.; Stewart, A.C. The Reduction of Iron(III) Chloride with Lithium Aluminohydride and Lithium Borohydride: Iron(II) Borohydride. *J. Am. Soc.* **1956**, *78*, 729–733. [CrossRef]

131. Varin, R.A.; Bidabadi, A.S. Rapid, ambient temperature hydrogen generation from the solid state Li-B-Fe-H system by mechano-chemical activation synthesis. *J. Power Sources* **2015**, *284*, 554–565. [CrossRef]

132. Varin, R.A.; Shirani Bidabadi, A. Nanostructured, complex hydride systems for hydrogen generation. *AIMS Energy* **2015**, *3*, 121–143. [CrossRef]

133. Stewart, A.C.; Schaeffer, G.W. The reaction of cobalt(II) bromide with lithium borohydride and lithium aluminohydride. *J. Inorg. Nucl. Chem.* **1956**, *3*, 194–197. [CrossRef]

134. Raje, S.; Angamuthu, R. Solvent-free synthesis and reactivity of nickel(II) borohydride and nickel(II) hydride. *Green Chem.* **2019**, *21*, 2752–2758. [CrossRef]

135. Wiberg, E. Zur kenntnis eines kupfer-bor-wasserstoffs CuBH$_4$. *Z. Naturforsch. B* **1952**, *7b*, 582. [CrossRef]

136. Klingen, T.J. The Reaction of Copper(II) Chloride with Lithium Borohydride. *Inorg. Chem.* **1964**, *3*, 1058–1059. [CrossRef]

137. Wiberg, E.; Henle, W. Notizen: Zur Kenntnis eines Silber-bor-wasserstoffs AgBH$_4$. *Z. Naturforsch. B* **1952**, *7*, 575–576. [CrossRef]

138. Wiberg, E. Neuere Ergebnisse der praparativen Hydrid-Forschung. *Angew. Chemie* **1953**, *65*, 16–33. [CrossRef]

139. Musaev, D.G.; Morokuma, K. Does the Tetrahydroborate Species AuBH$_4$ Exist? Ab Initio MO Study of the Structure and Stability of CuBH$_4$, AgBH$_4$, and AuBH$_4$. *Organometallics* **1995**, *14*, 3327–3334. [CrossRef]

140. Wiberg, E.; Henle, W. Notizen: Zur Kenntnis eines ätherlöslichen Zink-bor-wasser-stoffs Zn(BH$_4$)$_2$. *Z. Naturforsch. B* **1952**, *7*, 579–580. [CrossRef]

141. Nöth, H.; Wiberg, E.; Winter, L.P. Boranate und Boranato-metallate. I. Zur Kenntnis von Solvaten des Zinkboranats. *Z. Anorg. Allg. Chemie* **1969**, *370*, 209–223. [CrossRef]

142. Narasimhan, S.; Balakumar, R. Synthetic applications of zinc borohydride. *Aldrichimica Acta* **1998**, *31*, 19–26.

143. Friedrichs, O.; Borgschulte, A.; Kato, S.; Buchter, F.; Gremaud, R.; Remhof, A.; Züttel, A. Low-Temperature Synthesis of LiBH$_4$ by Gas-Solid Reaction. *Chem. A Eur. J.* **2009**, *15*, 5531–5534. [CrossRef]

144. Choudhury, P.; Bhethanabotla, V.R.; Stefanakos, E. Identification of a stable phase for the high-capacity hydrogen-storage material $Zn(BH_4)_2$ from density functional theory and lattice dynamics. *Phys. Rev. B Condens. Matter Mater. Phys.* **2008**, *77*. [CrossRef]

145. Huan, T.D.; Amsler, M.; Tuoc, V.N.; Willand, A.; Goedecker, S. Low-energy structures of zinc borohydride $Zn(BH_4)_2$. *Phys. Rev. B Condens. Matter Mater. Phys.* **2012**, *86*, 1–8. [CrossRef]

146. Aidhy, D.S.; Wolverton, C. First-principles prediction of phase stability and crystal structures in Li-Zn and Na-Zn mixed-metal borohydrides. *Phys. Rev. B Condens. Matter Mater. Phys.* **2011**, *83*, 1–8. [CrossRef]

147. Ravnsbæk, D.; Filinchuk, Y.; Cerenius, Y.; Jakobsen, H.J.; Besenbacher, F.; Skibsted, J.; Jensen, T.R. A series of mixed-metal borohydrides. *Angew. Chemie Int. Ed.* **2009**, *48*, 6659–6663. [CrossRef] [PubMed]

148. Jeon, E.; Cho, Y.W. Mechanochemical synthesis and thermal decomposition of zinc borohydride. *J. Alloys Compd.* **2006**, *422*, 273–275. [CrossRef]

149. Srinivasan, S.; Escobar, D.; Jurczyk, M.; Goswami, Y.; Stefanakos, E. Nanocatalyst doping of $Zn(BH_4)_2$ for on-board hydrogen storage. *J. Alloys Compd.* **2008**, *462*, 294–302. [CrossRef]

150. Srinivasan, S.; Escobar, D.; Goswami, Y.; Stefanakos, E. Effects of catalysts doping on the thermal decomposition behavior of $Zn(BH_4)_2$. *Int. J. Hydrog. Energy* **2008**, *33*, 2268–2272. [CrossRef]

151. Yang, B.; Li, S.; Wang, H.; Xiang, J.; Yang, Q. Effect of MWCNTs additive on desorption properties of $Zn(BH_4)_2$ composite prepared by mechanical alloying. *J. Mater. Sci. Technol.* **2013**, *29*, 715–719. [CrossRef]

152. Nakagawa, T.; Ichikawa, T.; Kojima, Y.; Fujii, H. Gas emission properties of the MgH_x-$Zn(BH_4)_2$ systems. *Mater. Trans.* **2007**, *48*, 556–559. [CrossRef]

153. Park, H.R.; Kwak, Y.J.; Song, M.Y. Role of the Added Ni in Hydrogen-Storage Reactions of MgH_2-$Zn(BH_4)_2$-Tm (Ni, Ti, or Fe) Alloys. *Mater. Sci.* **2018**, *24*. [CrossRef]

154. Song, M.Y.; Kwak, Y.J. Comparison of the Hydrogen Release Properties of $Zn(BH_4)_2$-Added MgH_2 Alloy and $Zn(BH_4)_2$ and Ni-Added MgH_2 Alloy. *Korean J. Met. Mater.* **2018**, *56*. [CrossRef]

155. Černý, R.; Chul Kim, K.; Penin, N.; D'Anna, V.; Hagemann, H.; Sholl, D.S. $AZn_2(BH_4)_5$ (A = Li, Na) and $NaZn(BH_4)_3$: Structural Studies. *J. Phys. Chem. C* **2010**, *114*, 19127–19133. [CrossRef]

156. Ravnsbæk, D.B.; Frommen, C.; Reed, D.; Filinchuk, Y.; Sørby, M.; Hauback, B.C.; Jakobsen, H.J.; Book, D.; Besenbacher, F.; Skibsted, J.; et al. Structural studies of lithium zinc borohydride by neutron powder diffraction, Raman and NMR spectroscopy. *J. Alloys Compd.* **2011**, *509*, 698–704. [CrossRef]

157. Ravnsbæk, D.B.; Filinchuk, Y.; Černý, R.; Jensen, T.R. Powder diffraction methods for studies of borohydride-based energy storage materials. *Z. Krist.* **2010**, *225*, 557–569. [CrossRef]

158. Wang, Y.; Zhang, Y.; Wolverton, C. First-principles studies of phase stability and crystal structures in Li-Zn mixed-metal borohydrides. *Phys. Rev. B Condens. Matter Mater. Phys.* **2013**, *88*, 1–10. [CrossRef]

159. Xia, G.; Li, L.; Guo, Z.; Gu, Q.; Guo, Y.; Yu, X.; Liu, H.; Liu, Z. Stabilization of $NaZn(BH_4)_3$ via nanoconfinement in SBA-15 towards enhanced hydrogen release. *J. Mater. Chem. A* **2013**, *1*, 250–257. [CrossRef]

160. Černý, R.; Ravnsbæk, D.B.; Schouwink, P.; Filinchuk, Y.; Penin, N.; Teyssier, J.; Smrčok, L.; Jensen, T.R. Potassium zinc borohydrides containing triangular $[Zn(BH_4)_3]$-and tetrahedral $[Zn(BH_4)_xCl_{4-x}]^{2-}$ anions. *J. Phys. Chem. C* **2012**, *116*, 1563–1571. [CrossRef]

161. Albanese, E.; Kalantzopoulos, G.N.; Vitillo, J.G.; Pinatel, E.; Civalleri, B.; Deledda, S.; Bordiga, S.; Hauback, B.C.; Baricco, M. Theoretical and experimental study on $Mg(BH_4)_2$-$Zn(BH_4)_2$ mixed borohydrides. *J. Alloys Compd.* **2013**, *580*, S282–S286. [CrossRef]

162. Kalantzopoulos, G.N.; Vitillo, J.G.; Albanese, E.; Pinatel, E.; Civalleri, B.; Deledda, S.; Bordiga, S.; Baricco, M.; Hauback, B.C. Hydrogen storage of Mg-Zn mixed metal borohydrides. *J. Alloys Compd.* **2014**, *615*, S702–S705. [CrossRef]

163. Albanese, E.; Civalleri, B.; Casassa, S.; Baricco, M. Investigation on the decomposition enthalpy of novel mixed $Mg_{(1-x)}Zn_x(BH_4)_2$ borohydrides by means of periodic DFT calculations. *J. Phys. Chem. C* **2014**, *118*, 23468–23475. [CrossRef]

164. Ravnsbæk, D.B.; Sørensen, L.H.; Filinchuk, Y.; Reed, D.; Book, D.; Jakobsen, H.J.; Besenbacher, F.; Skibsted, J.; Jensen, T.R. Mixed-anion and mixed-cation borohydride $KZn(BH_4)Cl_2$: Synthesis, structure and thermal decomposition. *Eur. J. Inorg. Chem.* **2010**, 1608–1612. [CrossRef]

165. Wiberg, E.; Henle, W. Zur Kenntnis eines Cadmium-bor-wasserstoffs $Cd(BH_4)_2$. *Z. Naturforschg. B* **1952**, *7*, 582. [CrossRef]

166. Nöth, H.; Winter, L.P. Metallboranate und Boranato-metallate. V. Solvate des Cadmiumboranats und Boranatocadmate. *Z. Anorg. Allg. Chemie* **1972**, *389*, 225–234. [CrossRef]

167. Ravnsbaek, D.B.; Sørensen, L.H.; Filinchuk, Y.; Besenbacher, F.; Jensen, T.R. Screening of Metal Borohydrides by Mechanochemistry and Diffraction. *Angew. Chemie Int. Ed.* **2012**, *51*, 3582–3586. [CrossRef] [PubMed]

168. Blanchard, D.; Zatti, M.; Vegge, T. Analysis of the decomposition gases from α and β-$Cd(BH_4)_2$ synthesized by temperature controlled mechanical milling. *J. Alloys Compd.* **2013**, *547*, 76–80. [CrossRef]

169. Nöth, H.; Thomann, M. Metal Tetrahydroborates and Tetrahydroborato Metalates, 17/Bonding in Cadmium Bis(tetrahydroborate), and the Reaction with Lithium Tetrahydroborate. *Z. Naturforsch. B* **1990**, *45*, 1482–1486. [CrossRef]

170. Linti, G.; Nöth, H.; Thomann, M. Metal Tetrahydroborates and Tetrahydroborato Metalates, 15 [1] An ^{11}B and [113]Cd NMR Study of MBH_4-$CdCl_2$ Systems in Dimethylformamide and the X-Ray Structure of $CdCl_2 \cdot 2$ DMF. *Z. Naturforsch. Sect. B J. Chem. Sci.* **1990**, *45*, 1463–1471. [CrossRef]

171. Nöth, H.; Thomann, M. Metal Tetrahydroborates and Tetrahydroboratometalates, 18 [1] Studies on the Formation of Cadmium(II)-tetrahydroborates with Tetrahydroborate and Iodide. *Z. Naturforsch. Sect. B J. Chem. Sci.* **1994**, *49*, 9–14. [CrossRef]

172. Schlesinger, H.I.; Sanderson, R.T.; Burg, A.B. A Volatile Compound of Aluminum, Boron and Hydrogen. *J. Am. Chem. Soc.* **1939**, *61*, 536. [CrossRef]

173. Schlesinger, H.I.; Sanderson, R.T.; Burg, A.B. Metallo Borohydrides. I. Aluminum Borohydride. *J. Am. Chem. Soc.* **1940**, *62*, 3421–3425. [CrossRef]

174. Rulon, R.M.; Mason, L.S. The Heat of Formation of Aluminum Borohydride. *J. Am. Chem. Soc.* **1951**, *73*, 5491–5493. [CrossRef]

175. Schlesinger, H.I.; Brown, H.C.; Hyde, E.K. The Preparation of Other Borohydrides by Metathetical Reactions Utilizing the Alkali Metal Borohydrides. *J. Am. Chem. Soc.* **1953**, *75*, 209–213. [CrossRef]

176. Aldridge, S.; Blake, A.J.; Downs, A.J.; Gould, R.O.; Parsons, S.; Pulham, C.R. Some tetrahydroborate derivatives of aluminium: Crystal structures of dimethylaluminium tetrahydroborate and the α and β phases of aluminium tris(tetrahydroborate) at low temperature. *J. Chem. Soc. Dalt. Trans.* **1997**, 1007–1012. [CrossRef]

177. Almenningen, A.; Gundersen, G.; Haaland, A.; Haug, A.; Enzell, C.; Francis, G. On the Molecular Structure of Aluminium Borohydride, $Al(BH_4)_3$. *Acta Chem. Scand.* **1968**, *22*, 328–334. [CrossRef]

178. Bauer, S.H.; Bauer, S.H. The Structure of the Hydrides of Boron. VI. AlB_3H_{12}. *J. Am. Chem. Soc.* **1940**, *62*, 3440–3442.

179. Coe, D.A.; Nibler, J.W. Infrared and Raman spectra of aluminum borohydride, $Al(BH_4)_3$. *Spectrochim. Acta Part A Mol. Spectrosc.* **1973**, *29*, 1789–1804. [CrossRef]

180. Al-Kahtani, A.; Williams, D.L.; Nibler, J.W.; Sharpe, S.W. High-resolution infrared studies of $Al(BH_4)_3$ and $Al(BD_4)_3$. *J. Phys. Chem. A* **1998**, *102*, 537–544. [CrossRef]

181. Miwa, K.; Ohba, N.; Towata, S.I.; Nakamori, Y.; Züttel, A.; Orimo, S. Ichi First-principles study on thermodynamic stability of metal borohydrides: Aluminum borohydride $Al(BH_4)_3$. *J. Alloys Compd.* **2007**, *446–447*, 310–314. [CrossRef]

182. Harrison, D.; Thonhauser, T. Suppressing diborane production during the hydrogen release of metal borohydrides: The example of alloyed $Al(BH_4)_3$. *Int. J. Hydrog. Energy* **2016**, *41*, 3571–3578. [CrossRef]

183. Paduani, C.; Wu, M.M.; Willis, M.; Jena, P. Theoretical study of the stability and electronic structure of $Al(BH_4)_{n=1\rightarrow4}$ and $Al(BF_4)_{n=1\rightarrow4}$ and their hyperhalogen behavior. *J. Phys. Chem. A* **2011**, *115*, 10237–10243. [CrossRef]

184. Dovgaliuk, I.; Safin, D.A.; Tumanov, N.A.; Morelle, F.; Moulai, A.; Černý, R.; Łodziana, Z.; Devillers, M.; Filinchuk, Y. Solid Aluminum Borohydrides for Prospective Hydrogen Storage. *ChemSusChem* **2017**, *10*, 4725–4734. [CrossRef]

185. Dovgaliuk, I.; Ban, V.; Sadikin, Y.; Černý, R.; Aranda, L.; Casati, N.; Devillers, M.; Filinchuk, Y. The first halide-free bimetallic aluminum borohydride: Synthesis, structure, stability, and decomposition pathway. *J. Phys. Chem. C* **2014**, *118*, 145–153. [CrossRef]

186. Lindemann, I.; Ferrer, R.D.; Dunsch, L.; Filinchuk, Y.; Černý, R.; Hagemann, H.; D'Anna, V.; Daku, L.M.L.; Schultz, L.; Gutfleisch, O. $Al_3Li_4(BH_4)_{13}$: A complex double-cation borohydride with a new structure. *Chem. A Eur. J.* **2010**, *16*, 8707–8712. [CrossRef] [PubMed]

187. Lindemann, I.; Borgschulte, A.; Callini, E.; Züttel, A.; Schultz, L.; Gutfleisch, O. Insight into the decomposition pathway of the complex hydride $Al_3Li_4(BH_4)_{13}$. *Int. J. Hydrog. Energy* **2013**, *38*, 2790–2795. [CrossRef]

188. Knight, D.A.; Zidan, R.; Lascola, R.; Mohtadi, R.; Ling, C.; Sivasubramanian, P.; Kaduk, J.A.; Hwang, S.J.; Samanta, D.; Jena, P. Synthesis, characterization, and atomistic modeling of stabilized highly pyrophoric $Al(BH_4)_3$ via the formation of the hypersalt $K[Al(BH_4)_4]$. *J. Phys. Chem. C* **2013**, *117*, 19905–19915. [CrossRef]

189. Downs, A.J.; Thomas, P.D.P. Gallium borohydrides: The synthesis and properties of $HGa(BH_4)_2$. *J. Chem. Soc. Chem. Commun.* **1976**, 825. [CrossRef]

190. Pulham, C.R.; Brain, P.T.; Downs, A.J.; Rankin, D.W.H.; Robertson, H.E. Gallaborane, $H_2Ga(\mu-H)_2BH_2$: Synthesis, properties, and structure of the gaseous molecule as determined by electron diffraction. *J. Chem. Soc., Chem. Commun.* **1990**, 177–178. [CrossRef]

191. Barlow, M.T.; Dain, C.J.; Downs, A.J.; Laurenson, G.S.; Rankin, D.W.H. Group 3 tetrahydroborates. Part 4. The molecular structure of hydridogallium bis(tetrahydroborate) in the gas phase as determined by electron diffraction. *J. Chem. Soc. Dalt. Trans.* **1982**, 597. [CrossRef]

192. Downs, A.J.; Harman, L.A.; Thomas, P.D.P.; Pulham, C.R. Hydridogallium bis(tetrahydroborate), $HGa(BH_4)_2$: Synthesis and properties. *Polyhedron* **1995**, *14*, 935–945. [CrossRef]

193. Wiberg, E.; Nöth, H. Notizen: Über Wasserstoff-Verbindungen des Indiums. *Z. Naturforsch. B* **1957**, *12*, 59–60. [CrossRef]

194. Wiberg, E.; Dittmann, O.; Nöth, H.; Schmidt, M. Notizen: Über Wasserstoff-Verbindungen des Thalliums. V. Zur Kenntnis eines Thallium(I)-boranats TlBH4 und Thallium(I)-alanats TlAlH4. *Z. Naturforsch. B* **1957**, *12*, 62–63. [CrossRef]

195. Wiberg, E.; Nöth, H. Notizen: Über Wasserstoff-Verbindungen des Thalliums. VI. Zur Kenntnis eines Thallium(III)-boranats TlCl(BH4)2. *Z. Naturforsch. B* **1957**, *12*, 63–65. [CrossRef]

196. Stadie, N.P.; Callini, E.; Richter, B.; Jensen, T.R.; Borgschulte, A.; Züttel, A. Supercritical N_2 processing as a route to the clean dehydrogenation of porous $Mg(BH_4)_2$. *J. Am. Chem. Soc.* **2014**, *136*, 8181–8184. [CrossRef]

197. Frommen, C.; Sørby, M.; Heere, M.; Humphries, T.; Olsen, J.; Hauback, B. Rare Earth Borohydrides—Crystal Structures and Thermal Properties. *Energies* **2017**, *10*, 2115. [CrossRef]

198. Olsen, J.E.; Frommen, C.; Sørby, M.H.; Hauback, B.C. Crystal structures and properties of solvent-free $LiYb(BH_4)_{4-x}Cl_x$, $Yb(BH_4)_3$ and $Yb(BH_4)_{2-x}Cl_x$. *RSC Adv.* **2013**, *3*, 10764–10774. [CrossRef]

199. Zhang, B.J.; Liu, B.H.; Li, Z.P. Destabilization of LiBH$_4$ by (Ce, La)(Cl, F)$_3$ for hydrogen storage. *J. Alloys Compd.* **2011**, *509*, 751–757. [CrossRef]
200. Ley, M.B.; Jørgensen, M.; Černý, R.; Filinchuk, Y.; Jensen, T.R. From M(BH$_4$)$_3$ (M = La, Ce) Borohydride Frameworks to Controllable Synthesis of Porous Hydrides and Ion Conductors. *Inorg. Chem.* **2016**, *55*, 9748–9756. [CrossRef]
201. GharibDoust, S.H.P.; Brighi, M.; Sadikin, Y.; Ravnsbæk, D.B.; Černý, R.; Skibsted, J.; Jensen, T.R. Synthesis, Structure, and Li-Ion Conductivity of LiLa(BH$_4$)$_3$X, X = Cl, Br, I. *J. Phys. Chem. C* **2017**, *121*, 19010–19021. [CrossRef]
202. Payandeh Gharibdoust, S.; Heere, M.; Sørby, M.H.; Ley, M.B.; Ravnsbæk, D.B.; Hauback, B.C.; Černý, R.; Jensen, T.R. Synthesis, structure and properties of new bimetallic sodium and potassium lanthanum borohydrides. *Dalt. Trans.* **2016**, *45*, 19002–19011. [CrossRef] [PubMed]
203. Brighi, M.; Schouwink, P.; Sadikin, Y.; Černý, R. Fast ion conduction in garnet-type metal borohydrides Li$_3$K$_3$Ce$_2$(BH$_4$)$_{12}$ and Li$_3$K$_3$La$_2$(BH$_4$)$_{12}$. *J. Alloys Compd.* **2016**, *662*, 388–395. [CrossRef]
204. Payandeh Gharibdoust, S.; Ravnsbæk, D.B.; Černý, R.; Jensen, T.R. Synthesis, structure and properties of bimetallic sodium rare-earth (RE) borohydrides, NaRE(BH$_4$)$_4$, RE = Ce, Pr, Er or Gd. *Dalt. Trans.* **2017**, *46*, 13421–13431. [CrossRef] [PubMed]
205. Gennari, F.C.; Esquivel, M.R. Synthesis and dehydriding process of crystalline Ce(BH$_4$)$_3$. *J. Alloys Compd.* **2009**, *485*, 47–51. [CrossRef]
206. Luo, X.; Aguey-Zinsou, K.-F. Correlations between the ionic conductivity and cation size in complex borohydrides. *Ionics* **2020**, *26*, 5287–5291. [CrossRef]
207. Wu, H. Strategies for the Improvement of the Hydrogen Storage Properties of Metal Hydride Materials. *ChemPhysChem* **2008**, *9*, 2157–2162. [CrossRef]
208. Davies, R.A.; Hewett, D.R.; Anderson, P.A. Enhancing ionic conductivity in lithium amide for improved energy storage materials. *Adv. Nat. Sci. Nanosci. Nanotechnol.* **2014**, *6*, 015005. [CrossRef]
209. Anderson, P.A.; Chater, P.A.; Hewett, D.R.; Slater, P.R. Hydrogen storage and ionic mobility in amide–halide systems. *Faraday Discuss.* **2011**, *151*, 271. [CrossRef] [PubMed]
210. Gennari, F.C.; Albanesi, L.F.; Puszkiel, J.A.; Larochette, P.A. Reversible hydrogen storage from 6LiBH$_4$-MCl$_3$ (M = Ce, Gd) composites by in-situ formation of MH$_2$. *Int. J. Hydrog. Energy* **2011**, *36*, 563–570. [CrossRef]
211. Heere, M.; Payandeh GharibDoust, S.H.; Frommen, C.; Humphries, T.D.; Ley, M.B.; Sørby, M.H.; Jensen, T.R.; Hauback, B.C. The influence of LiH on the rehydrogenation behavior of halide free rare earth (RE) borohydrides (RE = Pr, Er). *Phys. Chem. Chem. Phys.* **2016**, *18*, 24387–24395. [CrossRef]
212. Humphries, T.D.; Ley, M.B.; Frommen, C.; Munroe, K.T.; Jensen, T.R.; Hauback, B.C. Crystal structure and in situ decomposition of Eu(BH$_4$)$_2$ and Sm(BH$_4$)$_2$. *J. Mater. Chem. A* **2015**, *3*, 691–698. [CrossRef]
213. Møller, K.T.; Jørgensen, M.; Fogh, A.S.; Jensen, T.R. Perovskite alkali metal samarium borohydrides: Crystal structures and thermal decomposition. *Dalt. Trans.* **2017**, *46*, 11905–11912. [CrossRef]
214. Olsen, J.E.; Frommen, C.; Jensen, T.R.; Riktor, M.D.; Sørby, M.H.; Hauback, B.C. Structure and thermal properties of composites with RE-borohydrides (RE = La, Ce, Pr, Nd, Sm, Eu, Gd, Tb, Er, Yb or Lu) and LiBH$_4$. *RSC Adv.* **2014**, *4*, 1570–1582. [CrossRef]
215. Sharma, M.; Didelot, E.; Spyratou, A.; Lawson Daku, L.M.; Černý, R.; Hagemann, H. Halide Free M(BH$_4$)$_2$ (M = Sr, Ba, and Eu) Synthesis, Structure, and Decomposition. *Inorg. Chem.* **2016**, *55*, 7090–7097. [CrossRef]
216. Rossmanith, K. Herstellung von Europium(II)-bromid-boranat. *Monatshefte für Chemie* **1966**, *97*, 863–865. [CrossRef]
217. Borisov, V.D.; Makahaev, A.P. tetrahydridoborates of divalent Samarium, Europium, and Ytterbium. *Russ. J. Inorg. Chem.* **1999**, *44*, 1411–1413.
218. Andrade-Gamboa, J.; Puszkiel, J.A.; Fernández-Albanesi, L.; Gennari, F.C. A novel polymorph of gadolinium tetrahydroborate produced by mechanical milling. *Int. J. Hydrog. Energy* **2010**, *35*, 10324–10328. [CrossRef]
219. Ley, M.B.; Paskevicius, M.; Schouwink, P.; Richter, B.; Sheppard, D.A.; Buckley, C.E.; Jensen, T.R. Novel solvates M(BH$_4$)$_3$S(CH$_3$)$_2$ and properties of halide-free M(BH$_4$)$_3$ (M = y or Gd). *Dalt. Trans.* **2014**, *43*, 13333–13342. [CrossRef]
220. Wegner, W.; Jaroń, T.; Grochala, W. Polymorphism and hydrogen discharge from holmium borohydride, Ho(BH$_4$)$_3$, and KHo(BH$_4$)$_4$. *Int. J. Hydrog. Energy* **2014**, *39*, 20024–20030. [CrossRef]
221. Wegner, W.; Jaroń, T.; Grochala, W. MYb(BH$_4$)$_4$ (M = K, Na) from laboratory X-ray powder data. *Acta Crystallogr. Sect. C Cryst. Struct. Commun.* **2013**, *69*, 1289–1291. [CrossRef] [PubMed]
222. Banks, R.H.; Edelstein, N.M. Synthesis and Characterization of Protactinium(IV), Neptunium(IV), and Plutonium (IV) Borohydrides. In *Lanthanide and Actinide Chemistry and Spectroscopy*; American Chemical Society Publications: Washington, DC, USA, 1980; pp. 331–348. [CrossRef]
223. Rajnak, K.; Gamp, E.; Shinomoto, R.; Edelstein, N. Optical and magnetic properties of uranium borohydride and tetrakismethyl-borohydride. *J. Chem. Phys.* **1984**, *80*, 5942–5950. [CrossRef]
224. Bernstein, E.R.; Hamilton, W.C.; Keiderling, T.A.; La Placa, S.J.; Lippard, S.J.; Mayerle, J.J. 14-Coordinate uranium(IV). Structure of uranium borohydride by single-crystal neutron diffraction. *Inorg. Chem.* **1972**, *11*, 3009–3016. [CrossRef]
225. Banks, R.H.; Edelstein, N.M.; Rietz, R.R.; Templeton, D.H.; Zalkin, A. Preparation and properties of the actinide borohydrides: Protactinium(IV), neptunium(IV), and plutonium(IV) borohydrides. *J. Am. Chem. Soc.* **1978**, *100*, 1957–1958. [CrossRef]
226. Schlesinger, H.I.; Brown, H.C. Uranium(IV) Borohydride 1. *J. Am. Chem. Soc.* **1953**, *75*, 219–221. [CrossRef]
227. Bernstein, E.R.; Keiderling, T.A. Optical and magnetic resonance spectra of inorganic molecular crystals-uranium borohydride [U(BH$_4$)$_4$] in hafnium borohydride [Hf(BH$_4$)$_4$]. *J. Chem. Phys.* **1973**, *59*, 2105–2122. [CrossRef]

228. Ghiassee, N.; Clay, P.G.; Walton, G.N. Photolytic decomposition of uranium tetrahydroborate vapour, $U(BH_4)_4$. *Inorg. Nucl. Chem. Lett.* **1980**, *16*, 149–153. [CrossRef]

229. Ghiassee, N.; Clay, P.G.; Walton, G.N. Thermal decomposition of $U(BH_4)_4$. *J. Inorg. Nucl. Chem.* **1981**, *43*, 2909–2913. [CrossRef]

230. Paine, R.T.; Schonberg, P.R.; Light, R.W.; Danen, W.C.; Freund, S.M. Photochemistry of $U(BH_4)_4$ and $U(BD_4)_4$. *J. Inorg. Nucl. Chem.* **1979**, *41*, 1577–1578. [CrossRef]

231. Rajnak, K.; Banks, R.H.; Gamp, E.; Edelstein, N. Analysis of the optical spectrum of $Np(BD_4)_4$ diluted in $Zr(BD_4)_4$ and the magnetic properties of $Np(BH_4)_4$ and $Np(BH_3CH_3)_4$. *J. Chem. Phys.* **1984**, *80*, 5951–5962. [CrossRef]

232. Schlapbach, L.; Züttel, A. Hydrogen-storage materials for mobile applications. *Nature* **2001**, *414*, 353–358. [CrossRef] [PubMed]

233. Li, H.W.; Orimo, S.; Nakamori, Y.; Miwa, K.; Ohba, N.; Towata, S.; Züttel, A. Materials designing of metal borohydrides: Viewpoints from thermodynamical stabilities. *J. Alloys Compd.* **2007**, *446–447*, 315–318. [CrossRef]

234. Błoński, P.; Łodziana, Z. Correlation between the ionic potential and thermal stability of metal borohydrides: First-principles investigations. *Phys. Rev. B* **2014**, *90*, 054114. [CrossRef]

235. Łodziana, Z.; Błoński, P.; Yan, Y.; Rentsch, D.; Remhof, A. NMR Chemical Shifts of ^{11}B in Metal Borohydrides from First-Principle Calculations. *J. Phys. Chem. C* **2014**, *118*, 6594–6603. [CrossRef]

236. Mauron, P.; Buchter, F.; Friedrichs, O.; Remhof, A.; Bielmann, M.; Zwicky, C.N.; Züttel, A. Stability and reversibility of $LiBH_4$. *J. Phys. Chem. B* **2008**, *112*, 906–910. [CrossRef]

237. Züttel, A.; Rentsch, S.; Fischer, P.; Wenger, P.; Sudan, P.; Mauron, P.; Emmenegger, C. Hydrogen storage properties of $LiBH_4$. *J. Alloys Compd.* **2003**, *356–357*, 515–520. [CrossRef]

238. Liu, H.; Wang, X.; Zhou, H.; Gao, S.; Ge, H.; Li, S.; Yan, M. Improved hydrogen desorption properties of $LiBH_4$ by AlH_3 addition. *Int. J. Hydrog. Energy* **2016**, *41*, 22118–22127. [CrossRef]

239. Zhang, B.J.; Liu, B.H. Hydrogen desorption from $LiBH_4$ destabilized by chlorides of transition metal Fe, Co, and Ni. *Int. J. Hydrog. Energy* **2010**, *35*, 7288–7294. [CrossRef]

240. Yu, X.B.; Grant, D.M.; Walker, G.S. Dehydrogenation of $LiBH_4$ Destabilized with Various Oxides. *J. Phys. Chem. C* **2009**, *113*, 17945–17949. [CrossRef]

241. Ngene, P.; van den Berg, R.; Verkuijlen, M.H.W.; de Jong, K.P.; de Jongh, P.E. Reversibility of the hydrogen desorption from $NaBH_4$ by confinement in nanoporous carbon. *Energy Environ. Sci.* **2011**, *4*, 4108. [CrossRef]

242. Martelli, P.; Caputo, R.; Remhof, A.; Mauron, P.; Borgschulte, A.; Züttel, A. Stability and decomposition of $NaBH_4$. *J. Phys. Chem. C* **2010**, *114*, 7173–7177. [CrossRef]

243. Mao, J.; Guo, Z.; Nevirkovets, I.P.; Liu, H.K.; Dou, S.X. Hydrogen De-/Absorption Improvement of $NaBH_4$ Catalyzed by Titanium-Based Additives. *J. Phys. Chem. C* **2012**, *116*, 1596–1604. [CrossRef]

244. Mao, J.F.; Yu, X.B.; Guo, Z.P.; Liu, H.K.; Wu, Z.; Ni, J. Enhanced hydrogen storage performances of $NaBH_4$-MgH_2 system. *J. Alloys Compd.* **2009**, *479*, 619–623. [CrossRef]

245. Kumar, S.; Jain, A.; Miyaoka, H.; Ichikawa, T.; Kojima, Y. Study on the thermal decomposition of $NaBH_4$ catalyzed by $ZrCl_4$. *Int. J. Hydrog. Energy* **2017**, *42*, 22432–22437. [CrossRef]

246. Mao, J.F.; Yu, X.B.; Guo, Z.P.; Poh, C.K.; Liu, H.K.; Wu, Z.; Ni, J. Improvement of the $LiAlH_4$-$NaBH_4$ system for reversible hydrogen storage. *J. Phys. Chem. C* **2009**, *113*, 10813–10818. [CrossRef]

247. Kumar, S.; Kojima, Y.; Dey, G.K. Synergic effect of $ZrCl_4$ on thermal dehydrogenation kinetics of KBH_4. *J. Alloys Compd.* **2017**, *718*, 134–138. [CrossRef]

248. Dematteis, E.M.; Santoru, A.; Poletti, M.G.; Pistidda, C.; Klassen, T.; Dornheim, M.; Baricco, M. Phase stability and hydrogen desorption in a quinary equimolar mixture of light-metals borohydrides. *Int. J. Hydrog. Energy* **2018**, *43*, 16793–16803. [CrossRef]

249. Ley, M.B.; Roedern, E.; Jensen, T.R. Eutectic melting of $LiBH_4$ –KBH_4. *Phys. Chem. Chem. Phys.* **2014**, *16*, 24194–24199. [CrossRef]

250. Züttel, A.; Borgschulte, A.; Orimo, S.I. Tetrahydroborates as new hydrogen storage materials. *Scr. Mater.* **2007**, *56*, 823–828. [CrossRef]

251. Newhouse, R.J.; Stavila, V.; Hwang, S.-J.; Klebanoff, L.E.; Zhang, J.Z. Reversibility and Improved Hydrogen Release of Magnesium Borohydride. *J. Phys. Chem. C* **2010**, *114*, 5224–5232. [CrossRef]

252. Soloveichik, G.; Gao, Y.; Rijssenbeek, J.; Andrus, M.; Kniajanski, S.; Bowmanjr, R.; Hwang, S.; Zhao, J. Magnesium borohydride as a hydrogen storage material: Properties and dehydrogenation pathway of unsolvated $Mg(BH_4)_2$. *Int. J. Hydrog. Energy* **2009**, *34*, 916–928. [CrossRef]

253. Matsunaga, T.; Buchter, F.; Miwa, K.; Towata, S.; Orimo, S.; Züttel, A. Magnesium borohydride: A new hydrogen storage material. *Renew. Energy* **2008**, *33*, 193–196. [CrossRef]

254. Dematteis, E.M.; Baricco, M. Hydrogen Desorption in $Mg(BH_4)_2$-$Ca(BH_4)_2$ System. *Energies* **2019**, *12*, 3230. [CrossRef]

255. Chu, H.; Wu, G.; Zhang, Y.; Xiong, Z.; Guo, J.; He, T.; Chen, P. Improved dehydrogenation properties of calcium borohydride combined with alkaline-earth metal amides. *J. Phys. Chem. C* **2011**, *115*, 18035–18041. [CrossRef]

256. Comănescu, C.; Capurso, G.; Maddalena, A. Nanoconfinement in activated mesoporous carbon of calcium borohydride for improved reversible hydrogen storage. *Nanotechnology* **2012**, *23*, 385401. [CrossRef]

257. Rönnebro, E.; Majzoub, E.H. Calcium borohydride for hydrogen storage: Catalysis and reversibility. *J. Phys. Chem. B* **2007**, *111*, 12045–12047. [CrossRef] [PubMed]

258. Chu, H.; Wu, G.; Xiong, Z.; Guo, J.; He, T.; Chen, P. Structure and Hydrogen Storage Properties of Calcium Borohydride Diammoniate. *Chem. Mater.* **2010**, *22*, 6021–6028. [CrossRef]

259. Ravnsbæk, D.B.; Nickels, E.A.; Černý, R.; Olesen, C.H.; David, W.I.F.; Edwards, P.P.; Filinchuk, Y.; Jensen, T.R. Novel Alkali Earth Borohydride $Sr(BH_4)_2$ and Borohydride-Chloride $Sr(BH_4)Cl$. *Inorg. Chem.* **2013**, *52*, 10877–10885. [CrossRef] [PubMed]

260. Wiberg, E.; Nöth, H.; Hartwimmer, R. Notizen: Zur Kenntnis von Erdalkaliboranaten $Me[BH_4]_2$. *Z. Naturforsch. B* **1955**, *10*, 292–294. [CrossRef]

261. Borgschulte, A.; Callini, E.; Probst, B.; Jain, A.; Kato, S.; Friedrichs, O.; Remhof, A.; Bielmann, M.; Ramirez-Cuesta, A.J.; Züttel, A. Impurity gas analysis of the decomposition of complex hydrides. *J. Phys. Chem. C* **2011**, *115*, 17220–17226. [CrossRef]

262. Callini, E.; Borgschulte, A.; Ramirez-cuesta, J.; Züttel, A. Diborane release and structure distortion in borohydrides. *Dalton Trans.* **2012**, *2*, 719–725. [CrossRef]

263. Pitt, M.P.; Paskevicius, M.; Brown, D.H.; Sheppard, D.A.; Buckley, C.E. Thermal stability of $Li_2B_{12}H_{12}$ and its role in the decomposition of $LiBH_4$. *J. Am. Chem. Soc.* **2013**, *135*, 6930–6941. [CrossRef] [PubMed]

264. Friedrichs, O.; Remhof, A.; Hwang, S.J.; Züttel, A. Role of $Li_2B_{12}H_{12}$ for the formation and decomposition of $LiBH_4$. *Chem. Mater.* **2010**, *22*, 3265–3268. [CrossRef]

265. Her, J.H.; Yousufuddin, M.; Zhou, W.; Jalisatgi, S.S.; Kulleck, J.G.; Zan, J.A.; Hwang, S.J.; Bowman, R.C.; Udovic, T.J. Crystal structure of $Li_2B_{12}H_{12}$: A possible intermediate species in the decomposition of $LiBH_4$. *Inorg. Chem.* **2008**, *47*, 9757–9759. [CrossRef] [PubMed]

266. Beall, H.; Gaines, D.F. Mechanistic aspects of boron hydride reactions. *Inorg. Chim. Acta* **1999**, *289*, 1–10. [CrossRef]

267. Grahame, A.; Aguey-Zinsou, K.F. Properties and applications of metal (M) dodecahydro-closo-dodecaborates ($M_{n=1,2}B_{12}H_{12}$) and their implications for reversible hydrogen storage in the borohydrides. *Inorganics* **2018**, *6*, 106. [CrossRef]

268. Černý, R.; Brighi, M.; Murgia, F. The Crystal Chemistry of Inorganic Hydroborates. *Chemistry* **2020**, *2*, 805–826. [CrossRef]

269. Wong, S.S.; Li, W.K.; Paddon-Row, M.N. On the structure and stability of the AlH_4 radical and its potential energy surface for rearrangement and dissociation: An ab initio MO study. *J. Mol. Struct. Theochem* **1991**, *226*, 285–301. [CrossRef]

270. Barkhordarian, G.; Klassen, T.; Dornheim, M.; Bormann, R. Unexpected kinetic effect of MgB_2 in reactive hydride composites containing complex borohydrides. *J. Alloys Compd.* **2007**, *440*, 18–21. [CrossRef]

271. Gennari, F.C. Improved hydrogen storage reversibility of $LiBH_4$ destabilized by $Y(BH_4)_3$ and YH_3. *Int. J. Hydrog. Energy* **2012**, *37*, 18895–18903. [CrossRef]

272. Liu, X.; Peaslee, D.; Jost, C.Z.; Baumann, T.F.; Majzoub, E.H. Systematic Pore-Size Effects of Nanoconfinement of $LiBH_4$: Elimination of Diborane Release and Tunable Behavior for Hydrogen Storage Applications. *Chem. Mater.* **2011**, *23*, 1331–1336. [CrossRef]